KA-TP-4-2001

The Masses of the Neutral $\mathcal{CP}$-even Higgs Bosons in the MSSM: Two-Loop Calculations in the Feynman-Diagrammatic Approach

S. Heinemeyer[1*], W. Hollik[2†] and G. Weiglein[3‡]

[1] *HET, Physics Department, Brookhaven Natl. Lab., Upton NY 11973, USA*

[2] *Institut für Theoretische Physik, Universität Karlsruhe, D–76128 Karlsruhe, Germany*

[3] *Theoretical Physics Division, CERN, CH-1211 Geneva 23, Switzerland*

Abstract

We present detailed results of a Feynman-diagrammatic (FD) calculation of the leading two-loop QCD corrections to the masses of the neutral $\mathcal{CP}$-even Higgs bosons in the Minimal Supersymmetric Standard Model (MSSM). The dominant two-loop contributions together with subdominant electroweak corrections are incorporated into the full diagrammatic one-loop result. The dependence of the results for the Higgs boson masses on the various MSSM parameters is analyzed in detail. For the mass of the lightest Higgs boson, m_h, a parameter scan has been performed, yielding an upper limit on m_h which depends only on $\tan\beta$, reaching $m_h \lesssim 130$ GeV for $M_{SUSY} = 1$ TeV, $m_t = 175$ GeV and large $\tan\beta$. A compact analytical approximation formula is derived for the neutral $\mathcal{CP}$-even Higgs boson masses. These formulas, after performing the transition to the $\overline{\rm MS}$ scheme, are analytically compared with results obtained by renormalization group (RG) methods. The difference, arising from genuine non-logarithmic two-loop contributions, is identified, and its effect on the maximal value of m_h is discussed. Finally it is shown that in a simple analytic approximation to the Higgs mass, the leading two-loop radiative corrections can be absorbed to a large extent into an effective one-loop expression by evaluating the running top quark mass at appropriately chosen energy scales.

*email: Sven.Heinemeyer@bnl.gov
†email: Wolfgang.Hollik@physik.uni-karlsruhe.de
‡email: Georg.Weiglein@cern.ch

1 Introduction

The search for the lightest Higgs boson is a crucial test of Supersymmetry (SUSY) [1] which can be performed with the present and the next generation of accelerators. The prediction of a relatively light Higgs boson is common to all supersymmetric models whose couplings remain in the perturbative regime up to a very high energy scale [2]. A precise prediction for the mass of the lightest Higgs boson in terms of the relevant SUSY parameters is necessary in order to determine the discovery and exclusion potential of LEP2 and the upgraded Tevatron, and for physics at the LHC and future linear colliders, where eventually a high-precision measurement of the mass of this particle might be possible. A precise knowledge of the dependence of the masses and mixing angles of the Higgs sector of the MSSM on the relevant SUSY parameters is necessary for a detailed analysis of SUSY phenomenology at LEP2, the upgraded Tevatron, and also for the LHC and a future linear e^+e^- collider, where high-precision measurements in the Higgs sector might become possible.

The mass of the lightest $\mathcal{CP}$-even MSSM Higgs boson, m_h, is bounded from above by about $m_h \lesssim 135$ GeV, including radiative corrections up to the two-loop level [3–14]. The mixing angle $\alpha_{\rm eff}$ that diagonalizes the neutral $\mathcal{CP}$-even Higgs sector receives the same kind of corrections. By incorporating $\alpha_{\rm eff}$ into the calculations for Higgs productions or for the Higgs decay widths, the leading electroweak corrections to the production and decay of the neutral $\mathcal{CP}$-even Higgs bosons are taken into account, see Refs. [15, 16] and references therein.

In this paper we present in detail the Feynman-diagrammatic on-shell calculation at the two-loop level [7, 8]. This result is incorporated into the full diagrammatic one-loop result obtained in the on-shell scheme [5] and supplemented by subdominant electroweak two-loop and higher order QCD corrections. The results for the masses of the neutral $\mathcal{CP}$-even Higgs bosons are analyzed in terms of the relevant parameters of the MSSM. A parameter scan for the lightest Higgs boson mass is performed yielding an upper bound for m_h within the MSSM (apart from certain threshold regions which correspond to very specific configurations of the MSSM parameters) given exclusively in terms of $\tan\beta$. Compact analytical approximation formulas for the higher order corrections in the $\mathcal{CP}$-even Higgs sector are presented [17]. It is shown that these formulas approximate m_h better than 2 GeV for most of the MSSM parameter space. The results for m_h are compared with the corresponding results obtained by renormalization group (RG) methods [17, 18]. After transforming the FD result into the $\overline{\rm MS}$ scheme, it is shown that the logarithmic contributions of both approaches coincide. The difference, arising from genuine non-logarithmic two-loop contributions, is identified, and its effect on the maximal value of m_h is discussed. Finally it is shown that in a simple analytic approximation to the Higgs mass, the leading two-loop radiative corrections can be absorbed to a large extent into an effective one-loop expression by evaluating the running top quark mass at appropriately chosen energy scales.

The paper is organized as follows: Section 2 contains our notations and a description of the renormalization procedure as required for the corrections in the MSSM Higgs sector in $\mathcal{O}(\alpha\alpha_s)$. The main features of the calculation are discussed in section 3. In section 4 we present a detailed numerical analysis of the results for the neutral $\mathcal{CP}$-even Higgs boson

masses as functions of the different SUSY parameters. A scan for m_h over the parameters $m_{\tilde{g}}, M_A, M, \mu$ and the $\tilde{t}$-mixing parameter is performed. The maximal possible values of m_h as a function of $\tan\beta$ is obtained. In section 5 a compact analytical approximation formula is derived and a comparison with the full result is performed. Section 6 contains the comparison with the RG result. The conclusions are given in section 7.

2 Renormalization

2.1 The Higgs sector of the MSSM

Contrary to the Standard Model (SM), in the MSSM two Higgs doublets are required. The Higgs potential [19]

$$\begin{aligned} V &= m_1^2|\mathcal{H}_1|^2 + m_2^2|\mathcal{H}_2|^2 - m_{12}^2(\epsilon_{ab}\mathcal{H}_1^a\mathcal{H}_2^b + \text{h.c.}) \\ &\quad + \frac{1}{8}({g_1}^2 + {g_2}^2)\left[|\mathcal{H}_1|^2 - |\mathcal{H}_2|^2\right]^2 + \frac{1}{2}{g_2}^2|\mathcal{H}_1^\dagger\mathcal{H}_2|^2 \ , \end{aligned} \tag{1}$$

contains m_1, m_2, m_{12} as soft SUSY breaking parameters; g, g' are the $SU(2)$ and $U(1)$ gauge couplings, and $\epsilon_{12} = -1$.

The doublet fields H_1 and H_2 are decomposed in the following way:

$$\begin{aligned} \mathcal{H}_1 &= \begin{pmatrix} \mathcal{H}_1^0 \\ \mathcal{H}_1^- \end{pmatrix} = \begin{pmatrix} v_1 + \frac{1}{\sqrt{2}}(\phi_1^0 + i\chi_1^0) \\ -\phi_1^- \end{pmatrix} \\ \mathcal{H}_2 &= \begin{pmatrix} \mathcal{H}_2^+ \\ \mathcal{H}_2^0 \end{pmatrix} = \begin{pmatrix} \phi_2^+ \\ v_2 + \frac{1}{\sqrt{2}}(\phi_2^0 + i\chi_2^0) \end{pmatrix} \ . \end{aligned} \tag{2}$$

The potential (1) can be described with the help of two independent parameters (besides g and g'): $\tan\beta = v_2/v_1$ and $M_A^2 = -m_{12}^2(\tan\beta + \cot\beta)$, where M_A is the mass of the $\mathcal{CP}$-odd A boson.

The diagonalization of the bilinear part of the Higgs potential, i.e. the Higgs mass matrices, is performed via the orthogonal transformations

$$\begin{pmatrix} H^0 \\ h^0 \end{pmatrix} = \begin{pmatrix} \cos\alpha & \sin\alpha \\ -\sin\alpha & \cos\alpha \end{pmatrix} \begin{pmatrix} \phi_1^0 \\ \phi_2^0 \end{pmatrix} \tag{3}$$

$$\begin{pmatrix} G^0 \\ A^0 \end{pmatrix} = \begin{pmatrix} \cos\beta & \sin\beta \\ -\sin\beta & \cos\beta \end{pmatrix} \begin{pmatrix} \chi_1^0 \\ \chi_2^0 \end{pmatrix} \tag{4}$$

$$\begin{pmatrix} G^\pm \\ H^\pm \end{pmatrix} = \begin{pmatrix} \cos\beta & \sin\beta \\ -\sin\beta & \cos\beta \end{pmatrix} \begin{pmatrix} \phi_1^\pm \\ \phi_2^\pm \end{pmatrix} \ . \tag{5}$$

The mixing angle α is determined through

$$\tan 2\alpha = \tan 2\beta \, \frac{M_A^2 + M_Z^2}{M_A^2 - M_Z^2}; \qquad -\frac{\pi}{2} < \alpha < 0 \ . \tag{6}$$

One gets the following Higgs spectrum:

$$\begin{aligned} \text{2 neutral bosons, } \mathcal{CP}=+1 &: \; h^0, H^0 \\ \text{1 neutral boson, } \mathcal{CP}=-1 &: \; A^0 \\ \text{2 charged bosons} &: \; H^+, H^- \\ \text{3 unphysical Goldstone bosons} &: \; G^0, G^+, G^-. \end{aligned} \tag{7}$$

The masses of the gauge bosons are given in analogy to the SM:

$$M_W^2 = \frac{1}{2} g_2^2 (v_1^2 + v_2^2); \qquad M_Z^2 = \frac{1}{2}(g_1^2 + g_2^2)(v_1^2 + v_2^2); \qquad M_\gamma = 0. \tag{8}$$

At tree level the mass matrix of the neutral $\mathcal{CP}$-even Higgs bosons is given in the ϕ_1-ϕ_2-basis in terms of M_Z, M_A, and $\tan\beta$ by

$$\begin{aligned} M_{\text{Higgs}}^{2,\text{tree}} &= \begin{pmatrix} m_{\phi_1}^2 & m_{\phi_1\phi_2}^2 \\ m_{\phi_1\phi_2}^2 & m_{\phi_2}^2 \end{pmatrix} \\ &= \begin{pmatrix} M_A^2 \sin^2\beta + M_Z^2 \cos^2\beta & -(M_A^2 + M_Z^2)\sin\beta\,\cos\beta \\ -(M_A^2 + M_Z^2)\sin\beta\,\cos\beta & M_A^2\cos^2\beta + M_Z^2 \sin^2\beta \end{pmatrix}, \end{aligned} \tag{9}$$

which by diagonalization according to eq. (3) yields the tree-level Higgs boson masses

$$M_{\text{Higgs}}^{2,\text{tree}} \xrightarrow{\alpha} \begin{pmatrix} m_{H,\text{tree}}^2 & 0 \\ 0 & m_{h,\text{tree}}^2 \end{pmatrix}. \tag{10}$$

In order to slightly simplify the two-loop calculation, we have chosen to perform it in the ϕ_1-ϕ_2-basis. In this way the angle α does not appear in the calculation of the two-loop self-energies, but enters at the end when the rotation into the physical basis is performed.

In order to deal with the arising divergences and to establish the meaning of the physical parameters beyond the tree level, one has to renormalize the Higgs and the scalar top sector of the MSSM. For the corrections of $\mathcal{O}(\alpha\alpha_s)$ to the Higgs boson masses, in the focus of this discussion here, renormalization up to the two-loop level is needed. In the following we specify the renormalization for the relevant quantities in this calculation (explicitly listed are only those terms that actually contribute at $\mathcal{O}(\alpha\alpha_s)$). The renormalization of the complete one-loop contributions to the neutral $\mathcal{CP}$-even Higgs boson masses has been performed according to Ref. [5].

We use the following notation: $\Sigma^{(1)}$ and $\Sigma^{(2)}$ denote the one- and two-loop part of an unrenormalized self-energy, $\hat{\Sigma}^{(1)}$ and $\hat{\Sigma}^{(2)}$ denote the one- and two-loop part of a renormalized self-energy, and $\Sigma'(k^2) = \frac{\partial}{\partial k^2}\Sigma(k^2)$. t_1 and t_2 denote the unrenormalized tadpoles; $t^{(1)}$ and $t^{(2)}$ represent the one- and two-loop part of an unrenormalized tadpole, and $\hat{t}_1, \hat{t}_2$ denote the renormalized tadpoles.

The renormalization of the masses and fields is performed as follows:

$$
\begin{aligned}
M_Z^2 &\to M_Z^2 + \delta M_Z^{2\,(1)} + \delta M_Z^{2\,(2)}, && (11)\\
M_A^2 &\to M_A^2 + \delta M_A^{2\,(1)} + \delta M_A^{2\,(2)}, && (12)\\
\varphi_1 &\to \varphi_1 Z_{\mathcal{H}_1}^{1/2}, \quad \varphi_1 = \phi_1^0, \chi_1^0, \phi_1^-, && (13)\\
\varphi_2 &\to \varphi_2 Z_{\mathcal{H}_2}^{1/2}, \quad \varphi_2 = \phi_2^0, \chi_2^0, \phi_2^+, && (14)\\
& Z_{\mathcal{H}_i} = 1 + \delta Z_{\mathcal{H}_i}^{(1)} + \delta Z_{\mathcal{H}_i}^{(2)} && (15)\\
\tan\beta &\to \tan\beta\,(1 + \delta\tan\beta^{\,(1)} + \delta\tan\beta^{\,(2)}), && (16)\\
t_i &\to t_i + \delta t_i^{(1)} + \delta t_i^{(2)} \quad (i = 1,2)\ . && (17)
\end{aligned}
$$

This yields for the renormalized two-loop self-energies of ϕ_1 and ϕ_2:

$$
\begin{aligned}
\hat{\Sigma}_{\phi_1}^{(2)}(k^2) &= \Sigma_{\phi_1}^{(2)}(k^2) + k^2\delta Z_{H_1}^{(2)} - \delta V_{\phi_1}^{(2)}, && (18)\\
\hat{\Sigma}_{\phi_2}^{(2)}(k^2) &= \Sigma_{\phi_2}^{(2)}(k^2) + k^2\delta Z_{H_2}^{(2)} - \delta V_{\phi_2}^{(2)}, && (19)\\
\hat{\Sigma}_{\phi_1\phi_2}^{(2)}(k^2) &= \Sigma_{\phi_1\phi_2}^{(2)}(k^2) - \delta V_{\phi_1\phi_2}^{(2)}, && (20)
\end{aligned}
$$

where it is understood that the unrenormalized self-energies at two-loop order also contain the contributions arising from the subloop renormalization. The expressions $\delta V_{\phi_1}^{(2)}, \delta V_{\phi_2}^{(2)}$ and $\delta V_{\phi_1\phi_2}^{(2)}$ are the two-loop counterterm contributions from the Higgs potential:

$$
\begin{aligned}
\delta V_{\phi_1}^{(2)} &= \delta M_Z^{2\,(2)}\cos^2\beta\ + \delta M_A^{2\,(2)}\sin^2\beta\ - \delta t_1^{(2)}\frac{e}{2M_W s_W}\cos\beta\,(1+\sin^2\beta\,)\\
&\quad + \delta t_2^{(2)}\frac{e}{2M_W s_W}\cos^2\beta\ \sin\beta\ + \delta Z_{H_1}^{(2)}\left(M_Z^2\cos^2\beta\ + M_A^2\sin^2\beta\,\right)\\
&\quad + \delta\tan\beta^{\,(2)}\cos^2\beta\ \sin^2\beta\,(M_A^2 - M_Z^2), && (21)\\
\delta V_{\phi_2}^{(2)} &= \delta M_Z^{2\,(2)}\sin^2\beta\ + \delta M_A^{2\,(2)}\cos^2\beta\ - \delta t_2^{(2)}\frac{e}{2M_W s_W}\sin\beta\,(1+\cos^2\beta\,)\\
&\quad + \delta t_1^{(2)}\frac{e}{2M_W s_W}\sin^2\beta\ \cos\beta\ + \delta Z_{H_2}^{(2)}\left(M_Z^2\sin^2\beta\ + M_A^2\cos^2\beta\,\right)\\
&\quad - \delta\tan\beta^{\,(2)}\cos^2\beta\ \sin^2\beta\,(M_A^2 - M_Z^2), && (22)\\
\delta V_{\phi_1\phi_2}^{(2)} &= -\delta M_Z^{2\,(2)}\sin\beta\ \cos\beta\ - \delta M_A^{2\,(2)}\sin\beta\ \cos\beta\ - \delta t_1^{(2)}\frac{e}{2M_W s_W}\sin^3\beta\\
&\quad - \delta t_2^{(2)}\frac{e}{2M_W s_W}\cos^3\beta\ - \delta Z_{H_1}^{(2)}\frac{\sin\beta\ \cos\beta}{2}\left(M_A^2 - M_Z^2\right)\\
&\quad - \delta Z_{H_2}^{(2)}\frac{\sin\beta\ \cos\beta}{2}\left(M_A^2 - M_Z^2\right)\\
&\quad - \delta\tan\beta^{\,(2)}\frac{1}{2}\sin 2\beta\ \cos 2\beta\,(M_A^2 + M_Z^2), && (23)
\end{aligned}
$$

with the electroweak mixing angle $s_W^2 = 1 - c_W^2$, $c_W^2 = M_W^2/M_Z^2$.

The counterterms are fixed by imposing on-shell renormalization conditions for the renormalized self-energies. For the A boson this reads:

$$
\mathrm{Re}\,\hat{\Sigma}_A(M_A^2) = 0\ . \qquad (24)
$$

The tadpole conditions are:

$$\hat{t}_1 = 0, \quad \hat{t}_2 = 0 \ . \tag{25}$$

The conditions for the tadpoles have the consequence that the v_i remain the minima of the Higgs potential also at the two-loop level.

The resulting expressions for the renormalization constants contributing to the leading two-loop corrections to the neutral $\mathcal{CP}$-even Higgs boson masses, expressed in terms of unrenormalized self-energies and tadpoles, are given in Sec. 3.1.

2.2 The scalar quark sector of the MSSM

Renormalization in the squark sector is needed in the present calculation at the one-loop level, i.e. at $\mathcal{O}(\alpha_s)$. As above, we work in the on-shell scheme. In the following the formulas are written for one flavor.

The squark mass term of the MSSM Lagrangian is given by

$$\mathcal{L}_{m_{\tilde{f}}} = -\frac{1}{2}\left(\tilde{f}_L^\dagger, \tilde{f}_R^\dagger\right) \mathbf{Z} \begin{pmatrix} \tilde{f}_L \\ \tilde{f}_R \end{pmatrix} \ , \tag{26}$$

where

$$\mathbf{Z} = \begin{pmatrix} M_{\tilde{Q}}^2 + M_Z^2 \cos 2\beta \, (I_3^f - Q_f s_W^2) + m_f^2 & m_f(A_f - \mu\{\cot\beta \, ; \tan\beta \,\}) \\ m_f(A_f - \mu\{\cot\beta; \tan\beta\}) & M_{\tilde{Q}'}^2 + M_Z^2 \cos 2\beta \, Q_f s_W^2 + m_f^2 \end{pmatrix}, \tag{27}$$

and $\{\cot\beta \, ; \tan\beta \,\}$ corresponds to $\{u; d\}$-type squarks. The soft SUSY breaking term $M_{\tilde{Q}'}$ is given by:

$$M_{\tilde{Q}'} \ = \ \begin{cases} M_{\tilde{U}} & \text{for right handed } u\text{-type squarks} \\ M_{\tilde{D}} & \text{for right handed } d\text{-type squarks} \end{cases} \ . \tag{28}$$

In order to diagonalize the mass matrix and to determine the physical mass eigenstates the following rotation has to be performed:

$$\begin{pmatrix} \tilde{f}_1 \\ \tilde{f}_2 \end{pmatrix} = \begin{pmatrix} \cos\theta_{\tilde{f}} & \sin\theta_{\tilde{f}} \\ -\sin\theta_{\tilde{f}} & \cos\theta_{\tilde{f}} \end{pmatrix} \begin{pmatrix} \tilde{f}_L \\ \tilde{f}_R \end{pmatrix}. \tag{29}$$

The mixing angle $\theta_{\tilde{f}}$ is given for $\tan\beta \ > 1$ by:

$$\cos\theta_{\tilde{f}} \ = \ \sqrt{\frac{(m_{\tilde{f}_R}^2 - m_{\tilde{f}_1}^2)^2}{m_f^2 \, (A_f - \mu\{\cot\beta \, ; \tan\beta \,\})^2 + (m_{\tilde{f}_R}^2 - m_{\tilde{f}_1}^2)^2}} \tag{30}$$

$$\begin{aligned} \sin\theta_{\tilde{f}} \ &= \ \mp \, sgn\Big[A_f - \mu\{\cot\beta \, ; \tan\beta \,\}\Big] \\ &\quad \times \sqrt{\frac{m_f^2 \, (A_f - \mu\{\cot\beta \, ; \tan\beta \,\})^2}{m_f^2 \, (A_f - \mu\{\cot\beta \, ; \tan\beta \,\})^2 + (m_{\tilde{f}_R}^2 - m_{\tilde{f}_1}^2)^2}} \ . \end{aligned} \tag{31}$$

The negative sign in (31) corresponds to u-type squarks, the positive sign to d-type ones. $m^2_{\tilde{f}_R} = M^2_{\tilde{Q}'} + M_Z^2 \cos 2\beta\, Q_f s_W^2 + m_f^2$ denotes the lower right entry in the squark mass matrix (27). The masses are given by the eigenvalues of the mass matrix:

$$
\begin{aligned}
m^2_{\tilde{f}_{1,2}} &= \frac{1}{2}\left[M^2_{\tilde{Q}} + M^2_{\tilde{Q}'}\right] + \frac{1}{2} M_Z^2 \cos 2\beta\, I_3^f + m_f^2 \\
&\quad \left\{ \begin{array}{l} \pm \dfrac{c_f}{2} \sqrt{\left[M^2_{\tilde{Q}} - M^2_{\tilde{Q}'} + M_Z^2 \cos 2\beta\, (I_3^f - 2Q_f s_W^2)\right]^2 + 4 m_f^2 \left(A_u - \mu \cot\beta\right)^2} \\ \pm \dfrac{c_f}{2} \sqrt{\left[M^2_{\tilde{Q}} - M^2_{\tilde{Q}'} + M_Z^2 \cos 2\beta\, (I_3^f - 2Q_f s_W^2)\right]^2 + 4 m_f^2 \left(A_d - \mu \tan\beta\right)^2} \end{array} \right. \qquad (32) \\
c_f &= sgn\left[M^2_{\tilde{Q}} - M^2_{\tilde{Q}'} + M_Z^2 \cos 2\beta\, (I_3^f - 2Q_f s_W^2)\right] \qquad (33)
\end{aligned}
$$

for u-type and d-type squarks, respectively. For most of our discussions (see Sec. 4) we make the choice

$$M_{\tilde{Q}} = M_{\tilde{Q}'} =: m_{\tilde{q}} \ . \qquad (34)$$

Since the non-diagonal entry of the mass matrix eq. (27) is proportional to the fermion mass, mixing becomes particularly important for $\tilde{f}_1 = \tilde{t}$, in the case of $\tan\beta \gg 1$ also for $\tilde{f}_1 = \tilde{b}$.

For an on-shell renormalization it is convenient to express the squark mass matrix in terms of the physical masses $m_{\tilde{f}_1}, m_{\tilde{f}_2}$ and the mixing angle $\theta_{\tilde{f}}$:

$$\mathbf{Z} = \begin{pmatrix} \cos^2\theta_{\tilde{f}} m^2_{\tilde{f}_1} + \sin^2\theta_{\tilde{f}} m^2_{\tilde{f}_2} & \sin\theta_{\tilde{f}}\cos\theta_{\tilde{f}} (m^2_{\tilde{f}_1} - m^2_{\tilde{f}_2}) \\ \sin\theta_{\tilde{f}}\cos\theta_{\tilde{f}} (m^2_{\tilde{f}_1} - m^2_{\tilde{f}_2}) & \sin^2\theta_{\tilde{f}} m^2_{\tilde{f}_1} + \cos^2\theta_{\tilde{f}} m^2_{\tilde{f}_2} \end{pmatrix} \ . \qquad (35)$$

A_f can be written as follows:

$$A_f = \frac{\sin\theta_{\tilde{f}}\cos\theta_{\tilde{f}} (m^2_{\tilde{f}_1} - m^2_{\tilde{f}_2})}{m_f} + \mu\{\cot\beta\,;\tan\beta\,\}. \qquad (36)$$

The renormalization of the fields, the masses, and the mixing angle is then performed via

$$
\begin{aligned}
\tilde{f}_L &\to \tilde{f}_L (1 + \frac{1}{2}\delta Z_{\tilde{f}_L}) && (37) \\
\tilde{f}_R &\to \tilde{f}_R (1 + \frac{1}{2}\delta Z_{\tilde{f}_R}) && (38) \\
m^2_{\tilde{f}_i} &\to m^2_{\tilde{f}_i} + \delta m^2_{\tilde{f}_i} && (39) \\
\theta_{\tilde{f}} &\to \theta_{\tilde{f}} + \delta\theta_{\tilde{f}}. && (40)
\end{aligned}
$$

In the mass eigenstate basis, the field renormalization reads:

$$\begin{pmatrix} \tilde{f}_1 \\ \tilde{f}_2 \end{pmatrix} \to \begin{pmatrix} 1 + \frac{1}{2}\delta Z_{\tilde{f}_1} & \frac{1}{2}\delta Z_{\tilde{f}_{12}} \\ \frac{1}{2}\delta Z_{\tilde{f}_{21}} & 1 + \frac{1}{2}\delta Z_{\tilde{f}_2} \end{pmatrix} \begin{pmatrix} \tilde{f}_1 \\ \tilde{f}_2 \end{pmatrix}, \qquad (41)$$

with

$$\begin{pmatrix} \delta Z_{\tilde{f}_1} \\ \delta Z_{\tilde{f}_2} \end{pmatrix} = \begin{pmatrix} \cos^2\theta_{\tilde{f}} & \sin^2\theta_{\tilde{f}} \\ \sin^2\theta_{\tilde{f}} & \cos^2\theta_{\tilde{f}} \end{pmatrix} \begin{pmatrix} \delta Z_{\tilde{f}_L} \\ \delta Z_{\tilde{f}_R} \end{pmatrix} \tag{42}$$

$$\begin{aligned} \delta Z_{\tilde{f}_{12}} &= \sin\theta_{\tilde{f}}\cos\theta_{\tilde{f}}(\delta Z_{\tilde{f}_R} - \delta Z_{\tilde{f}_L}) = \delta Z_{\tilde{f}_{21}} \qquad (43)\\ &= \frac{\sin\theta_{\tilde{f}}\cos\theta_{\tilde{f}}}{\cos^2\theta_{\tilde{f}} - \sin^2\theta_{\tilde{f}}}(\delta Z_{\tilde{f}_2} - \delta Z_{\tilde{f}_1}). \end{aligned}$$

The renormalized diagonal and non-diagonal self-energies in this basis have the following structure:

$$\hat{\Sigma}_{\tilde{f}_1}(k^2) = \Sigma_{\tilde{f}_1}(k^2) - \delta m^2_{\tilde{f}_1} + (k^2 - m^2_{\tilde{f}_1})\delta Z_{\tilde{f}_1} \tag{44}$$

$$\hat{\Sigma}_{\tilde{f}_2}(k^2) = \Sigma_{\tilde{f}_2}(k^2) - \delta m^2_{\tilde{f}_2} + (k^2 - m^2_{\tilde{f}_2})\delta Z_{\tilde{f}_2} \tag{45}$$

$$\hat{\Sigma}_{\tilde{f}_1\tilde{f}_2}(k^2) = \Sigma_{\tilde{f}_1\tilde{f}_2}(k^2) - (m^2_{\tilde{f}_1} - m^2_{\tilde{f}_2})\delta\theta_{\tilde{f}} + (k^2 - \frac{1}{2}(m^2_{\tilde{f}_1} + m^2_{\tilde{f}_2}))\delta Z_{\tilde{f}_{12}}. \tag{46}$$

We impose the following on-shell renormalization conditions:

$$\mathrm{Re}\,\hat{\Sigma}_{\tilde{f}_1}(m^2_{\tilde{f}_1}) = 0 \tag{47}$$

$$\mathrm{Re}\,\hat{\Sigma}'_{\tilde{f}_1}(m^2_{\tilde{f}_1}) = 0 \tag{48}$$

$$\mathrm{Re}\,\hat{\Sigma}_{\tilde{f}_2}(m^2_{\tilde{f}_2}) = 0 \tag{49}$$

$$\mathrm{Re}\,\hat{\Sigma}'_{\tilde{f}_2}(m^2_{\tilde{f}_1}) = -\mathrm{Re}\,\Sigma'_{\tilde{f}_1}(m^2_{\tilde{f}_1}) + \mathrm{Re}\,\Sigma'_{\tilde{f}_2}(m^2_{\tilde{f}_2}) \tag{50}$$

$$\mathrm{Re}\,\hat{\Sigma}_{\tilde{f}_1\tilde{f}_2}(m^2_{\tilde{f}_1}) = 0, \tag{51}$$

which determines the renormalization constants to be

$$\delta m^2_{\tilde{f}_1} = \mathrm{Re}\,\Sigma_{\tilde{f}_1}(m^2_{\tilde{f}_1}) \tag{52}$$

$$\delta m^2_{\tilde{f}_2} = \mathrm{Re}\,\Sigma_{\tilde{f}_1}(m^2_{\tilde{f}_2}) \tag{53}$$

$$\delta Z_{\tilde{f}_1} = -\Sigma'_{\tilde{f}_1}(m^2_{\tilde{f}_1}) \tag{54}$$

$$\delta Z_{\tilde{f}_2} = \delta Z_{\tilde{f}_1} \quad \Rightarrow \quad \delta Z_{\tilde{f}_{12}} = 0 \tag{55}$$

$$\delta\theta_{\tilde{f}} = \frac{1}{m^2_{\tilde{f}_1} - m^2_{\tilde{f}_2}}\Sigma_{\tilde{f}_1\tilde{f}_2}(m^2_{\tilde{f}_1}). \tag{56}$$

The unsymmetric renormalization condition (50) is chosen for convenience since it leads to $\delta Z_{\tilde{f}_2} = \delta Z_{\tilde{f}_1}$ and accordingly to $\delta Z_{\tilde{f}_{12}} = 0$, which simplifies the expression for the counterterm of the mixing angle. In eq. (51) we have imposed the condition that the non-diagonal self-energy vanishes at $q^2 = m^2_{\tilde{f}_1}$. Alternatively one could choose $q^2 = m^2_{\tilde{f}_2}$, instead; the numerical difference arising from these different choices is irrelevant for the results of the Higgs boson masses, as we have checked explicitly.

Taking into account that neither $\delta\mu$ nor $\delta\tan\beta$ are of $\mathcal{O}(\alpha_s)$, one obtains from eq. (36):

$$\delta A_f = \frac{\sin\theta_{\tilde{f}}\cos\theta_{\tilde{f}}(m^2_{\tilde{f}_1} - m^2_{\tilde{f}_2})}{m_f}\left[\frac{1 - 2\sin^2\theta_{\tilde{f}}}{\sin\theta_{\tilde{f}}\cos\theta_{\tilde{f}}}\delta\theta_{\tilde{f}} + \frac{\delta m^2_{\tilde{f}_1} - \delta m^2_{\tilde{f}_2}}{m^2_{\tilde{f}_1} - m^2_{\tilde{f}_2}} - \frac{\delta m_f}{m_f}\right]. \tag{57}$$

For completeness we also list the expression for the quark mass counterterm in the on-shell scheme,

$$\delta m_f = m_f \left(\Sigma_f^V(m_f^2) + \Sigma_f^S(m_f^2) \right), \tag{58}$$

where the scalar functions in the decomposition of the fermion self-energy $\Sigma_f(p)$ are defined according to

$$\Sigma_f(p) = \not{p}\Sigma_f^V(p^2) + \not{p}\gamma_5\Sigma_f^A(p^2) + m_f\Sigma_f^S(p^2). \tag{59}$$

3 Calculation of the neutral $\mathcal{CP}$-even Higgs boson masses

3.1 Leading two-loop contributions to the Higgs boson self-energies

The dominant one-loop contributions to the Higgs boson mass matrix in eq. (9) are given by terms of the form $G_F m_t^4 \ln(m_{\tilde{t}_1} m_{\tilde{t}_2}/m_t^2)$, which arise from t- and $\tilde{t}$-loops. They can be obtained by evaluating the contribution of the t–$\tilde{t}$-sector to the $\phi_{1,2}$ self-energies at zero external momentum from the Yukawa part of the theory (neglecting the gauge couplings). Accordingly, the leading contributions to the one-loop corrected Higgs boson masses are derived by diagonalizing the matrix

$$M_{\rm Higgs}^{2,1-\rm loop} = \begin{pmatrix} m_{\phi_1}^2 - \hat{\Sigma}_{\phi_1}^{(1)}(0) & m_{\phi_1\phi_2}^2 - \hat{\Sigma}_{\phi_1\phi_2}^{(1)}(0) \\ m_{\phi_1\phi_2}^2 - \hat{\Sigma}_{\phi_1\phi_2}^{(1)}(0) & m_{\phi_2}^2 - \hat{\Sigma}_{\phi_2}^{(1)}(0) \end{pmatrix}, \tag{60}$$

where the $\hat{\Sigma}^{(1)}$ denote the one-loop Yukawa contributions of the t–$\tilde{t}$-sector to the renormalized one-loop $\phi_{1,2}$ self-energies. For completeness, we list here the explicit form of these dominant one-loop corrections (in the numerical results given in Sec. 4 we use the complete one-loop on-shell result as given in Ref. [5]):

$$\begin{aligned}
\hat{\Sigma}_{\phi_1}^{(1)}(0) &= \frac{3G_F m_t^4}{\sqrt{2}\pi^2 \sin^2\beta} \frac{\mu^2 (A_t - \mu\cot\beta)^2}{(m_{\tilde{t}_1}^2 - m_{\tilde{t}_2}^2)^2} \left(1 - \frac{m_{\tilde{t}_1}^2 + m_{\tilde{t}_2}^2}{m_{\tilde{t}_1}^2 - m_{\tilde{t}_2}^2} \ln\frac{m_{\tilde{t}_1}}{m_{\tilde{t}_2}} \right), \\
\hat{\Sigma}_{\phi_1\phi_2}^{(1)}(0) &= \frac{3G_F m_t^4}{2\sqrt{2}\pi^2 \sin^2\beta} \left[-\frac{\mu(A_t - \mu\cot\beta)}{m_{\tilde{t}_1}^2 - m_{\tilde{t}_2}^2} \ln\frac{m_{\tilde{t}_1}^2}{m_{\tilde{t}_2}^2} \right. \\
&\quad \left. - \frac{2\mu A_t (A_t - \mu\cot\beta)^2}{(m_{\tilde{t}_1}^2 - m_{\tilde{t}_2}^2)^2} \left(1 - \frac{m_{\tilde{t}_1}^2 + m_{\tilde{t}_2}^2}{m_{\tilde{t}_1}^2 - m_{\tilde{t}_2}^2} \ln\frac{m_{\tilde{t}_1}}{m_{\tilde{t}_2}} \right) \right], \\
\hat{\Sigma}_{\phi_2}^{(1)}(0) &= \frac{3G_F m_t^4}{\sqrt{2}\pi^2 \sin^2\beta} \left[\ln\left(\frac{m_{\tilde{t}_1} m_{\tilde{t}_2}}{m_t^2} \right) + \frac{A_t(A_t - \mu\cot\beta)}{m_{\tilde{t}_1}^2 - m_{\tilde{t}_2}^2} \ln\frac{m_{\tilde{t}_1}^2}{m_{\tilde{t}_2}^2} \right. \\
&\quad \left. + \frac{A_t^2 (A_t - \mu\cot\beta)^2}{(m_{\tilde{t}_1}^2 - m_{\tilde{t}_2}^2)^2} \left(1 - \frac{m_{\tilde{t}_1}^2 + m_{\tilde{t}_2}^2}{m_{\tilde{t}_1}^2 - m_{\tilde{t}_2}^2} \ln\frac{m_{\tilde{t}_1}}{m_{\tilde{t}_2}} \right) \right].
\end{aligned} \tag{61}$$

By comparison with the full one-loop result [5,6] it has been shown that these contributions indeed contain the bulk of the one-loop corrections. They typically approximate the full one-loop result within 5 GeV.

In order to derive the leading two-loop contributions to the masses of the neutral $\mathcal{CP}$-even Higgs bosons we have evaluated the QCD corrections to eq. (60) [7]. Accordingly, we have calculated the $\mathcal{O}(\alpha\alpha_s)$ contribution of the t–$\tilde{t}$-sector to the $\phi_{1,2}$ self-energies at zero momentum transfer, neglecting the gauge couplings. Because of the large value of the strong coupling constant these are expected to be the most sizable two-loop corrections (see also Ref. [12]).

The leading two-loop contributions to the $\phi_{1,2}$ self-energies are given, according to Eqs. (18)-(20), by

$$\hat{\Sigma}^{(2)}_{\phi_1}(0) = \Sigma^{(2)}_{\phi_1}(0) - \delta V^{(2)}_{\phi_1}, \tag{62}$$

$$\hat{\Sigma}^{(2)}_{\phi_2}(0) = \Sigma^{(2)}_{\phi_2}(0) - \delta V^{(2)}_{\phi_2}, \tag{63}$$

$$\hat{\Sigma}^{(2)}_{\phi_1\phi_2}(0) = \Sigma^{(2)}_{\phi_1\phi_2}(0) - \delta V^{(2)}_{\phi_1\phi_2}, \tag{64}$$

and for the leading contributions the potential counterterms eqs. (21)–(23) simplify to

$$\begin{aligned}\delta V^{(2)}_{\phi_1} &= +\delta M_A^{2\,(2)} \sin^2\beta \; - \delta t_1^{(2)} \frac{e}{2M_W s_W} \cos\beta \,(1+\sin^2\beta\,) \\ &\quad +\delta t_2^{(2)} \frac{e}{2M_W s_W} \cos^2\beta \, \sin\beta \,,\end{aligned} \tag{65}$$

$$\begin{aligned}\delta V^{(2)}_{\phi_2} &= +\delta M_A^{2\,(2)} \cos^2\beta \; - \delta t_2^{(2)} \frac{e}{2M_W s_W} \sin\beta \,(1+\cos^2\beta\,) \\ &\quad +\delta t_1^{(2)} \frac{e}{2M_W s_W} \sin^2\beta \, \cos\beta \,,\end{aligned} \tag{66}$$

$$\begin{aligned}\delta V^{(2)}_{\phi_1\phi_2} &= -\delta M_A^{2\,(2)} \sin\beta \, \cos\beta \; - \delta t_1^{(2)} \frac{e}{2M_W s_W} \sin^3\beta \\ &\quad -\delta t_2^{(2)} \frac{e}{2M_W s_W} \cos^3\beta \,.\end{aligned} \tag{67}$$

From the on-shell renormalization conditions eqs. (24)–(25) we obtain for the counterterms in eqs. (65)–(67)

$$\delta M_A^{2\,(2)} = \Sigma^{(2)}_A(0) \tag{68}$$

and

$$\delta t_1^{(2)} = -t_1^{(2)}, \quad \delta t_2^{(2)} = -t_2^{(2)}. \tag{69}$$

3.2 Evaluation of the relevant Feynman diagrams

The calculations have been performed using Dimensional Reduction (DRED) [20], which is necessary in order to preserve the relevant SUSY relations. Naive application (without an appropriate shift in the couplings) of Dimensional Regularization (DREG) [21], on the other hand, does not lead to a finite result. The same observation has also been made in Ref. [12].

The Feynman diagrams contributing to the ϕ_1, ϕ_2 and A self-energies are depicted in Fig. 1.[1] The Feynman diagrams for the tadpole diagrams are shown in Fig. 2.

There are three classes of diagrams: pure scalar diagrams (Fig. 1a–c, Fig 2a), diagrams with gluon exchange (Fig. 1d–h, Fig 2b–c), and diagrams with gluino exchange (Fig. 1i–l, Fig 2d–e). These diagrams have to be supplemented by the corresponding one-loop diagrams with counterterm insertions, which are depicted in Fig. 3 and in Fig. 4. The counterterm insertions are generated by the renormalization in the top and scalar top sector (see Sect. 2.2). They are calculated from the Feynman diagrams in Fig. 5.

The gluon-exchange contribution of $\mathcal{O}(\alpha_s)$ to the quark mass counterterm reads in DRED:

$$\delta^g m_q = \frac{\alpha_s}{\pi} m_q \left(-\frac{1}{\delta} + \gamma_{\rm E} + \ln\left(\frac{m_q^2}{4\pi\mu^2}\right) - \frac{5}{3} \right) + \mathcal{O}(\delta), \tag{70}$$

where $2\delta = 4 - n$ with n the space–time dimension, $\gamma_{\rm E}$ is Euler's constant, and μ is the 't Hooft scale. The explicit form of the other counterterms of the quark and scalar quark sector can be found in Ref. [22].

Some of the diagrams shown in Figs. 1, 2 vanish when they are combined with the corresponding counterterm contributions of Figs. 3, 4. From the pure scalar diagrams only Fig. 1a yields a non-vanishing contribution. The diagrams Fig. 1b–c are canceled exactly with their corresponding counterterm diagrams. Here the mass renormalization for the diagonal terms (with two identical squarks) and the mixing-angle renormalization for the non-diagonal terms (with two different squarks) are needed. The same applies for the tadpole diagram Fig. 2a together with the counterterm diagram Fig. 4b. The diagrams Fig. 1f are exactly canceled with the corresponding diagram with counterterm insertion Fig. 3b. The same applies for the tadpole diagrams Fig. 2b together with the counterterm diagram Fig. 4b.

We now briefly describe the evaluation of the two-loop diagrams. As explained above, the calculation involves irreducible two-loop diagrams at zero momentum-transfer and counterterm diagrams. In deriving our results we have made strong use of computer algebra tools: the diagrams were generated with the Mathematica package *FeynArts* [23, 24]. For this purpose we have implemented a model file which contains the relevant part of the MSSM Lagrangian, i.e. all SUSY propagators ($\tilde{t}_1, \tilde{t}_2, \tilde{b}_1, \tilde{b}_2, \tilde{g}$) needed for the QCD-corrections and the appropriate vertices (Higgs boson-squark vertices, squark-gluon and squark-gluino vertices). The program inserts propagators and vertices into the graphs in all possible ways and creates the amplitudes including all symmetry factors. The evaluation of the two-loop diagrams and counterterms was performed with the Mathematica package *TwoCalc* [25]. By means of two-loop tensor integral decompositions it reduces the amplitudes to a minimal set of standard scalar integrals, consisting in this case of products of the basic one-loop integrals A_0, B_0 [26] (the B_0 functions originate from the counterterm contributions only) and the two-loop function T_{134}, which is the genuine two-loop scalar integral at zero momentum-transfer (vacuum integral). This integral is known for arbitrary internal masses and admits

[1] The diagrams with a closed gluon line give zero contribution in DREG and DRED, they are omitted here.

a compact representation for $\delta \to 0$ in terms of logarithms and dilogarithms (see for instance Ref. [27]). It should be noted that from the expansion of the one-loop two-point function B_0,

$$B_0(q^2, m_a, m_b) = \frac{1}{\delta} + B_0^{\rm fin}(q^2, m_a, m_b) + \delta\, B_0^{\delta}(q^2, m_a, m_b), \tag{71}$$

only the term $B_0^{\rm fin}$ contributes, while B_0^{δ} drops out in our final result. From the output generated with *TwoCalc* a `FORTRAN` code was created which allows a fast calculation for a given set of parameters. This code has been implemented into the `FORTRAN` program *FeynHiggs* [28], see the corresponding LC note [29] and below.

Our results for the two-loop $\phi_{1,2}$ self-energies are given in terms of the SUSY parameters $\tan\beta$, M_A, μ, $m_{\tilde{t}_1}$, $m_{\tilde{t}_2}$, $\theta_{\tilde{t}}$, and $m_{\tilde{g}}$. In the general case the results are by far too lengthy to be given here explicitly. In the special case of vanishing mixing in the $\tilde{t}$-sector, $\mu = 0$, and $m_{\tilde{t}_1} = m_{\tilde{t}_2} = m_{\tilde{t}}$, a relatively compact expression can be derived which is given in Ref. [7]. We have performed an expansion of this result for large values of $m_{\tilde{g}}$. It yields for the leading terms

$$\hat{\Sigma}^{(2)}_{\phi_2} = C_F \frac{\alpha}{\pi}\frac{\alpha_s}{\pi}\frac{3\, m_t^2}{2\, s_W^2 \sin^2\beta}\left[-\ln^2(m_{\tilde{g}}^2) + \ln(m_{\tilde{g}}^2)\right] + \mathcal{O}(m_{\tilde{g}}^0). \tag{72}$$

This shows that the gluino does not decouple from the two-loop result, contrary to the case of the two-loop QCD contributions to the ρ-parameter in the MSSM [22, 30].

In Ref. [12] a result for the limiting case

$$m_{\tilde{t}} = m_{\tilde{t}_1} = m_{\tilde{t}_2} = m_{\tilde{g}} \gg m_t, \qquad \tan\beta \to \infty \tag{73}$$

has been given. In this limit we obtain

$$\begin{aligned} \hat{\Sigma}^{(2)}_{\phi_1}(0) = 0, \quad \hat{\Sigma}^{(2)}_{\phi_1\phi_2}(0) = 0, \\ \hat{\Sigma}^{(2)}_{\phi_2}(0) \;=\; -C_F \frac{\alpha}{\pi}\frac{\alpha_s}{\pi}\frac{9\, m_t^4}{4 s_W^2 M_W^2} \ln\left(\frac{m_{\tilde{t}}^2}{m_t^2}\right)\left[\ln\left(\frac{m_{\tilde{t}}^2}{m_t^2}\right) + 2\right], \end{aligned} \tag{74}$$

which agrees with the corresponding result given in Ref. [12].

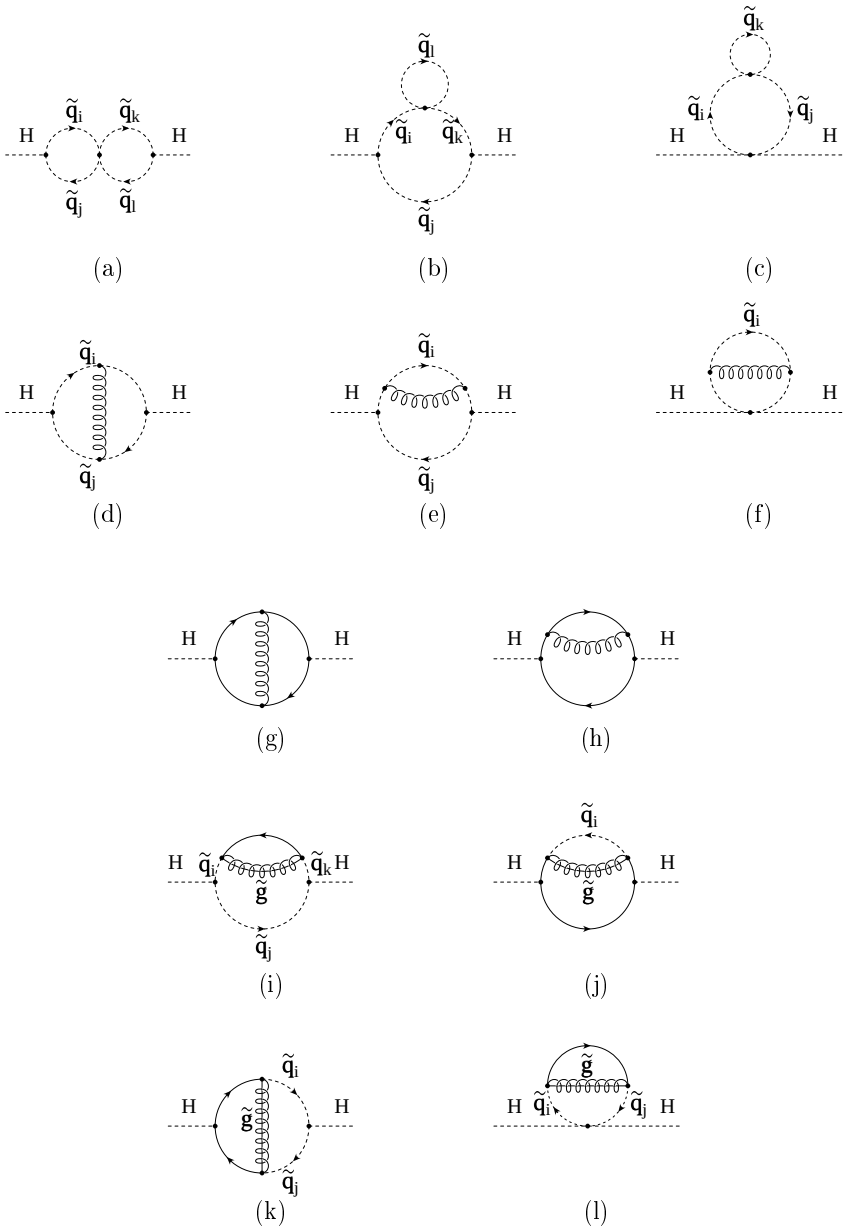

Figure 1: Feynman diagrams for the contribution of squark and quark loops to the Higgs boson self-energies at the two-loop level ($H = \phi_1, \phi_2, A$).

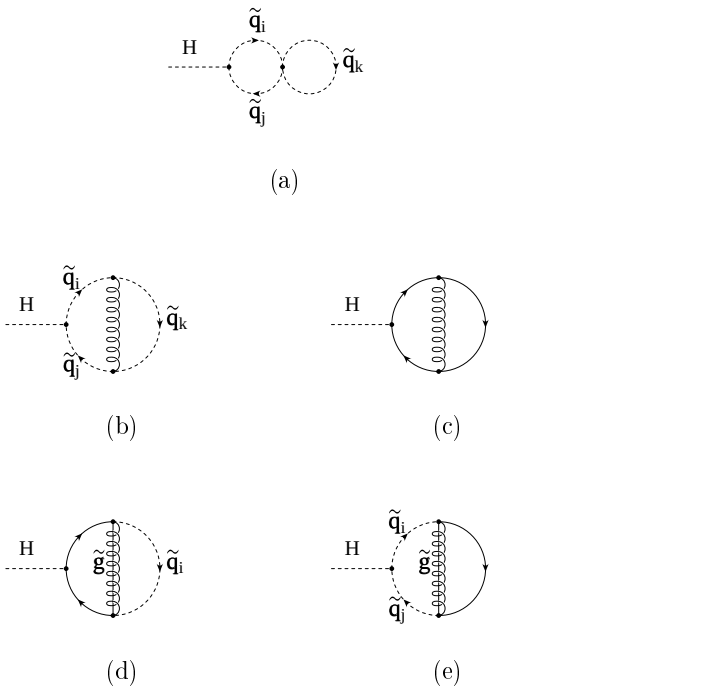

Figure 2: Feynman diagrams for the contributions of squark and quark loops to the Higgs boson tadpoles at the two-loop level ($H = \phi_1, \phi_2$).

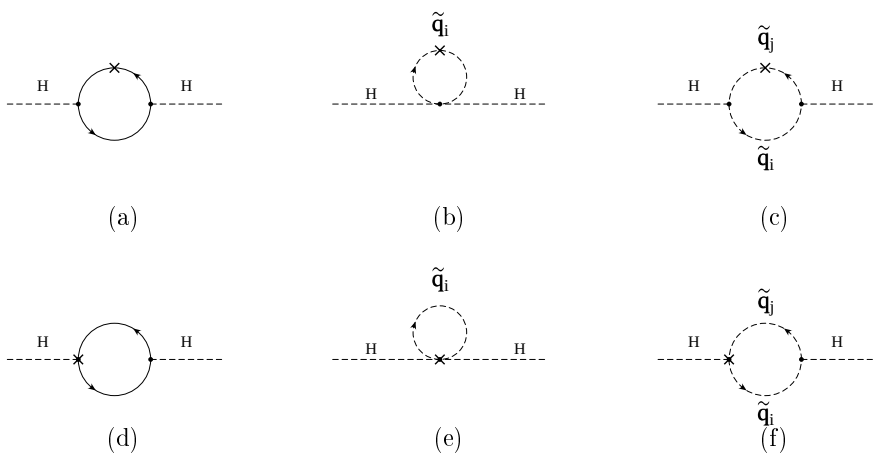

Figure 3: one-loop counterterm contributions to the Higgs boson self-energies at the two-loop level ($H = \phi_1, \phi_2, A$).

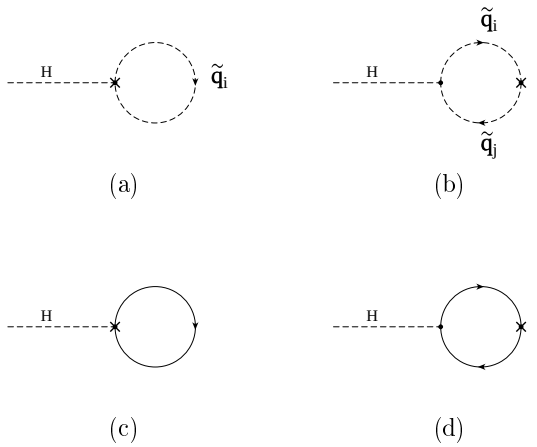

Figure 4: one-loop counterterm contributions to the Higgs boson tadpoles at the two-loop level ($H = \phi_1, \phi_2$).

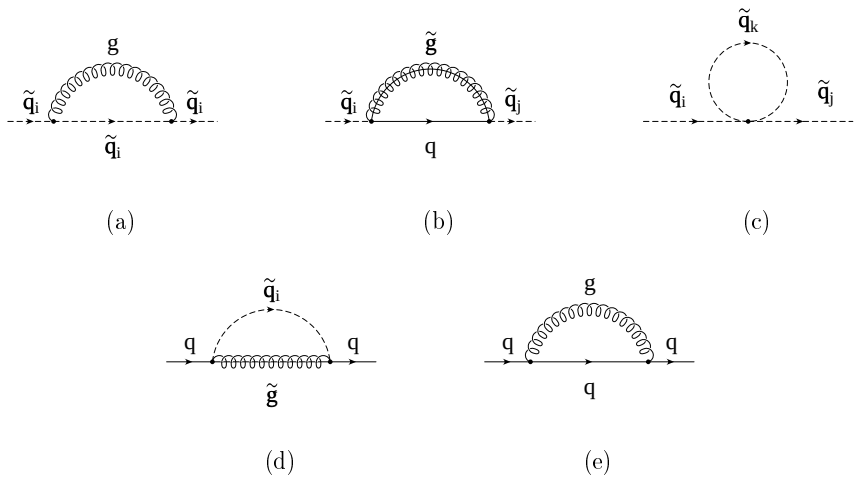

Figure 5: one-loop diagrams for the squark and quark mass counterterms and for the squark mixing-angle counterterm.

3.3 Determination of the Higgs boson masses

In the Feynman-diagrammatic approach the Higgs boson masses are derived beyond tree level by determining the poles of the $h - H$-propagator matrix whose inverse is given by

$$(\Delta_{\rm Higgs})^{-1} = -i \begin{pmatrix} q^2 - m^2_{H,\rm tree} + \hat{\Sigma}_H(q^2) & \hat{\Sigma}_{hH}(q^2) \\ \hat{\Sigma}_{hH}(q^2) & q^2 - m^2_{h,\rm tree} + \hat{\Sigma}_h(q^2) \end{pmatrix}, \tag{75}$$

where again the $\hat{\Sigma}$ denote the renormalized Higgs boson self-energies, now in the $h-H$-basis.

Determining the poles of the matrix $\Delta_{\rm Higgs}$ in eq. (75) is equivalent to solving the equation

$$\left[q^2 - m_h^2 + \hat{\Sigma}_{hh}(q^2)\right]\left[q^2 - m_H^2 + \hat{\Sigma}_{HH}(q^2)\right] - \left[\hat{\Sigma}_{hH}(q^2)\right]^2 = 0. \tag{76}$$

In our calculation the complete one-loop result for the Higgs boson self-energies in the on-shell scheme [5] is combined with the leading two-loop contributions, which have been outlined in the previous section. The matrix eq. (75) therefore contains the renormalized Higgs boson self-energies

$$\hat{\Sigma}_s(q^2) = \hat{\Sigma}_s^{(1)}(q^2) + \hat{\Sigma}_s^{(2)}(0), \quad s = h, H, hH, \tag{77}$$

where the momentum dependence is neglected only in the two-loop contribution.

Since the two-loop contribution has been calculated in the ϕ_1-ϕ_2-basis, a rotation into the h-H-basis, according to eq. (3), has to be performed:

$$\begin{aligned} \hat{\Sigma}_H^{(2)} &= \cos^2\alpha\, \hat{\Sigma}_{\phi_1}^{(2)} + \sin^2\alpha\, \hat{\Sigma}_{\phi_2}^{(2)} + 2\sin\alpha\, \cos\alpha\, \hat{\Sigma}_{\phi_1\phi_2}^{(2)} \\ \hat{\Sigma}_h^{(2)} &= \sin^2\alpha\, \hat{\Sigma}_{\phi_1}^{(2)} + \cos^2\alpha\, \hat{\Sigma}_{\phi_2}^{(2)} - 2\sin\alpha\, \cos\alpha\, \hat{\Sigma}_{\phi_1\phi_2}^{(2)} \\ \hat{\Sigma}_{hH}^{(2)} &= -\sin\alpha\, \cos\alpha\, \left(\hat{\Sigma}_{\phi_1}^{(2)} - \hat{\Sigma}_{\phi_2}^{(2)}\right) + (\cos^2\alpha\, - \sin^2\alpha\,)\hat{\Sigma}_{\phi_1\phi_2}^{(2)}. \end{aligned} \tag{78}$$

We have implemented two further corrections beyond $\mathcal{O}(\alpha\alpha_s)$ into the prediction for m_h, which are illustrated in Figs. 6, 7, 9 and 10. In order to take into account the leading electroweak two-loop contribution to the mass of the lightest Higgs boson, we have implemented the leading Yukawa correction of $\mathcal{O}(G_F^2 m_t^6)$, which gives a sizable contribution only for m_h. The formula is taken over from the result obtained by renormalization group methods. It only affects the renormalized ϕ_2 self-energy, which has to be inserted into eq. (78) and reads [10, 11]

$$\hat{\Sigma}_{\phi_2}^{(2)}(0) = -\frac{9}{16\pi^4}\frac{G_F^2 m_t^6}{\sin^2\beta}\left[\tilde{X}t + t^2\right] \tag{79}$$

$$\text{with} \qquad \tilde{X} = \left[\left(\frac{m^2_{\tilde{t}_2} - m^2_{\tilde{t}_1}}{4m_t^2}\sin^2 2\theta_{\tilde{t}}\right)^2 \left(2 - \frac{m^2_{\tilde{t}_2} + m^2_{\tilde{t}_1}}{m^2_{\tilde{t}_2} - m^2_{\tilde{t}_1}}\log\left(\frac{m^2_{\tilde{t}_2}}{m^2_{\tilde{t}_1}}\right)\right) + \frac{m^2_{\tilde{t}_2} - m^2_{\tilde{t}_1}}{2m_t^2}\sin^2 2\theta_{\tilde{t}}\log\left(\frac{m^2_{\tilde{t}_2}}{m^2_{\tilde{t}_1}}\right)\right], \tag{80}$$

$$t = \frac{1}{2}\log\left(\frac{m^2_{\tilde{t}_1} m^2_{\tilde{t}_2}}{m_t^4}\right). \tag{81}$$

The most recent calculation of the Yukawa corrections, containing also non-logarithmic contributions [14] may enhance m_h by up to one GeV. Since this calculation has not yet been confirmed by an independent calculation it is not taken into account in *FeynHiggs*.

The second step of refinement incorporated into *FeynHiggs* concerns leading QCD corrections beyond two-loop order. They are taken into account by using the $\overline{\rm MS}$ top mass

$$\overline{m}_t = \overline{m}_t(m_t) \approx \frac{m_t}{1 + \frac{4}{3\pi}\alpha_s(m_t)} \tag{82}$$

for the two-loop contributions of $\mathcal{O}(\alpha\alpha_s)$ and $\mathcal{O}(G_F^2 m_t^6)$ instead of the pole mass, $m_t = 175$ GeV. This three-loop effect gives rise to a shift up to 1.5 GeV in the prediction for m_h.

Neglecting the momentum dependence in the renormalized self-energies eq. (77), the Higgs boson masses m_h and m_H are obtained by diagonalizing the higher order corrected mass matrix with the mixing angle $\alpha_{\rm eff}$ (see also Sect. 5):

$$\alpha_{\rm eff} = \arctan\left[\frac{-(M_A^2 + M_Z^2)\sin\beta\,\cos\beta\, - \hat{\Sigma}_{\phi_1\phi_2}}{M_Z^2\cos^2\beta\, + M_A^2\sin^2\beta\, - \hat{\Sigma}_{\phi_1} - m_h^2}\right] , \quad -\frac{\pi}{2} < \alpha_{\rm eff} < \frac{\pi}{2} . \tag{83}$$

The complete one-loop calculation together with the leading two-loop corrections and the other corrections beyond $\mathcal{O}(\alpha\alpha_s)$ have been implemented into the `FORTRAN` code *FeynHiggs* [28]. This code can be linked to existing programs as a subroutine[2], thus providing an accurate calculation of m_h and m_H which can be used for further phenomenological analyses. *FeynHiggs* is available via its WWW page
`http://www.feynhiggs.de`.
See also the corresponding LC note Ref. [29].

4 Numerical results for m_h and m_H

4.1 Dependence of the results on the MSSM parameters

In this subsection we give a detailed discussion of the dependence of m_h on the parameters of the MSSM. For $\tan\beta$ we restrict ourselves to two typical values which are favored by SUSY-GUT scenarios [33]: $\tan\beta = 1.6$ for the $SU(5)$ scenario[3] and $\tan\beta = 40$ for the $SO(10)$ scenario. Other parameters are $M_Z = 91.187$ GeV, $M_W = 80.41$ GeV, $G_F = 1.16639\,10^{-5}$ GeV^{-2}, $\alpha_s(M_Z) = 0.118$, $m_t = 175$ GeV, and $m_b = 4.5$ GeV (if not indicated differently). The parameter $M(\equiv M_2)$ appearing in the plots is the $SU(2)$ gaugino mass parameter. The other gaugino mass parameter, M_1, is fixed via the GUT relation

$$M_1 = \frac{5}{3}\frac{s_W^2}{c_W^2} M . \tag{84}$$

[2]This has been carried out, for example, for the program HZHA [31, 32], into which *FeynHiggs* has been incorporated as a subroutine.

[3]The value $\tan\beta = 1.6$ is meanwhile ruled out by direct Higgs boson search (for $m_t = 175$ GeV and $M_{SUSY} \lesssim 1$ TeV) [34], but it still illustrates the general behavior of the Higgs boson sector for small $\tan\beta$, $\tan\beta \lesssim 5$.

The scalar top masses and the mixing angle are related to the parameters $M_{\tilde{t}_L}$, $M_{\tilde{t}_R}$ and X_t of the $\tilde{t}$ mass matrix, which reads

$$\mathcal{M}^2_{\tilde{t}} = \begin{pmatrix} M^2_{\tilde{t}_L} + m_t^2 + \cos 2\beta\,(\frac{1}{2} - \frac{2}{3}s^2_W)M^2_Z & m_t X_t \\ m_t X_t & M^2_{\tilde{t}_R} + m_t^2 + \frac{2}{3}\cos 2\beta\, s^2_W M^2_Z \end{pmatrix} , \tag{85}$$

with

$$X_t = A_t - \mu \cot\beta \ . \tag{86}$$

In the figures below we have chosen $m_{\tilde{q}} \equiv M_{\tilde{t}_L} = M_{\tilde{t}_R}$ (if not indicated differently).

Fig. 6 shows the result for m_h obtained from the diagrammatic calculation of the full one-loop and leading two-loop contributions. The two contributions beyond $\mathcal{O}(\alpha\alpha_s)$ discussed above are shown in separate curves. For comparison the pure one-loop result is also given. The results are plotted as a function of $X_t/m_{\tilde{q}}$, where $m_{\tilde{q}}$ is fixed to 500 GeV. The two-loop contributions give rise to a large reduction of the one-loop result of 10–20 GeV. The two corrections beyond $\mathcal{O}(\alpha\alpha_s)$ both increase m_h by up to 2 GeV. A minimum occurs around $X_t = 0$ GeV which we refer to as 'no mixing'. A maximum in the two-loop result for m_h is reached for about $X_t/m_{\tilde{q}} \approx \pm 2$ in the $\tan\beta = 1.6$ scenario as well as in the $\tan\beta = 40$ scenario. This case we refer to as 'maximal mixing'. The position of the maximum is shifted compared to its one-loop value of about $X_t/m_{\tilde{q}} \approx \pm 2.4$. The Yukawa correction and the insertion of the running top mass have only a negligible effect on the location of the maximum.

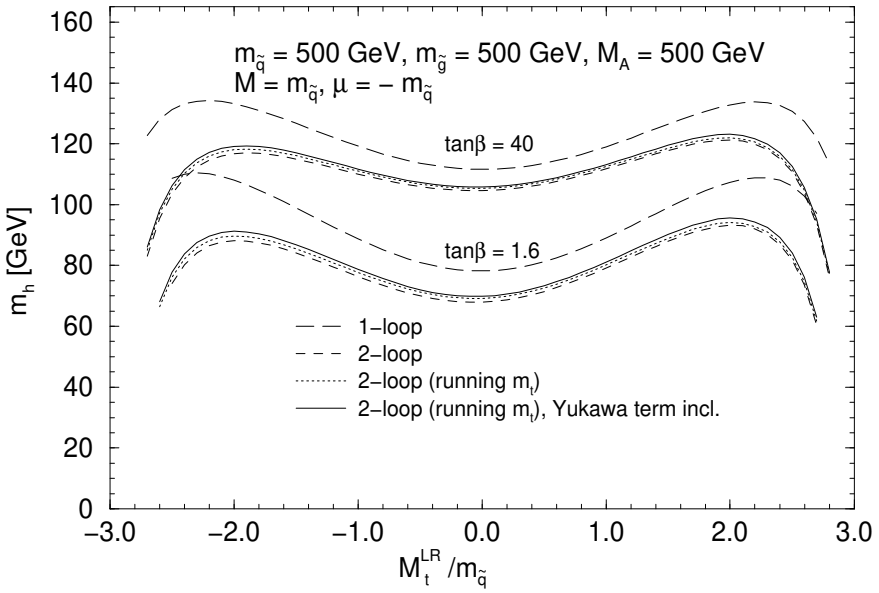

Figure 6: One- and two-loop results for m_h as a function of $X_t/m_{\tilde{q}}$ for two values of $\tan\beta$. The corrections beyond $\mathcal{O}(\alpha\alpha_s)$ discussed in the text are shown separately.

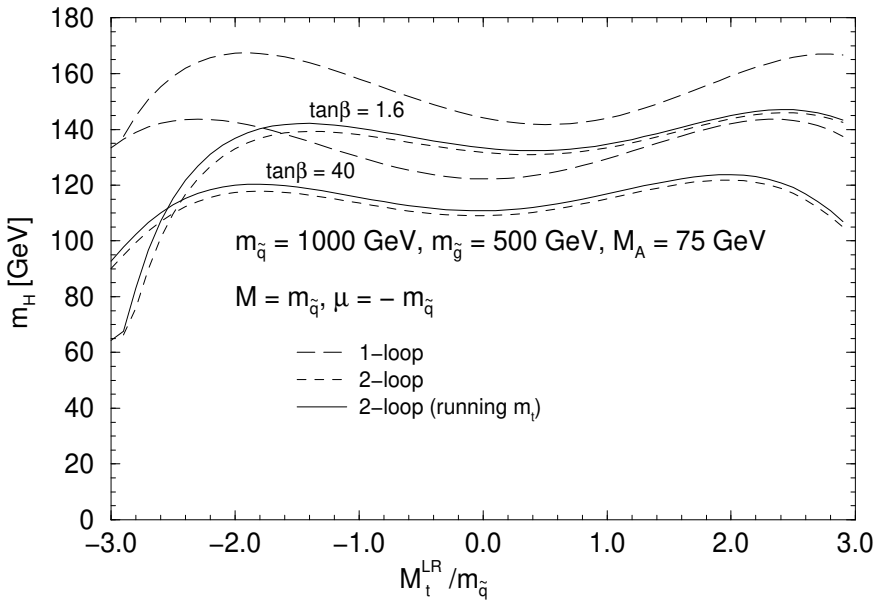

Figure 7: One- and two-loop results for m_H as a function of $X_t/m_{\tilde{q}}$ for two values of $\tan\beta$. The running top mass correction discussed in the text is shown separately.

Fig. 7 depicts the result for the heavy Higgs boson mass, m_H, obtained in the same way as m_h above. The only difference is that no Yukawa term has been included. In the plot we have chosen the small value $M_A = 75$ GeV, close to the lower experimental bound, since only for a light A boson the higher-order corrections give a sizable contribution (see also Fig. 8). Here the values for m_H obtained for small $\tan\beta$ are larger than for $\tan\beta = 40$. The values of $X_t/m_{\tilde{q}}$ for which m_H is maximal depend in this case on $\tan\beta$ and the sign of X_t.

Both Higgs boson masses are shown in Fig. 8 for low and high $\tan\beta$ and the no-mixing and the maximal-mixing case, where the latter case corresponds to the definition according to Fig. 6 for the light Higgs boson. For m_H sizable corrections at the one- and two-loop level are obtained only for $M_A \lesssim 200$ GeV for $\tan\beta = 1.6$ and for $M_A \lesssim 120$ GeV for $\tan\beta = 40$.

More relevant for todays' colliders is the mass of the lighter Higgs boson, m_h, on which we will focus in the following discussion. In Fig. 9 m_h is shown in the two scenarios with $\tan\beta = 1.6$ and $\tan\beta = 40$ as a function of $m_{\tilde{q}}$ for no mixing and maximal mixing and for $M_A = 200, 1000$ GeV. The tree-level, the one-loop and the two-loop results with the two corrections beyond $\mathcal{O}(\alpha\alpha_s)$ are shown (the values of $m_{\tilde{q}}$ are such that the corresponding $\tilde{t}$-masses lie within the experimentally allowed region). In all scenarios of Fig. 9 the two-loop corrections give rise to a large reduction of the one-loop value of m_h. The effect is generally larger in the low $\tan\beta$ scenario, and for maximal mixing and large M_A. The inclusion of the Yukawa correction and the running top mass leads to a slight shift in m_h towards higher

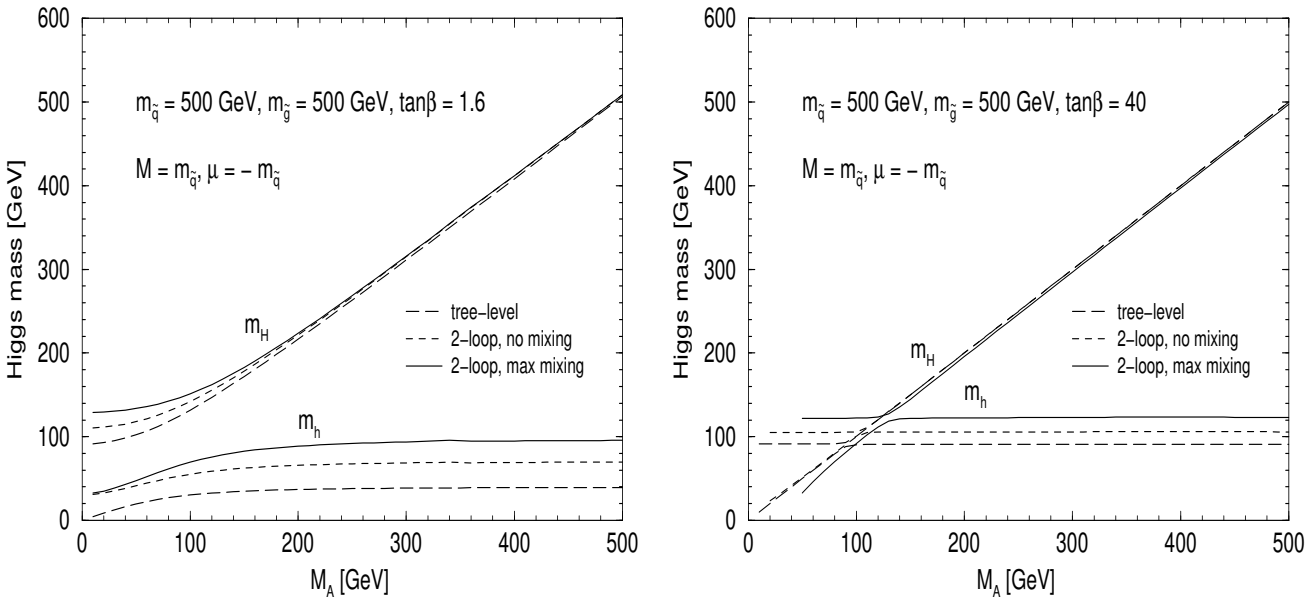

Figure 8: m_h and m_H are shown as a function of M_A for $\tan\beta = 1.6$ and $\tan\beta = 40$. The two-loop value for m_h contains both corrections beyond $\mathcal{O}(\alpha\alpha_s)$, whereas for m_H only the running top mass effect is included. The maximal-mixing scenario corresponds to the definition according to the discussion of Fig. 6.

values. This effect amounts up to 20% of the two-loop correction. In the low $\tan\beta$ scenario with $m_{\tilde{q}} = 1$ TeV, m_h reaches about 75 (81) GeV for $M_A = 200$ (1000) GeV in the no-mixing case, and 94 (101) GeV in the maximal-mixing case. For $\tan\beta = 40$ the respective values of m_h are 112 GeV in the no-mixing case, and 126 GeV in the maximal-mixing case for both values of M_A. The peaks in the plots for $M_A = 1$ TeV are due to the threshold $M_A = m_{\tilde{b}_1} + m_{\tilde{b}_2}$ in the one-loop contribution, originating from the sbottom-loop diagram in the A self-energy.

The dependence of m_h on M_A is depicted in Fig. 10 in the two scenarios with $\tan\beta = 1.6$ and $\tan\beta = 40$ for no mixing and maximal mixing for $m_{\tilde{q}} = 500, 1000$ GeV. In all scenarios of Fig. 10 the two-loop corrections give rise to a large reduction of the one-loop value of m_h. A saturation effect can be observed for $M_A \gtrsim 300$ (150) GeV in the $\tan\beta = 1.6$ (40) scenario. The peaks in the plots for $M_A = 350$ GeV are due to the threshold $M_A = 2\,m_t$ in the one-loop contribution, originating from the top-loop diagram in the A self-energy.

Allowing for a splitting between the parameters $M_{\tilde{t}_L}$, $M_{\tilde{t}_R}$ in the $\tilde{t}$ mass matrix yields maximal values of m_h which are approximately the same as for the case $m_{\tilde{q}} = M_{\tilde{t}_L} = M_{\tilde{t}_R}$, provided that one sets

$$m_{\tilde{q}}\Big|_{M_{\tilde{t}_L}=M_{\tilde{t}_R}} = \max\{M_{\tilde{t}_L}, M_{\tilde{t}_R}\}\Big|_{M_{\tilde{t}_L}\neq M_{\tilde{t}_R}} \quad , \tag{87}$$

see Fig. 11. However, the location of the maximal Higgs boson mass, depending on X_t, is

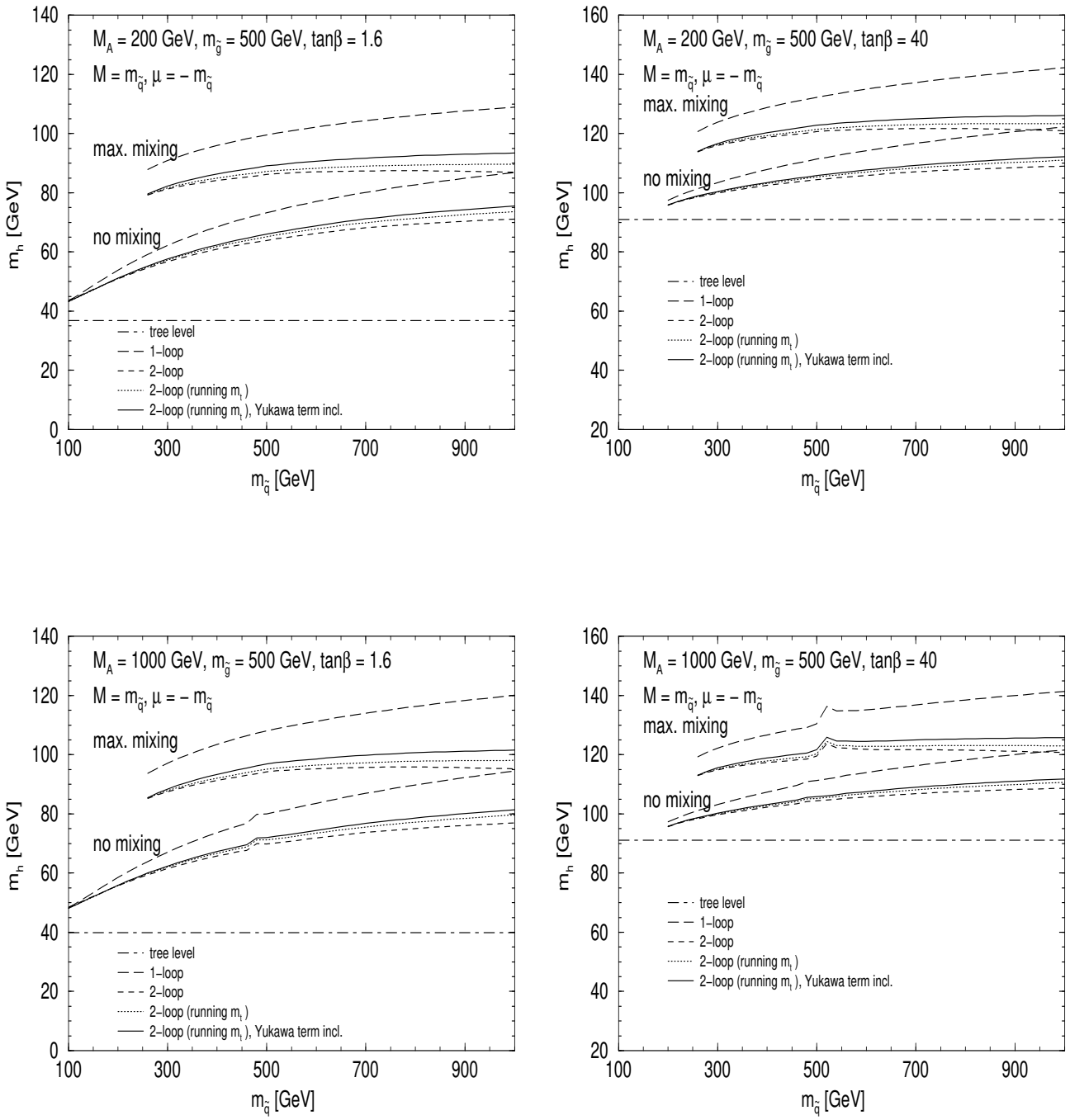

Figure 9: The mass of the lightest Higgs boson for $\tan\beta = 1.6$ and $\tan\beta = 40$. The tree-level, the one-loop and the two-loop results for m_h are shown as a function of $m_{\tilde{q}}$ for the no-mixing and the maximal-mixing case, and for $M_A = 200, 1000$ GeV.

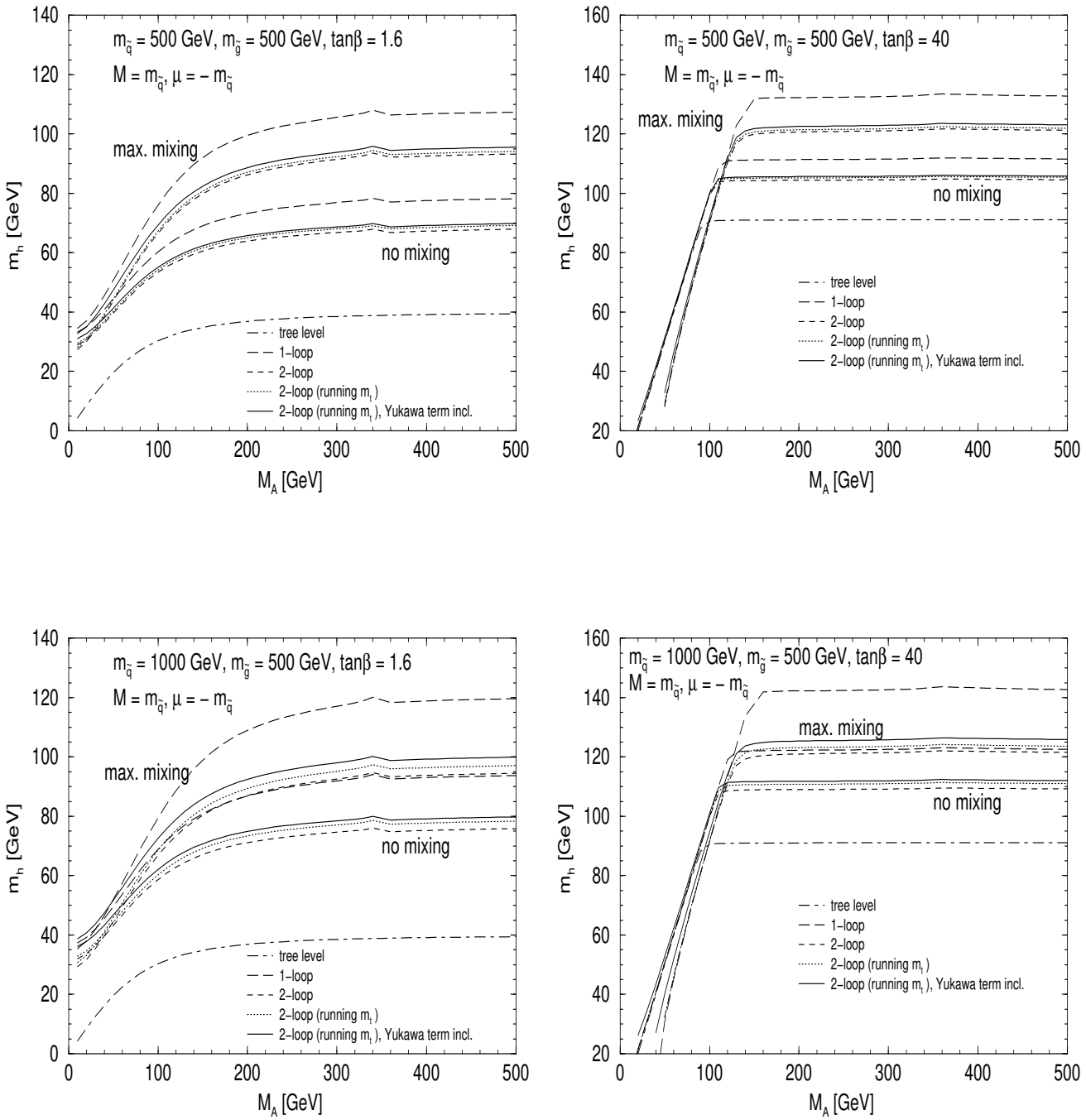

Figure 10: The mass of the lightest Higgs boson as a function of M_A for $\tan\beta = 1.6$ and $\tan\beta = 40$. The tree-level, the one-loop and the two-loop results for m_h are shown in the no-mixing and the maximal-mixing case, and for $m_{\tilde{q}} = 500, 1000$ GeV.

shifted towards smaller values, typically by about 40%. The numerical difference in m_h in the two splitting scenarios $M_{\tilde{t}_L}/M_{\tilde{t}_R} = 300/1000$ and $M_{\tilde{t}_L}/M_{\tilde{t}_R} = 1000/300$ is small. They differ by up to 2 GeV only in the large $\tan\beta$ scenario when $X_t > 1000$ GeV.

The variation of m_h with m_t is rather strong. The scenarios for no mixing and maximal mixing and for $\tan\beta = 1.6$ and $\tan\beta = 40$ are shown in Fig. 12, where m_t is varied around the central value of $m_t = 175$ GeV by ± 10 GeV. The variation of m_h is stronger for low $\tan\beta$ and larger $m_{\tilde{q}}$: in the low $\tan\beta$ scenario m_h varies by more than 10 GeV and about 20 GeV for no-mixing and maximal-mixing, respectively. In the $\tan\beta = 40$ scenario the respective values are less than 10 GeV and about 15 GeV.

Varying $\tan\beta$ around the value $\tan\beta = 1.6$ has a relatively large impact on m_h (higher values for m_h are obtained for larger $\tan\beta$), while the effect of varying $\tan\beta$ around $\tan\beta = 40$ is marginal. This is shown in Fig. 13 for $M_A = 200, 1000$ GeV, $m_{\tilde{q}} = 200, 1000$ GeV for the no-mixing and the maximal-mixing scenario. For $\tan\beta > 15$ the variation is less than 1 GeV[4].

In Fig. 14 m_h is shown as a function of M, the soft SUSY breaking parameter in the chargino and neutralino sector (see Sec. 84). In our calculation M enters only in the one-loop self-energies. The variation is less than 4 GeV for the whole M parameter space. For increasing M the result for m_h decreases in general.

The dependence of m_h on μ, the Higgs mixing parameter, is depicted in Fig. 15. The parameter μ enters via the non-diagonal Higgs-squark coupling at one- and two-loop order and via the chargino and neutralino sector in the one-loop self-energies. It should be noted that for the plots in Fig. 15 we have set $m_b = 0$, thus suppressing the contribution of the $b-\tilde{b}$-sector. The reason is that for large μ and for large $\tan\beta$ some Higgs-sbottom couplings can become rather large, which makes the perturbative calculation questionable in this case. The variation of m_h with μ in Fig. 15 is relatively weak, not exceeding 3 GeV. A maximum (for the choice $M = 400$ GeV) for m_h lies between $\mu = -200$ GeV and $\mu = -100$ GeV. For decreasing M the maximum is reached for slightly smaller values of μ, see also Sec. 4.2.

Finally we show the dependence on the gluino mass, $m_{\tilde{g}}$, which enters only at the two-loop level. Fig. 16 depicts m_h as a function of $m_{\tilde{g}}$ in the scenarios with $m_{\tilde{q}} = 500, 1000$ GeV for $\tan\beta = 1.6$ and $\tan\beta = 40$ in the no-mixing and the maximal-mixing case. Small variations below 1 GeV occur in the no-mixing scenario, while change in m_h up to 4 GeV arises in the maximal-mixing scenario. m_h reaches a maximum at about $m_{\tilde{g}} \approx 0.8\, m_{\tilde{q}}$. Since the parameter $m_{\tilde{g}}$ is absent in the RG approach, a variation of m_h with $m_{\tilde{g}}$ can directly be seen as a deviation of the diagrammatic result from the RG result, see Sec. 6.

As pointed out in Ref. [7,8] it is desirable to express the predictions for the observable m_h in terms of other physical observables. This provides the possibility to directly compare

[4] A non-negligible effect can arise for large $\tan\beta$ if μ is also large. This is briefly discussed below in the context of the μ-dependence of m_h.

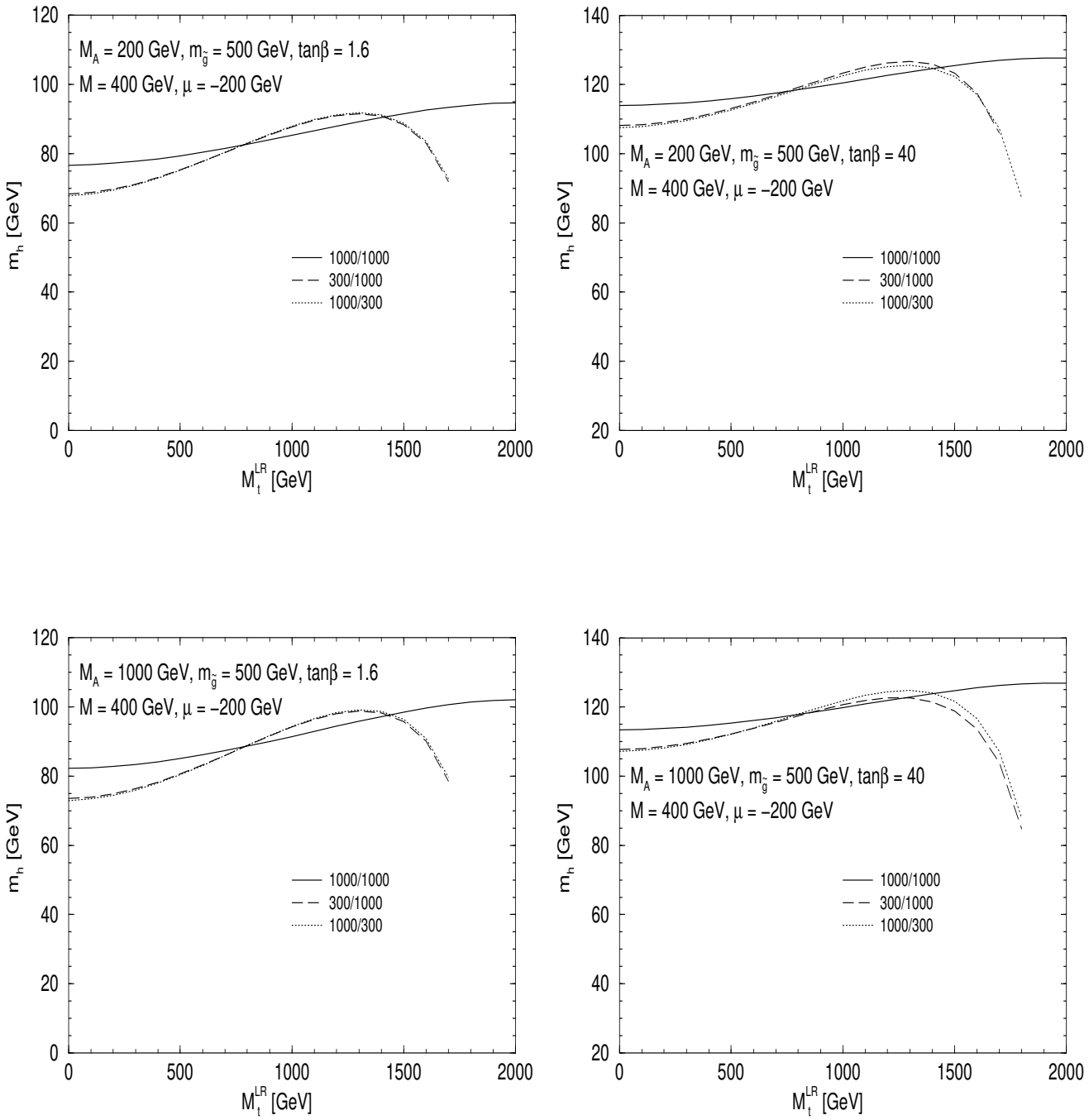

Figure 11: The mass of the lightest Higgs boson as a function of X_t for differently split values of the soft SUSY breaking terms. The curves in the plots correspond to the values $M_{\tilde{t}_L}/M_{\tilde{t}_R} = 1000/1000,\ 300/1000$ and $1000/300$.

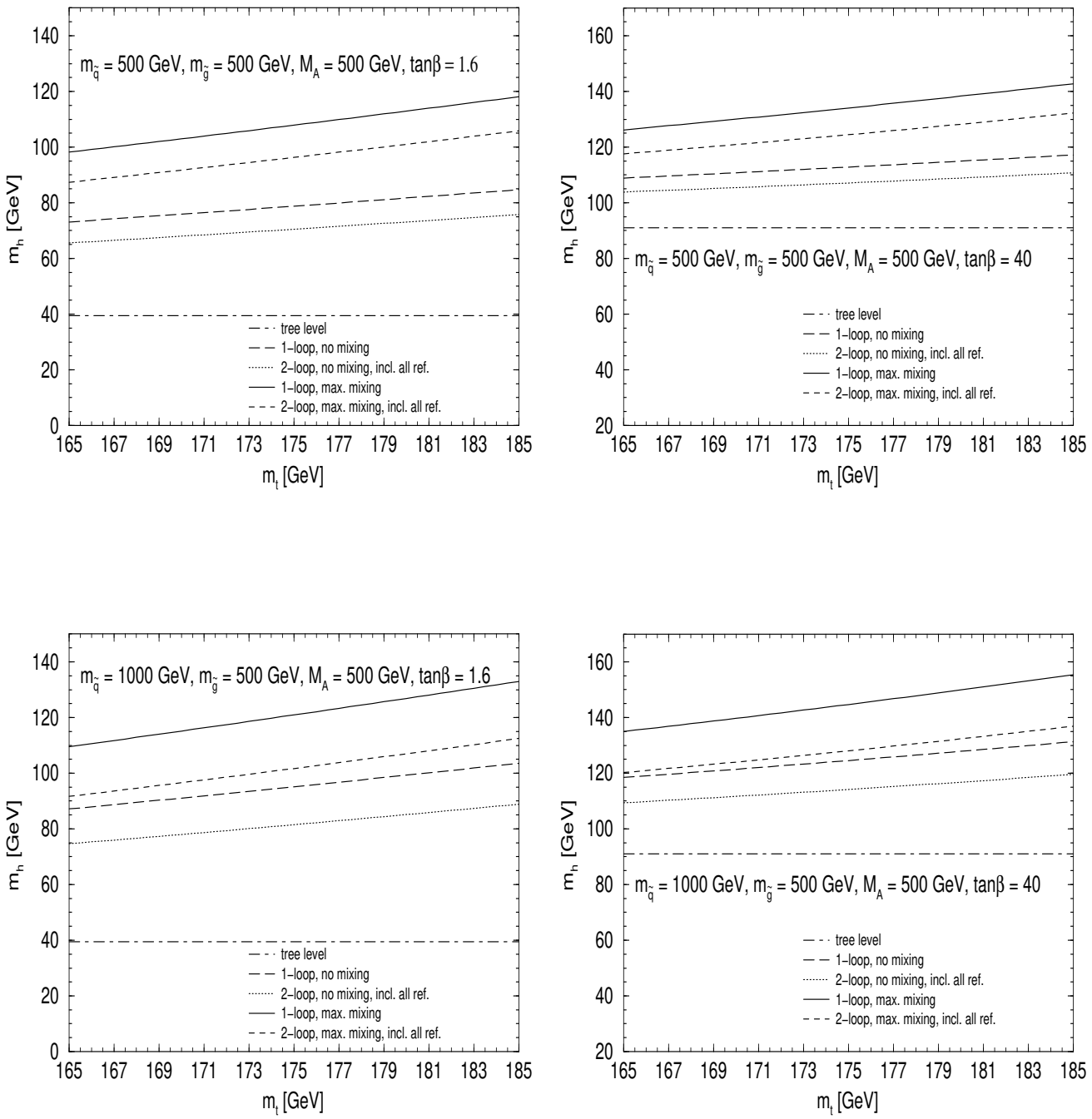

Figure 12: The mass of the lightest Higgs boson is shown as a function of m_t: the scenarios of no mixing and maximal mixing are depicted for low and high $\tan\beta$, and $\mu = -200$ GeV, $M = 400$ GeV.

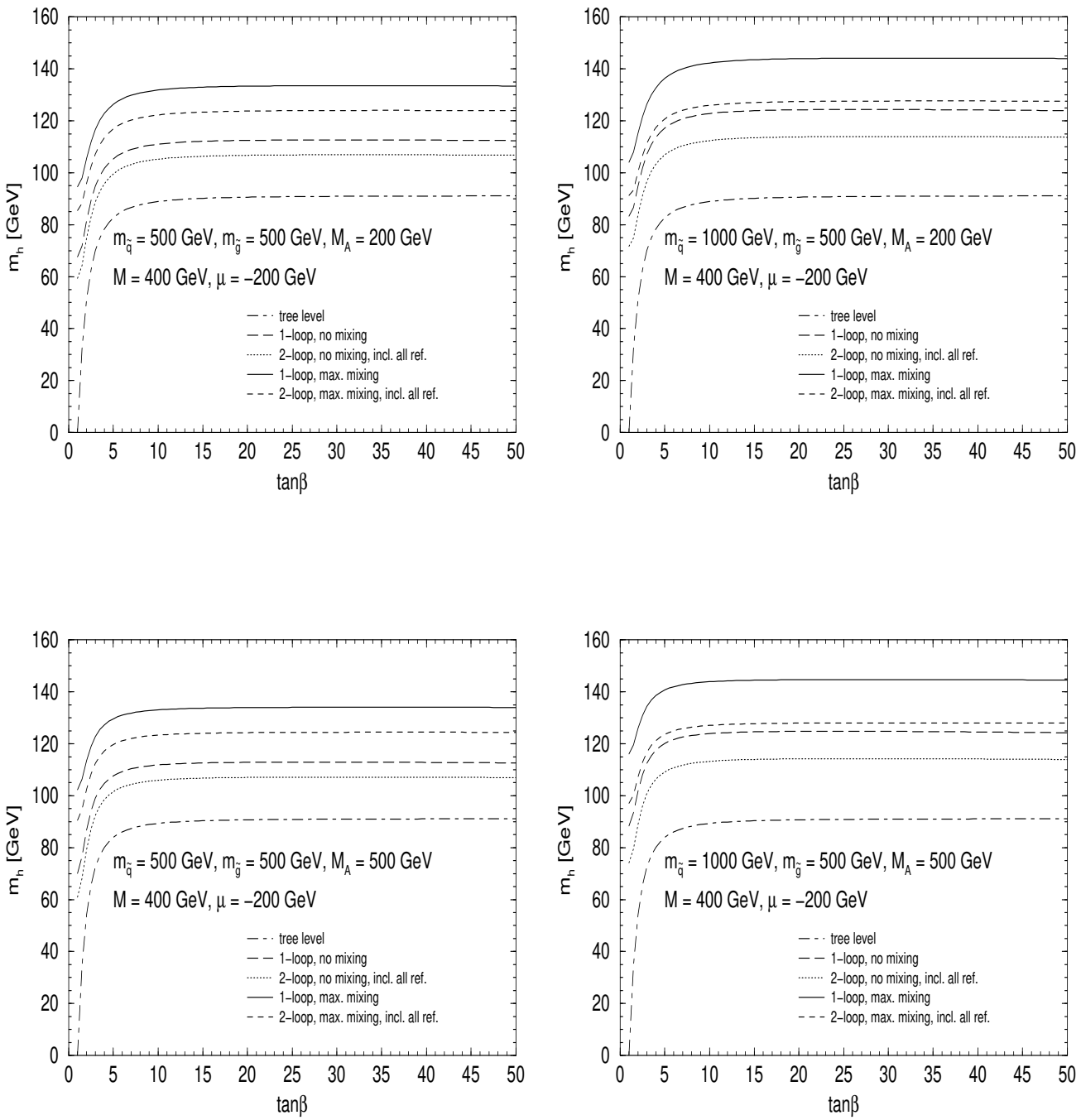

Figure 13: The mass of the lightest Higgs boson is shown as a function of $\tan\beta$. m_h is plotted for the scenarios with $M_A = 200, 500$ GeV and $m_{\tilde{q}} = 500, 1000$ GeV in the no-mixing and the maximal-mixing case.

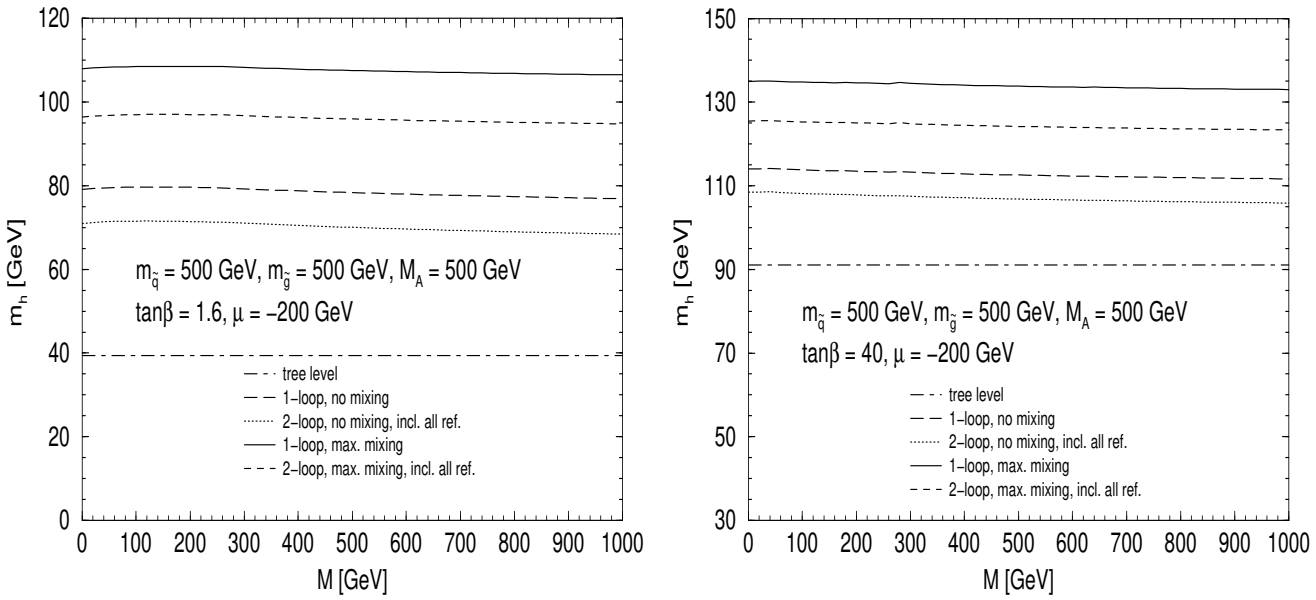

Figure 14: The mass of the lightest Higgs boson is shown as a function of M, the soft SUSY breaking parameter of the chargino and neutralino sector.

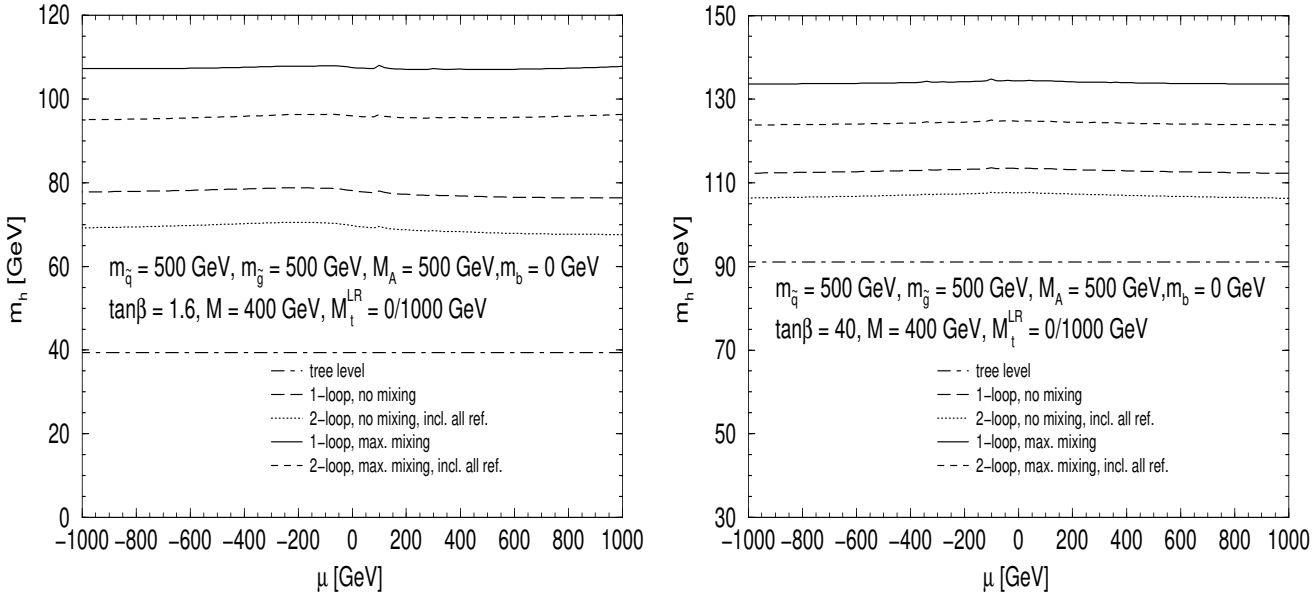

Figure 15: The mass of the lightest Higgs boson is shown as a function of μ, the Higgs mixing parameter. The mass of the bottom quark, m_b, is set to zero in order to avoid unnaturally large one-loop effects.

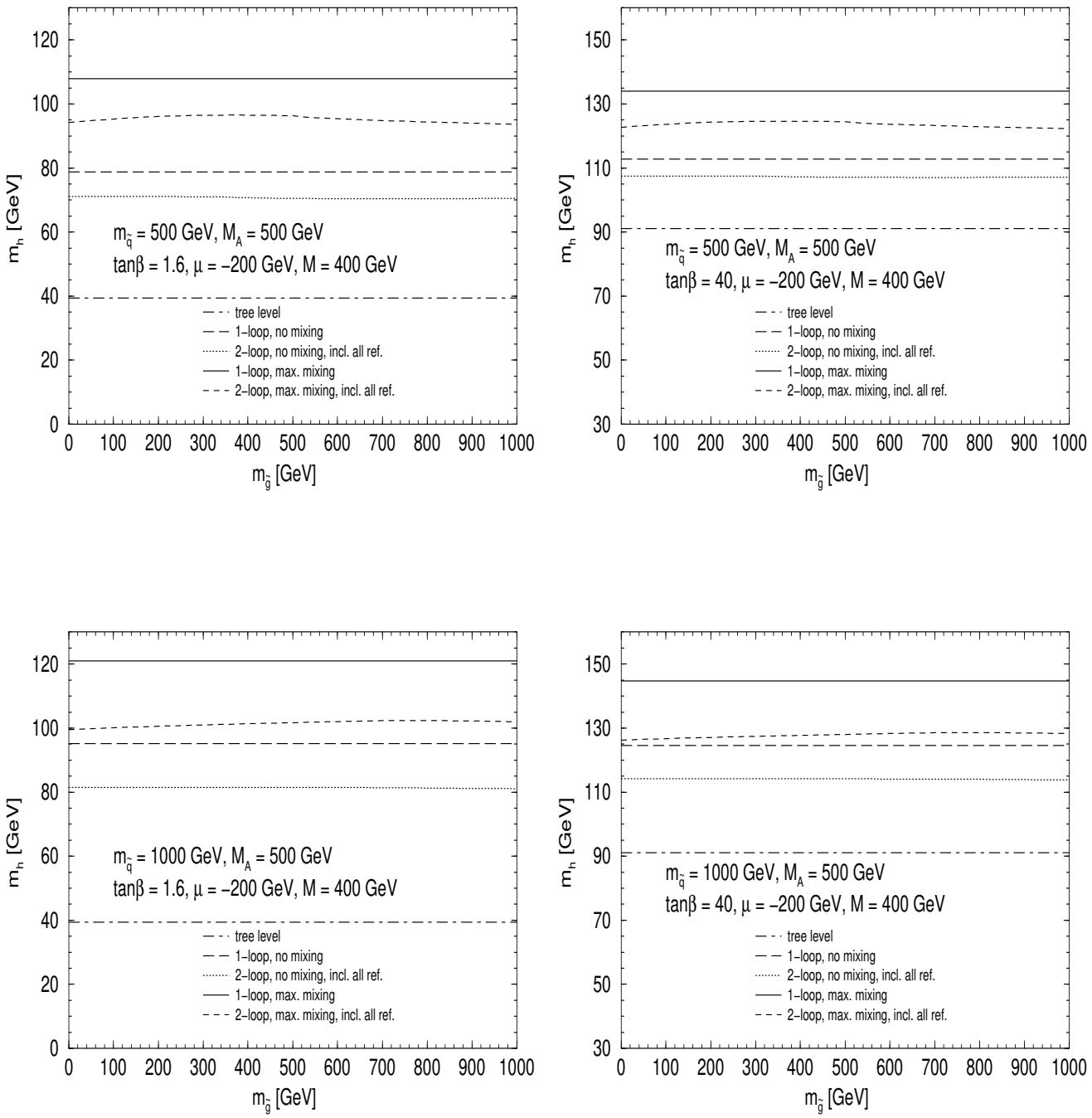

Figure 16: The mass of the lightest Higgs boson as a function of $m_{\tilde{g}}$ for a common value of $M_A = 500$ GeV, $m_{\tilde{q}} = 500, 1000$ GeV for the no-mixing and the maximal-mixing case and for low and high $\tan\beta$.

results obtained by different approaches making use of different renormalization schemes. Therefore we show in Fig. 17 the dependence of m_h on the parameters $m_{\tilde{t}_1}, m_{\tilde{t}_2}$ and $\theta_{\tilde{t}}$, which, since we are working in the on-shell scheme, directly correspond to the physical ones. We show m_h as a function of $m_{\tilde{t}_2}$ for $\Delta m_{\tilde{t}} = 0$ and $\theta_{\tilde{t}} = 0$ (no mixing) and for $\Delta m_{\tilde{t}} = 340$ GeV and $\theta_{\tilde{t}} = -\pi/4$ (maximal mixing), where $\Delta m_{\tilde{t}} \equiv m_{\tilde{t}_2} - m_{\tilde{t}_1}$. The choice of $\Delta m_{\tilde{t}} \approx 340$ GeV corresponds to $X_t/m_{\tilde{q}} \approx 2$ in terms of the soft SUSY breaking parameters. The two-loop results shown here contain also the corrections beyond $\mathcal{O}(\alpha\alpha_s)$. In these plots we have furthermore imposed the ρ-parameter constraint: We have required that the contribution of the third generation of scalar quarks to the ρ-parameter [22, 30] does not exceed the value of 2×10^{-3}, which corresponds approximately to the resolution of $\Delta\rho$ when it is determined from experimental data [35]. For $\tan\beta = 1.6$ m_h reaches about 76 (82) GeV for $M_A = 200$ (1000) GeV, $m_{\tilde{t}_2} = 1$ TeV and no mixing in the $\tilde{t}$-sector. In the maximal-mixing case the reached values of m_h are 94 (101) GeV. In the $\tan\beta = 40$ scenario, m_h reaches 114 (127) GeV in the no-mixing (maximal-mixing) case for both values of M_A. The peaks in the plots for $M_A = 1$ TeV and maximal mixing in the $\tilde{t}$-sector around $m_{\tilde{t}_2} = 660$ GeV are due to the threshold $M_A = m_{\tilde{t}_1} + m_{\tilde{t}_2}$ in the one-loop contribution, originating from the stop-loop diagram in the A self-energy.

4.2 Upper bound for m_h as a function of $\tan\beta$

Since, as shown in Fig. 13, smaller values for m_h are obtained for small $\tan\beta$, this part of the parameter space can to a large extend be covered at todays' colliders. The discovery limit for m_h at LEP2 is expected to be approximately 115 GeV [36]. In this context it is of special interest to know the maximally possible value for m_h as a function of $\tan\beta$ in the MSSM. To this end we have performed a parameter scan, varying $m_{\tilde{g}}, M, \mu, M_A$ and X_t for three values of m_t and fixed values of $m_{\tilde{q}}$ and $\tan\beta$. The maximal values for m_h, including also the Yukawa correction and the contribution from the running top mass, were reached (in the case $m_t = 175$ GeV) for[5]

$$\begin{aligned} m_{\tilde{g}} &\approx 0.8\, m_{\tilde{q}} \\ M &\approx 200 \text{ GeV} \\ \mu &\approx -200 \text{ GeV} \\ M_A &\approx 800 \text{ GeV} \\ X_t &\approx 2\, m_{\tilde{q}} \end{aligned} \tag{88}$$

in all scenarios. μ and M are chosen to avoid chargino masses already excluded by LEP2. Slightly higher m_h values could be obtained for smaller values of $|\mu|$ and M. The parameters in eq. (88) are usually called $m_h^{\max}$ scenario [37] and are used by the LEP collaborations to obtain conservative $\tan\beta$ bounds [34].

In Fig. 18 we show the maximal Higgs boson mass value, including also the corrections beyond $\mathcal{O}(\alpha\alpha_s)$, as a function of $\tan\beta$; the other parameters are chosen according to eqs. (88).

[5] Due to threshold effects very high values for m_h can occur. Since this is regarded as an accidental effect, these isolated points of parameter space are not considered here.

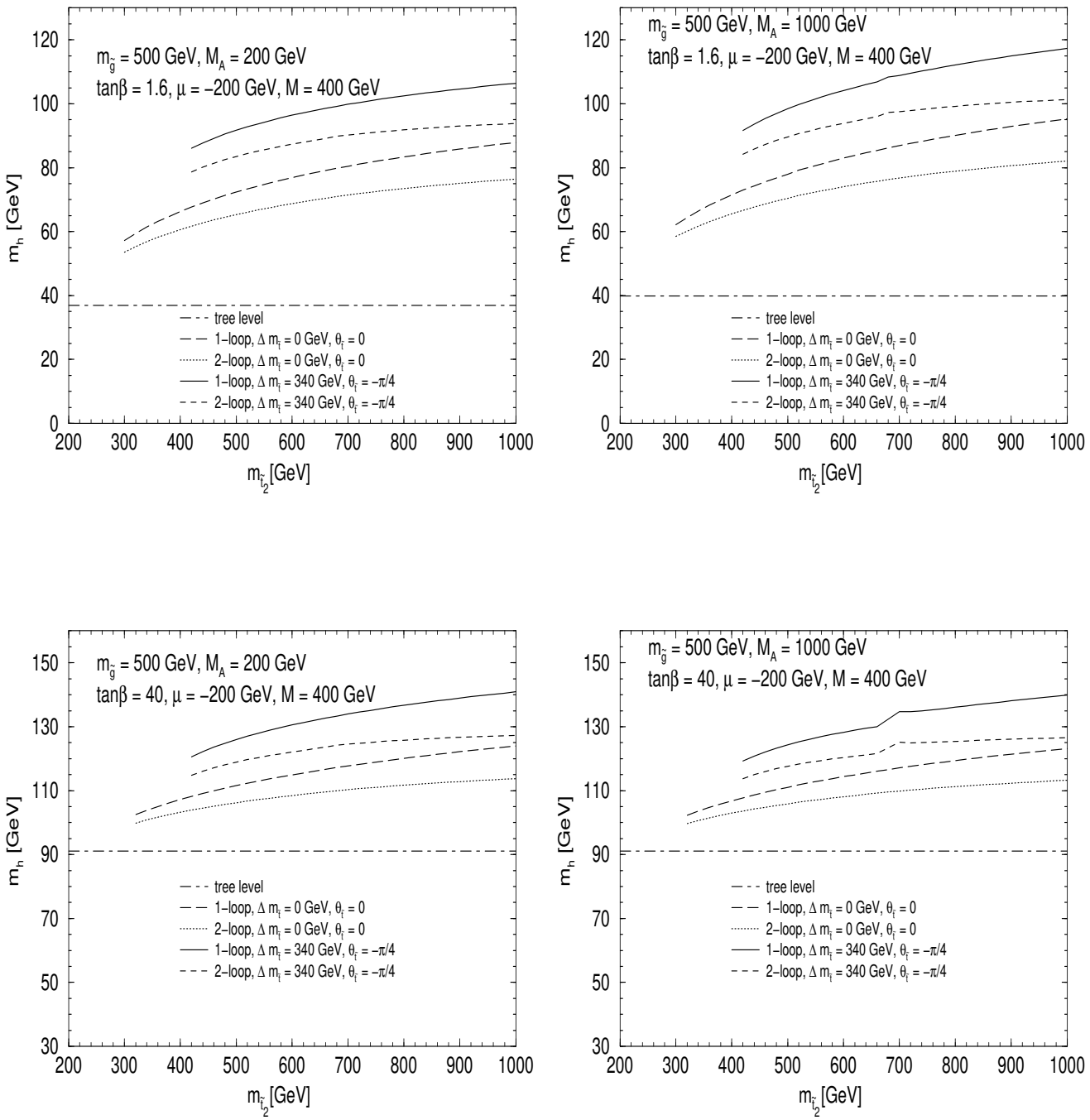

Figure 17: The mass of the lightest Higgs boson in terms of the physical parameters $m_{\tilde{t}_1}, m_{\tilde{t}_2}$ and $\theta_{\tilde{t}}$, where $\Delta m_{\tilde{t}} \equiv m_{\tilde{t}_2} - m_{\tilde{t}_1}$. The scenarios $\Delta m_{\tilde{t}} = 0, \theta_{\tilde{t}} = 0$ (no mixing) and $\Delta m_{\tilde{t}} = 340$ GeV$, \theta_{\tilde{t}} = -\pi/4$ (maximal mixing) are shown.

For the top-quark mass the most recent experimental value $m_t = 174.3$ GeV [38] is chosen.

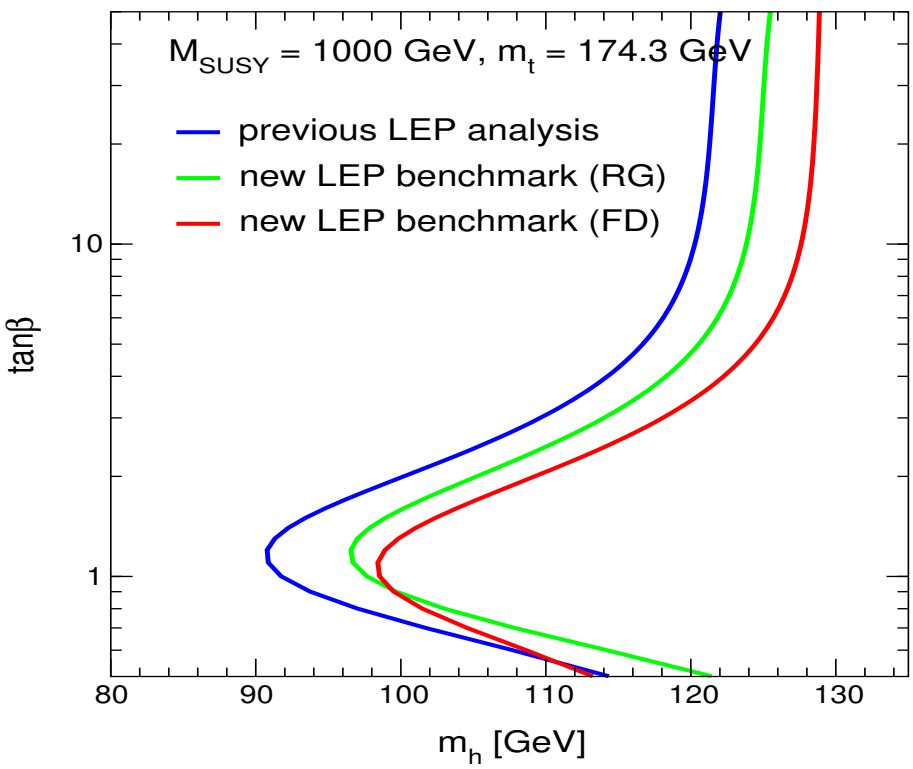

Figure 18: *m_h is shown as a function of* $\tan\beta$*. The blue curve displays the previous benchmark scenario. The green curve shows the $m_h^{\rm max}$-RG scenario (program* subhpole*), while the red curve represents the $m_h^{\rm max}$-FD scenario (program* FeynHiggs*).*

Since the dominant radiative corrections to the lightest Higgs-boson mass are proportional to m_t^4, the theoretical prediction for m_h depends sensitively on the precise value of the top-quark mass. The experimental uncertainty in the top-quark mass of currently $\Delta m_t = 5.1$ GeV [38] thus has a strong effect on the prediction for the upper bound on m_h, where larger values of m_t give rise to larger values of m_h. An increase in m_t by $\Delta m_t = 5.1$ GeV leads to an increase in m_h of up to 6 GeV, as shown in Fig. 19, where also the effect of increasing m_t by two standard deviations is displayed.

Besides the top-quark mass, the other main entry of the benchmark scenario is the choice $M_{SUSY} = 1$ TeV. Similarly to the case of m_t, allowing for higher values of M_{SUSY} leads to higher values of m_h. Since M_{SUSY} enters only logarithmically in the prediction for m_h, the dependence on it is more moderate. An increase of M_{SUSY} from 1 TeV to 2 TeV enhances m_h by up to 3 GeV (depending on $\tan\beta$).

Allowing values of m_t one or even two standard deviations above the current experimental central value and increasing also the input value of M_{SUSY} clearly has a large effect on possible $\tan\beta$ constraints. In Fig. 20 we show an "increased m_h" scenario, where $m_t =$

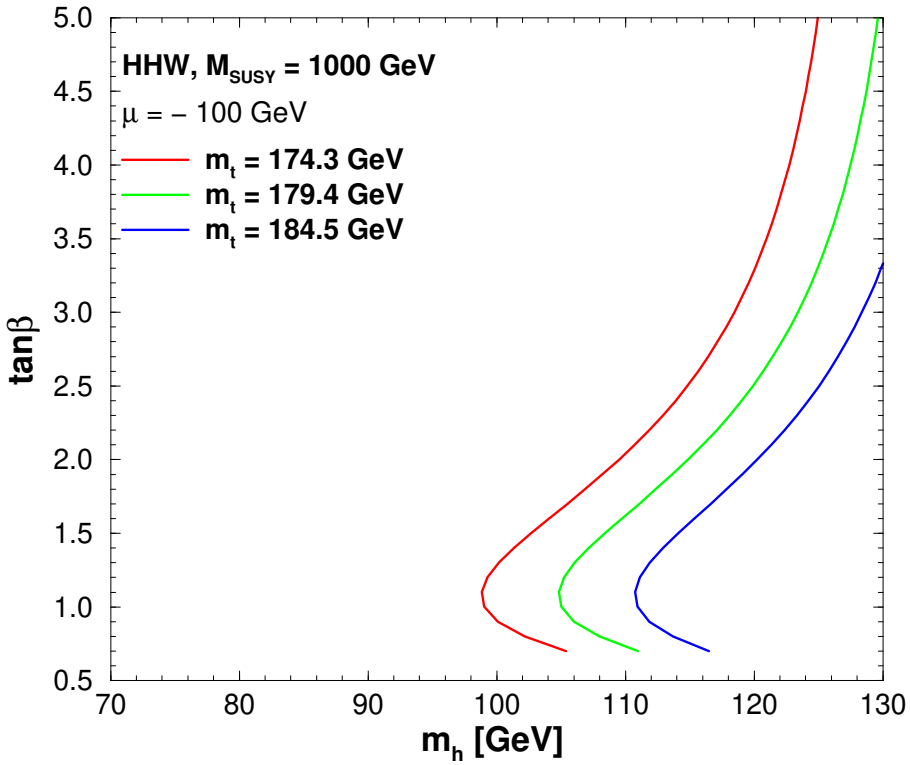

Figure 19: *m_h is shown as a function of* $\tan\beta$*, evaluated in the FD approach (HHW, program* FeynHiggs*). We give the results for three different values of the top-quark mass,* $m_t = 174.3, 179.4, 184.5$ GeV.

179.4 GeV has been chosen, i.e. one standard deviation above the current experimental value, and $M_{SUSY} = 2000$ GeV is taken. It is compared with the benchmark scenario in the RG calculation and with the $m_h^{\max}$-FD scenario. In the "increased m_h" scenario exclusion of a $\tan\beta$ range has only become possible, after the LEP exclusion limits have reached a region for m_h of more than about 110 GeV [34].

In this context one should keep in mind that the benchmark scenario contains not only an assumption about the SUSY parameters but also about the actual model which is tested, namely a SUSY model with a minimal Higgs sector that does not contain $\mathcal{CP}$-violating phases. The upper bound on m_h, however, stays the same also with complex parameters [39]. Extensions of the Higgs sector by additional particle representations can shift the upper bound on the mass of the lightest Higgs boson up to values of about 200 GeV [2].

The $m_h^{\max}$ scenario has been used to exclude $\tan\beta$ up to $\tan\beta \lesssim 2.3$ [34]. Concerning the large $\tan\beta$ region, the upgraded Tevatron, the LHC a future linear e^+e^--collider are needed in order to test the MSSM parameter space.

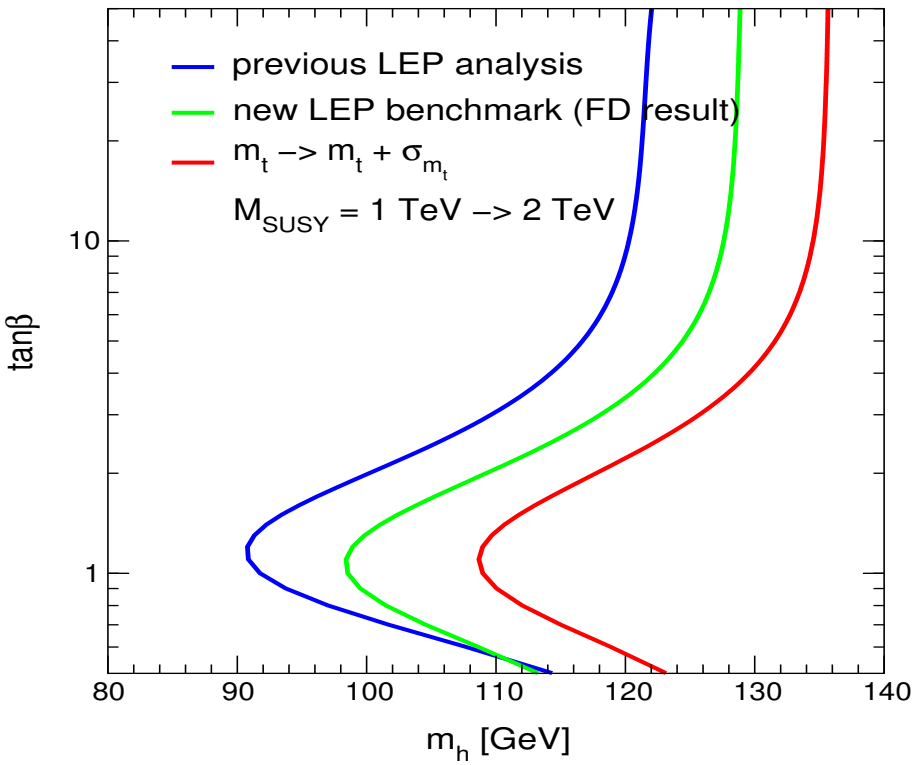

Figure 20: *m_h is shown as a function of* $\tan\beta$*. The blue curve displays the previous benchmark scenario in the RG approach, which has been used for phenomenological analyses until 1999. The green curve displays the $m_h^{\rm max}$-FD scenario, while the red curve corresponds to the "increased m_h" scenario with $m_t = 179.4$ GeV and $M_{SUSY} = 2000$ GeV.*

5 The compact analytical formula

5.1 Approximations in the scalar top sector

The mass matrix in the basis of the current eigenstates $\tilde{t}_L$ and $\tilde{t}_R$ as given in Sect. 4.1 is given by

$$\mathcal{M}^2_{\tilde{t}} = \begin{pmatrix} M^2_{\tilde{t}_L} + m_t^2 + \cos 2\beta\,(\frac{1}{2} - \frac{2}{3}s_W^2)M_Z^2 & m_t X_t \\ m_t X_t & M^2_{\tilde{t}_R} + m_t^2 + \frac{2}{3}\cos 2\beta\, s_W^2 M_Z^2 \end{pmatrix}, \tag{89}$$

where

$$m_t X_t = m_t(A_t - \mu \cot\beta\,) \ . \tag{90}$$

Neglecting the numerically small contributions proportional to M_Z^2 and setting[6]

$$M_{\tilde{t}_L} = M_{\tilde{t}_R} := m_{\tilde{q}}, \quad M_S^2 := m_{\tilde{q}}^2 + m_t^2 \tag{91}$$

[6]Later we will also discuss the case $M_{\tilde{t}_L} \neq M_{\tilde{t}_R}$, for which the same formalism applies, but with a different definition for M_S, see eq. (105).

one arrives at

$$\mathcal{M}^2_{\tilde{t}} = \begin{pmatrix} M_S^2 & m_t X_t \\ m_t X_t & M_S^2 \end{pmatrix} . \tag{92}$$

Diagonalizing the $\tilde{t}$ mass matrix (92) yields the mass eigenvalues $m_{\tilde{t}_1}, m_{\tilde{t}_2}$ and the $\tilde{t}$ mixing angle $\theta_{\tilde{t}}$, which relates the current eigenstates to the mass eigenstates:

$$\begin{pmatrix} \tilde{t}_1 \\ \tilde{t}_2 \end{pmatrix} = \begin{pmatrix} \cos\theta_{\tilde{t}} & \sin\theta_{\tilde{t}} \\ -\sin\theta_{\tilde{t}} & \cos\theta_{\tilde{t}} \end{pmatrix} \begin{pmatrix} \tilde{t}_L \\ \tilde{t}_R \end{pmatrix} . \tag{93}$$

In the above approximation, which we will use throughout the rest of this section, the $\tilde{t}$ masses and the mixing angle are given by

$$\begin{aligned} m^2_{\tilde{t}_1} &= M_S^2 - |m_t X_t| = M_S^2 \,(1 - \Delta_{\tilde{t}}) \,, \\ m^2_{\tilde{t}_2} &= M_S^2 + |m_t X_t| = M_S^2 \,(1 + \Delta_{\tilde{t}}) \,, \end{aligned} \tag{94}$$

$$\theta_{\tilde{t}} = \begin{cases} \frac{\pi}{4} & \text{for } X_t < 0 \\ 0 & \text{for } X_t = 0 \\ -\frac{\pi}{4} & \text{for } X_t > 0 \end{cases} , \tag{95}$$

with

$$\Delta_{\tilde{t}} = \frac{|m_t X_t|}{M_S^2} = \frac{m^2_{\tilde{t}_2} - m^2_{\tilde{t}_1}}{m^2_{\tilde{t}_2} + m^2_{\tilde{t}_1}} . \tag{96}$$

From the above definition it follows that $0 \leq \Delta_{\tilde{t}} \leq 1$, otherwise the $\tilde{t}$ mass matrix eq. (92) would have a negative eigenvalue.

5.2 Calculation of the mass of the lightest Higgs boson

The higher order corrected Higgs boson mass matrix in the ϕ_1-ϕ_2 basis reads:

$$M^2_{\rm Higgs} = \begin{pmatrix} m^2_{\phi_1} - \hat{\Sigma}_{\phi_1}(0) & m^2_{\phi_1\phi_2} - \hat{\Sigma}_{\phi_1\phi_2}(0) \\ m^2_{\phi_1\phi_2} - \hat{\Sigma}_{\phi_1\phi_2}(0) & m^2_{\phi_2} - \hat{\Sigma}_{\phi_2}(0) \end{pmatrix} , \tag{97}$$

where the $\hat{\Sigma}_s(0)$ ($s = \phi_1, \phi_1\phi_2, \phi_2$) denote the renormalized Higgs-boson self-energies (in the ϕ_1, ϕ_2 basis) as defined in Sect. 2.1. As a first step of approximation, the momentum dependence, which is numerically rather small, has been neglected in the $\hat{\Sigma}_s(p^2)$.

The mass of the lightest Higgs boson receives contributions from all sectors of the MSSM, but not all are numerically of equal relevance as has been shown in Sect. 4. In order to derive a compact analytical expression, we make the following further approximations:

The contributions from the $t, \tilde{t}$-sector up to the two-loop level: The contributions arising from the $t, \tilde{t}$-sector can be written as

$$\hat{\Sigma}_s(0) = \hat{\Sigma}^{(1)}_s(0) + \hat{\Sigma}^{(2)}_s(0), \;\; s = \phi_1, \phi_1\phi_2, \phi_2. \tag{98}$$

Here the $\hat{\Sigma}_s^{(1)}(0)$ denote the one-loop contributions of the $t, \tilde{t}$-sector to the renormalized Higgs-boson self-energies. Their explicit form (including also the momentum dependence) can be found e.g. in Ref. [5]. The $\hat{\Sigma}_s^{(2)}(0)$ denote the two-loop contributions from the $t, \tilde{t}$-sector at zero external momentum from the Yukawa part of the theory (neglecting the gauge couplings) [7]. We first consider the dependence of the mass shift Δm_h^2 ($m_h^2 = m_h^{2,\rm tree} + \Delta m_h^2$) on $\tan\beta$ and μ. For the leading contributions to Δm_h^2 from the Yukawa part of the theory the dependence on $\tan\beta$ and μ drops out in the limit $M_A \gg M_Z$.[7] This holds both for the contributions in $\mathcal{O}(\alpha)$ and $\mathcal{O}(\alpha\alpha_s)$. Since $\tan\beta$ and μ enter only via non-leading corrections in Δm_h^2, the dependence on them is relatively mild. We therefore use the approximation $\mu = 0$ in the $\hat{\Sigma}_s(0)$. We furthermore extract a common prefactor $(1/\sin^2\beta)$ and set otherwise $\sin\beta = 1$ in the non-logarithmic one-loop contributions, while the full dependence on $\sin\beta$ is kept in the logarithmic one-loop and the two-loop contributions. Since the variation of m_h with $m_{\tilde{g}}$ is ± 2 GeV at most, see Ref. [8], we have eliminated the dependence of the $\hat{\Sigma}_s^{(2)}(0)$ on the gluino mass by setting

$$m_{\tilde{g}} = M_{SUSY} \equiv \sqrt{M_S^2 - m_t^2}, \tag{99}$$

where in the case $M_{\tilde{t}_L} = M_{\tilde{t}_R} = m_{\tilde{q}}$ the SUSY scale is given by $M_{SUSY} = m_{\tilde{q}}$.

As the main step of our approximations, we have performed a Taylor expansion in $\Delta_{\tilde{t}}$ of the $\hat{\Sigma}_s(0)$ by inserting eq. (94) for the $\tilde{t}$ masses and eq. (95) for the $\tilde{t}$ mixing angle. For the one-loop correction we have expanded up to $\mathcal{O}(\Delta_{\tilde{t}}^8)$; all three renormalized one-loop Higgs-boson self-energies give a contribution. In the one-loop self-energies we have kept terms up to $\mathcal{O}(M_Z^4/m_t^4)$ while terms of $\mathcal{O}(M_Z^2/M_S^2)$ have been neglected. We have checked that the numerical effect of the latter terms is insignificant. Concerning the two-loop self-energies, the expansion has been carried out up to $\mathcal{O}(\Delta_{\tilde{t}}^4)$. With the above described approximations only $\hat{\Sigma}_{\phi_2}^{(2)}$ gives a non-zero contribution. The Taylor expanded self-energies have then been inserted into the Higgs-boson mass matrix eq. (97).

The one-loop contributions from the other sectors: For the one-loop corrections from the other sectors of the MSSM we use the logarithmic approximation given in Ref. [3]. In this approximation the scale of the soft SUSY-breaking parameter in the gaugino sector, M, is chosen as $M = M_{SUSY}$, where M_{SUSY} is defined as in eq. (99). Besides M_{SUSY}, this contribution is parameterized in terms of M_A, the mixing angle β, and the SM parameters, see eq. (111). A higher accuracy of the non-leading one-loop contributions in the approximation formula can be achieved by including further terms of the one-loop logarithmic approximation given in Ref. [11].

Corrections beyond $\mathcal{O}(\alpha\alpha_s)$: Leading contributions beyond $\mathcal{O}(\alpha\alpha_s)$ have been taken into account by as for the full calculation, see Sect. 3.3. The $\mathcal{O}(G_F^2 m_t^6)$ Yukawa term (79) is added to the ϕ_2 self-energy. Higher order QCD corrections are taken into account by means of the running top quark mass (82).

[7] Note that X_t is treated as a free parameter in eq. (90) and therefore does not depend on μ.

5.3 The analytical approximation formula for m_h

5.3.1 The case for general M_A

With the approximations described above we obtain the following contributions to the renormalized Higgs-boson self-energies from the $t, \tilde{t}$-sector (expressed in terms of the top-quark pole mass) at one-loop order:

$$\hat{\Sigma}^{(1)}_{\phi_1}(0) = \frac{G_F\sqrt{2}}{\pi^2} M_Z^4 \Lambda \cos^2\beta \, \log\left(\frac{m_t^2}{M_S^2}\right) \,, \tag{100}$$

$$\hat{\Sigma}^{(1)}_{\phi_1\phi_2}(0) = -\frac{G_F\sqrt{2}}{\pi^2} M_Z^2 \cot\beta \, \left[-\frac{3}{8} m_t^2 + M_Z^2 \Lambda \sin^2\beta\right] \log\left(\frac{m_t^2}{M_S^2}\right) \,, \tag{101}$$

$$\begin{aligned}
\hat{\Sigma}^{(1)}_{\phi_2}(0) = {} & \frac{G_F\sqrt{2}}{\pi^2} \frac{m_t^4}{8\sin^2\beta} \Bigg\{ -2\frac{M_Z^2}{m_t^2} + \frac{11}{10}\frac{M_Z^4}{m_t^4} \\
& + \left[12 - 6\frac{M_Z^2}{m_t^2}\sin^2\beta \; + 8\frac{M_Z^4}{m_t^4}\Lambda\sin^4\beta\right] \log\left(\frac{m_t^2}{M_S^2}\right) \\
& + \frac{X_t^2}{M_S^2}\left[-12 + 4\frac{M_Z^2}{m_t^2} + 6\frac{m_t^2}{M_S^2}\right] + \frac{X_t^4}{M_S^4}\left[1 - 4\,\frac{m_t^2}{M_S^2} + 3\frac{m_t^4}{M_S^4}\right] \\
& + \frac{X_t^6}{M_S^6}\left[\frac{3}{5}\frac{m_t^2}{M_S^2} - \frac{12}{5}\frac{m_t^4}{M_S^4} + 2\frac{m_t^6}{M_S^6}\right] \\
& + \frac{X_t^8}{M_S^8}\left[\frac{3}{7}\frac{m_t^4}{M_S^4} - \frac{12}{7}\frac{m_t^6}{M_S^6} + \frac{3}{2}\frac{m_t^8}{M_S^8}\right]\Bigg\} \,,
\end{aligned} \tag{102}$$

with

$$\Lambda = \left(\frac{1}{8} - \frac{1}{3}s_W^2 + \frac{4}{9}s_W^4\right), \qquad s_W^2 = 1 - \frac{M_W^2}{M_Z^2}. \tag{103}$$

The two-loop contributions read [17]:

$$\begin{aligned}
\hat{\Sigma}^{(2)}_{\phi_1}(0) &= 0 \,, \\
\hat{\Sigma}^{(2)}_{\phi_1\phi_2}(0) &= 0 \,, \\
\hat{\Sigma}^{(2)}_{\phi_2}(0) &= \frac{G_F\sqrt{2}}{\pi^2}\frac{\alpha_s}{\pi}\frac{m_t^4}{\sin^2\beta}\Bigg[3\log^2\left(\frac{m_t^2}{M_S^2}\right) - 6\log\left(\frac{m_t^2}{M_S^2}\right) - 6\frac{X_t}{M_S} \\
&\qquad - 3\frac{X_t^2}{M_S^2}\log\left(\frac{m_t^2}{M_S^2}\right) + \frac{3}{4}\frac{X_t^4}{M_S^4}\Bigg] \,.
\end{aligned} \tag{104}$$

M_S has to be chosen according to

$$M_S = \begin{cases} \sqrt{m_{\tilde{q}}^2 + m_t^2} & : \quad M_{\tilde{t}_L} = M_{\tilde{t}_R} = m_{\tilde{q}} \\ \left[M_{\tilde{t}_L}^2 M_{\tilde{t}_R}^2 + m_t^2(M_{\tilde{t}_L}^2 + M_{\tilde{t}_R}^2) + m_t^4\right]^{\frac{1}{4}} & : \quad M_{\tilde{t}_L} \neq M_{\tilde{t}_R} \end{cases} \tag{105}$$

The last formula requires some explanation: when performing the expansion in $\Delta_{\tilde{t}}$, it was assumed that $M_{\tilde{t}_L} = M_{\tilde{t}_R}$. Thus our result contains only one soft SUSY-breaking scale M_S.

For the case $M_{\tilde{t}_L} \neq M_{\tilde{t}_R}$, M_S is chosen to reproduce the argument of the leading log correctly. According to eq. (105) the log yields in both cases

$$\log\left(\frac{m_t^2}{M_S^2}\right) = \log\left(\frac{m_t^2}{m_{\tilde{t}_1}\, m_{\tilde{t}_2}}\right) + \mathcal{O}\left(\Delta_{\tilde{t}}\right) \tag{106}$$

in agreement with eq. (94).

The one-loop contributions from the other sectors of the MSSM are not listed here but can be found in Refs. [3, 11]. The combined self-energies have to be inserted into eq. (97). In order to incorporate the leading QCD corrections beyond $\mathcal{O}(\alpha\alpha_s)$, the top-quark pole mass should be replaced by the $\overline{\rm MS}$ top-quark mass eq. (82) in the two-loop contribution, as described above. Diagonalization of eq. (97) yields the square of the masses of the neutral $\mathcal{CP}$-even Higgs bosons. In order to incorporate leading contributions in $\mathcal{O}(G_F^2 m_t^6)$, the leading Yukawa correction, see eq. (79), can be added.

5.3.2 The case $M_A \gg M_Z$

The diagonalization of the mass matrix eq. (97) in the evaluation of m_h^2 incorporates contributions that are formally of higher order but are non-negligible in general. For large M_A these higher-order contributions are suppressed by inverse powers of M_A. Therefore it is possible in this case to perform an expansion in the loop order, leading to a very compact formula for m_h^2 of the form

$$m_h^2 = m_h^{2,\rm tree} + \Delta m_h^{2,\alpha,t/\tilde{t}} + \Delta m_h^{2,\alpha,\rm rest} + \Delta m_h^{2,\alpha\alpha_s} + \Delta m_h^{2,\alpha^2}. \tag{107}$$

At the two-loop level, only the ϕ_2 self-energy contributes in our approximation, yielding the term

$$\Delta m_h^{2,\alpha\alpha_s} = -\sin^2\beta\ \hat{\Sigma}^{(2)}_{\phi_2}(0) \tag{108}$$

with $\hat{\Sigma}^{(2)}_{\phi_2}(0)$ from eq. (104). In contrast to eqs. (100)–(104) we give here an expression for m_h in which the $\overline{\rm MS}$ top-quark mass is used everywhere. Inserting eq. (82) into $\hat{\Sigma}^{(1)}_{\phi_2}(0)$ yields additional contributions to $\Delta m_h^{2,\alpha\alpha_s}$, see eq. (113). From eq. (108) it becomes also clear that the β dependence of the leading two-loop contribution drops out, as mentioned above.
The tree-level and one-loop contributions of eq. (107) are given by

$$m_h^{2,\rm tree} = \frac{1}{2}\left[M_A^2 + M_Z^2 - \sqrt{(M_A^2+M_Z^2)^2 - 4M_Z^2 M_A^2\cos^2 2\beta}\right], \tag{109}$$

$$\begin{aligned}
\Delta m_h^{2,\alpha,t/\tilde{t}} = \frac{G_F\sqrt{2}}{\pi^2}\,\overline{m}_t^4 \Bigg[& \log\left(\frac{\overline{m}_t^2}{M_S^2}\right)\left\{-\frac{3}{2} - \frac{3}{4}\frac{M_Z^2}{\overline{m}_t^2}\cos 2\beta\ - \frac{M_Z^4}{\overline{m}_t^4}\Lambda\cos^2 2\beta\right. \\
& \left. - \frac{M_Z^2}{M_A^2}\cos^2\beta\ \cos 2\beta\ \left(6 + \frac{3}{2}\frac{M_Z^2}{\overline{m}_t^2}(1-4\sin^2\beta\,) - \frac{M_Z^4}{\overline{m}_t^4}8\Lambda\cos 2\beta\ \sin^2\beta\right)\right\} \\
& + \left\{\frac{1}{4}\frac{M_Z^2}{\overline{m}_t^2} - \frac{11}{80}\frac{M_Z^4}{\overline{m}_t^4} + \frac{X_t^2}{M_S^2}\left(\frac{3}{2} - \frac{1}{2}\frac{M_Z^2}{\overline{m}_t^2} - \frac{3}{4}\frac{\overline{m}_t^2}{M_S^2}\right)\right.
\end{aligned}$$

$$+\frac{X_t^4}{M_S^4}\left(-\frac{1}{8}+\frac{1}{2}\frac{\overline{m}_t^2}{M_S^2}-\frac{3}{8}\frac{\overline{m}_t^4}{M_S^4}\right)+\frac{X_t^6}{M_S^6}\left(-\frac{3}{40}\frac{\overline{m}_t^2}{M_S^2}+\frac{3}{10}\frac{\overline{m}_t^4}{M_S^4}-\frac{1}{4}\frac{\overline{m}_t^6}{M_S^6}\right)$$
$$+\frac{X_t^8}{M_S^8}\left(-\frac{3}{56}\frac{\overline{m}_t^4}{M_S^4}+\frac{3}{14}\frac{\overline{m}_t^6}{M_S^6}-\frac{3}{16}\frac{\overline{m}_t^8}{M_S^8}\right)\Bigg\}\left(1+4\frac{M_Z^2}{M_A^2}\cos^2\beta\,\cos 2\beta\right)\Bigg], \tag{110}$$

$$\Delta m_h^{2,\alpha,\mathrm{rest}} = \frac{G_F\sqrt{2}}{\pi^2}\frac{M_Z^4}{24}\Bigg[\log\left(\frac{M_{SUSY}^2}{M_Z^2}\right)\Bigg\{12N_c\frac{m_b^4}{M_Z^4}-6N_c\cos 2\beta\,\frac{m_b^2}{M_Z^2}+\cos^2 2\beta\,(P_b+P_f)$$
$$+(P_g+P_{2H})(\sin^4\beta\,+\cos^4\beta\,)-2\sin^2\beta\,\cos^2\beta\,(P_g'+P_{2H}')\Bigg\}+\frac{6N_cm_b^4}{M_Z^4}\times$$
$$\Bigg[2\frac{\left(M_b^{LR}\right)^2}{M_{SUSY}^2}\left(1-\frac{\left(M_b^{LR}\right)^2}{12\,M_{SUSY}^2}\right)-\frac{M_Z^2}{2\,m_b^2}\cos 2\beta\,\left(\frac{\left(M_b^{LR}\right)^2}{M_{SUSY}^2}+\frac{A_b^2-\mu^2\tan^2\beta}{3\,M_{SUSY}^2}\right)\Bigg]$$
$$-\log\left(\frac{M_A^2}{M_Z^2}\right)\Bigg\{(\cos^4\beta\,+\sin^4\beta\,)P_{2H}-2\cos^2\beta\,\sin^2\beta\,P_{2H}'-P_{1H}\Bigg\}\Bigg], \tag{111}$$

where Λ is defined as in eq. (103), and

$$\begin{aligned}
M_b^{LR} &= A_b-\mu\tan\beta\\
P_b &= N_c(1+4Q_bs_W^2+8Q_b^2s_W^4)\\
P_f &= N_c(N_g-1)(2-4s_W^2+8(Q_t^2+Q_b^2)s_W^4)+N_g(2-4s_W^2+8s_W^4)\\
P_g &= -44+106s_W^2-62s_W^4,\quad P_g' = 10+34s_W^2-26s_W^4\\
P_{1H} &= -9\cos^4 2\beta\,+(1-2s_W^2+2s_W^4)\cos^2 2\beta\\
P_{2H} &= -10+2s_W^2-2s_W^4,\quad P_{2H}' = 8-22s_W^2+10s_W^4\\
&Q_t=\frac{2}{3},\ Q_b=-\frac{1}{3},\ N_c=3,\ N_g=3\ .
\end{aligned} \tag{112}$$

The dominant two-loop contribution of $\mathcal{O}(\alpha\alpha_s)$ to m_h^2 reads:

$$\begin{aligned}
\Delta m_h^{2,\alpha\alpha_s} &= -\frac{G_F\sqrt{2}}{\pi^2}\frac{\alpha_s}{\pi}\,\overline{m}_t^4\Bigg[4+3\log^2\left(\frac{\overline{m}_t^2}{M_S^2}\right)+2\log\left(\frac{\overline{m}_t^2}{M_S^2}\right)-6\frac{X_t}{M_S}\\
&\quad-\frac{X_t^2}{M_S^2}\left\{3\log\left(\frac{\overline{m}_t^2}{M_S^2}\right)+8\right\}\\
&\quad+\frac{17}{12}\frac{X_t^4}{M_S^4}\Bigg]\left(1+4\frac{M_Z^2}{M_A^2}\cos^2\beta\,\cos 2\beta\right).
\end{aligned} \tag{113}$$

For the leading two-loop Yukawa correction we use the result given obtained from eq. (79) [10, 11]:

$$\Delta m_h^{2,\alpha^2} = \frac{9}{16\pi^4}G_F^2\overline{m}_t^6\left[\tilde{X}t+t^2\right]\ , \tag{114}$$

$$\begin{aligned}
\tilde{X} &= \Bigg[\left(\frac{m_{\tilde{t}_2}^2-m_{\tilde{t}_1}^2}{4\overline{m}_t^2}\sin^2 2\theta_{\tilde{t}}\right)^2\left(2-\frac{m_{\tilde{t}_2}^2+m_{\tilde{t}_1}^2}{m_{\tilde{t}_2}^2-m_{\tilde{t}_1}^2}\log\left(\frac{m_{\tilde{t}_2}^2}{m_{\tilde{t}_1}^2}\right)\right)\\
&\quad+\frac{m_{\tilde{t}_2}^2-m_{\tilde{t}_1}^2}{2\overline{m}_t^2}\sin^2 2\theta_{\tilde{t}}\log\left(\frac{m_{\tilde{t}_2}^2}{m_{\tilde{t}_1}^2}\right)\Bigg],\quad t=\frac{1}{2}\log\left(\frac{m_{\tilde{t}_1}^2m_{\tilde{t}_2}^2}{\overline{m}_t^4}\right).
\end{aligned} \tag{115}$$

Here M_S is chosen in analogy with eq. (105), where the top-quark pole mass m_t has to be replaced by the $\overline{\rm MS}$ top-quark mass $\overline{m}_t$.

In the contributions of the $t, \tilde{t}$-sector at one-loop and two-loop order, eqs. (110) and (113), we have included correction factors of $\mathcal{O}(M_Z^2/M_A^2)$. In this way the compact formula eq. (107) gives a reliable approximation for M_A values down to at least $M_A = 200$ GeV.

5.4 Implementation into *FeynHiggs* and *FeynHiggsFast*

The formulas given in the previous section have been implemented into the Fortran code *FeynHiggs* [28, 29], thus allowing a direct comparison between the full result described in Sect. 3.3 and the approximation formula (107).

We also provide the Fortran code *FeynHiggsFast* [28,29] in which only the formula for the compact approximation of m_h is implemented, thus allowing an approximate but much faster evaluation of the Higgs-boson mass m_h. This program is shorter by a factor of 50 and faster by a factor of 3×10^4 with respect to *FeynHiggs*; it needs only 2×10^{-5} seconds on a Sigma station (Alpha CPU, 600 MHz) for the evaluation of m_h for one set of parameters. The quality of the prediction of m_h is reasonably good for a large part of the MSSM parameter space, as will be discussed in the next section. Into *FeynHiggsFast* we have also implemented the calculation of the MSSM contributions to $\Delta\rho$ [22, 30]. Here the corrections arising from $\tilde{t}/\tilde{b}$ loops up to $\mathcal{O}(\alpha\alpha_s)$ have been taken into account, neglecting only the gluino-exchange contribution which is very lengthy and vanishes for large $m_{\tilde{g}}$. The ρ-parameter can be used as an additional constraint (besides the experimental bounds) on the squark masses. A value of $\Delta\rho$ outside the experimentally preferred region of $\Delta\rho^{\rm SUSY} \lesssim 2 \times 10^{-3}$ [35] indicates experimentally disfavored $\tilde{t}$ and $\tilde{b}$ masses.

Both Fortran codes can be obtained via the WWW page `www.feynhiggs.de` .

5.5 Discussion of the compact expression for m_h

In this section we analyze the quality of our compact approximation formula for m_h with respect to the full calculation, which contains the full diagrammatic one-loop contribution [5], the complete leading two-loop corrections in $\mathcal{O}(\alpha\alpha_s)$ [7,8], and the two contributions beyond $\mathcal{O}(\alpha\alpha_s)$, see eq. (82) and eq. (114). We use here the approximation formula for general M_A, as discussed in Sec. 5.3.1. As mentioned above, in the region $M_A \gtrsim 200$ GeV the compact formula given in Sec. 5.3.2 yields equally good results.

For $\tan\beta$ we restrict ourselves to two typical values which are favored by SUSY-GUT scenarios [33]: $\tan\beta = 1.6$ for the $SU(5)$ scenario and $\tan\beta = 40$ for the $SO(10)$ scenario, see Sect. 4.1. Other parameters are $M_Z = 91.187$ GeV, $M_W = 80.39$ GeV, $G_F = 1.16639 \times 10^{-5}$ GeV^{-2}, $\alpha_s(m_t) = 0.1095$, $m_t = 175$ GeV, and $m_b = 4.5$ GeV. In the numerical evaluation we have furthermore chosen $A_t = A_b$. If not indicated differently, we have chosen $M = m_{\tilde{q}}$ and $\mu = -m_{\tilde{q}}$.

In Fig. 21 we show m_h as a function of $X_t/m_{\tilde{q}}$ for $m_{\tilde{q}} = 200, 500, 1000$ GeV and $M_A = 500$ GeV. A maximum for m_h, evaluated with the full formula as well as with the approxi-

mation formula, is reached for about $X_t/m_{\tilde{q}} \approx \pm 1.9$ in the $\tan\beta = 1.6$ scenario and in the $\tan\beta = 40$ scenario. This case we refer to as 'maximal mixing'. A minimum is reached around $X_t/m_{\tilde{q}} \approx 0$ which we refer to as 'no mixing'. In general the approximation differs from the full result by less than 2 GeV up to $|X_t/m_{\tilde{q}}| \lesssim 2$. For larger $|X_t|$ sizeable deviations occur, which become very large for $|X_t/m_{\tilde{q}}| \gtrsim 2.5$. The reason is that the expansion parameter $\Delta_{\tilde{t}}$ becomes rather large and approaches 1 in this region. The effect of the non-logarithmic terms in the two-loop contribution in $\mathcal{O}(\alpha\alpha_s)$ reaches up to about 5 GeV for maximal mixing.

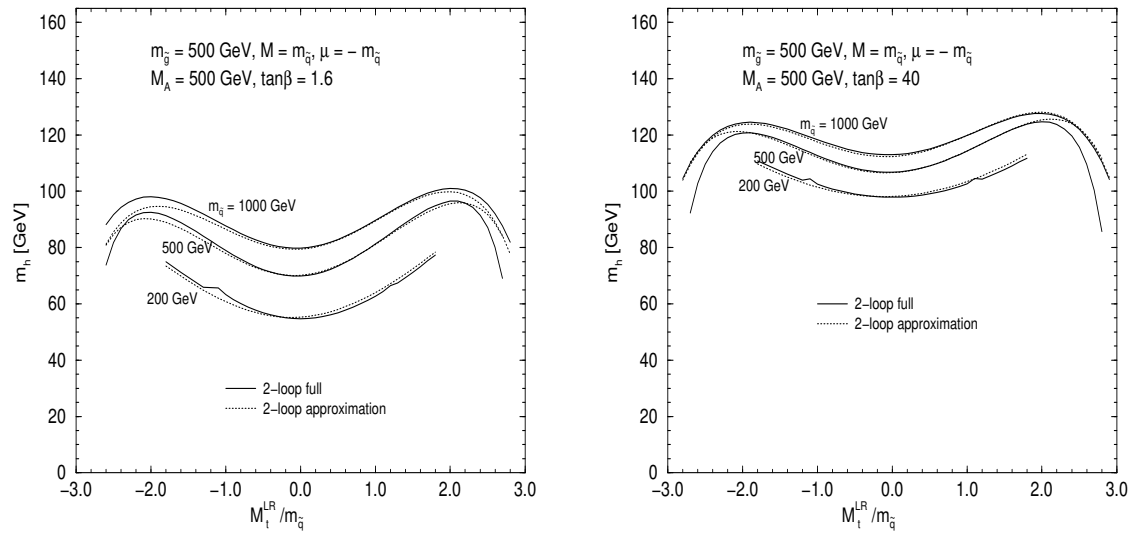

Figure 21: m_h as a function of $X_t/m_{\tilde{q}}$, calculated from the full formula and from the approximation formula for $M_A = 500$ GeV, $m_{\tilde{g}} = 500$ GeV and $\tan\beta = 1.6$ or 40.

The location of the extrema can be understood analytically as follows: taking into account only the leading one-loop corrections from the $t, \tilde{t}$-sector for the calculation of m_h, one can easily compute the values of $X_t/m_{\tilde{q}}$ for which m_h reaches a maximum or a minimum. The well known results are

$$\frac{X_t}{m_{\tilde{q}}} = \begin{cases} \sqrt{6} & \text{(maximum)} \\ 0 & \text{(minimum)} \\ -\sqrt{6} & \text{(maximum)} \end{cases} . \tag{116}$$

Taking into account the new two-loop corrections $\Delta m_h^{2,\alpha\alpha_s}$, given in eq. (113), the positions of the extrema in eq. (116) receive a shift, yielding up to $\mathcal{O}(\alpha\alpha_s)$:

$$\frac{X_t}{m_{\tilde{q}}} = \begin{cases} \sqrt{6} - \frac{\alpha_s}{\pi}\left[-1 + 3\sqrt{6} - \sqrt{6}\log\left(\frac{\overline{m}_t^2}{M_S^2}\right)\right] & (\approx +1.92 \text{ for } M_S = 1000 \text{ GeV; max.}) \\ -2\frac{\alpha_s}{\pi} & (\approx -0.07\text{; minimum}) \\ -\sqrt{6} + \frac{\alpha_s}{\pi}\left[1 + 3\sqrt{6} - \sqrt{6}\log\left(\frac{\overline{m}_t^2}{M_S^2}\right)\right] & (\approx -1.85 \text{ for } M_S = 1000 \text{ GeV; max.}) \end{cases} \tag{117}$$

The maxima are shifted to smaller absolute values of $X_t/m_{\tilde{q}}$, the minimum is shifted to a slightly negative value (see the discussion in Refs. [7, 8, 17]).

Fig. 22 shows the dependence of m_h on $m_{\tilde{q}}$ for the cases of no mixing and maximal mixing, and we have set $M_A = 500$ GeV. Very good agreement is found in the no-mixing scenario as well as in the maximal-mixing scenario, the deviation lies below 2 GeV.

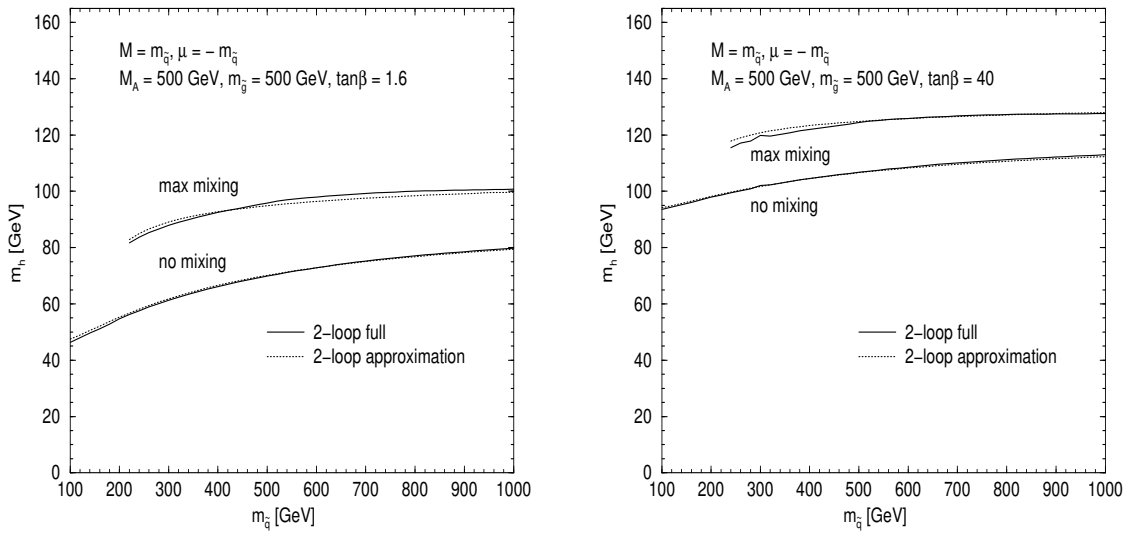

Figure 22: m_h as a function of $m_{\tilde{q}}$, calculated from the full formula and from the approximation formula for $M_A = 500$ GeV, $m_{\tilde{g}} = 500$ GeV and $\tan\beta = 1.6$ or 40.

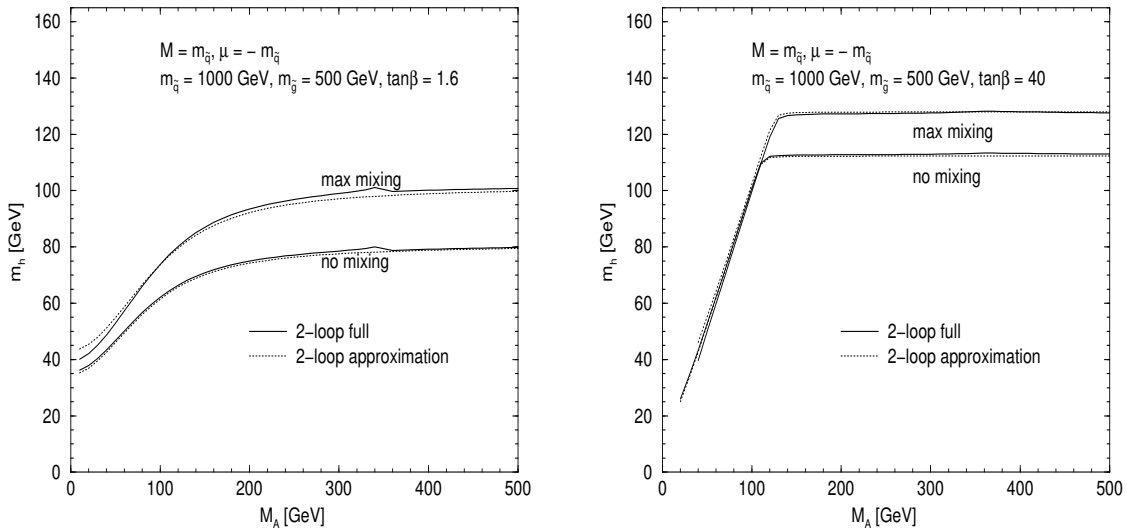

Figure 23: m_h as a function of M_A, calculated from the full formula and from the approximation formula for $m_{\tilde{q}} = 1000$ GeV, $m_{\tilde{g}} = 500$ GeV and $\tan\beta = 1.6$ or 40.

The dependence on M_A is shown in Fig. 23. The quality of the approximation is typically better than 1 GeV for the no-mixing case and better than 2 GeV for the maximal-mixing

case. Only for very small (and experimentally already excluded) values of M_A a deviation of 5 GeV occurs. The peaks in the plot for $\tan\beta = 1.6$ in the full result are due to the threshold $M_A = 2\,m_t$ in the one-loop contribution, originating from the top-loop diagram in the A self-energy. This peak does not occur in the approximation formula and can thus lead to a larger deviation around the threshold.

In deriving the leading and subleading corrections we have set $m_{\tilde{g}} = \sqrt{M_S^2 - m_t^2}$, thus eliminating this additional scale. A variation of $m_{\tilde{g}}$ in the full result directly corresponds to a shift relative to the approximation formula. As it was shown in Ref. [8] (see also Sect. 4.1, this deviation is negligible for the no-mixing case and lies within ± 2 GeV in the maximal-mixing case. There it was also analyzed in that the variation of m_h with the $SU(2)$ gaugino mass parameter $M(= M_2)$ and with the Higgs-mixing parameter μ is relatively weak. We have found only small deviations of the approximation formula with respect to the full result, not more than 2 GeV for small values of M, and 1.5 GeV for small values of μ.

Finally we consider the case when $M_{\tilde{t}_L} \neq M_{\tilde{t}_R}$, which is shown in Fig. 24. Here also the case $X_t = M_{\tilde{t}_L}$ is depicted, which we refer to as 'moderate mixing'. 'No mixing' here corresponds to $X_t = 0$, 'maximal mixing' corresponds to the choice $X_t = 2\ M_{\tilde{t}_L}$. For fixed $M_{\tilde{t}_R}$ this leads to a $\tilde{t}$ mass below the experimental lower bound for nearly the whole parameter space; thus we have omitted this case in this scenario (bottom of Fig. 24). Here we have made use of eq. (105). Agreement better than 2 GeV is found for all scenarios.

6 Comparison with the RG result

The two-loop diagrammatic computation of the dominant contributions at $\mathcal{O}(\alpha\alpha_s)$ to the neutral $\mathcal{CP}$-even Higgs boson masses [7] has been obtained first in the on-shell scheme, was subsequently combined [8] with the complete diagrammatic one-loop on-shell result of Ref. [5], see Sect. 3.3. Within the RG approach [9–11], on the other hand, the two-loop results was expressed in terms of the top-quark mass in the $\overline{\rm MS}$ scheme. By comparing the final expression of the FD approach with the results obtained in the RG approach, it was shown that the upper bound on the lightest Higgs mass was shifted upwards by up to 5 GeV, an effect that is more pronounced in the low $\tan\beta$ region [8, 17].

Besides the shift in the upper bound of m_h, apparent deviations between the explicit diagrammatic two-loop calculation and the results of the RG computation were observed in the dependence of m_h on the stop-mixing parameter X_t. While the value of X_t that maximizes the lightest $\mathcal{CP}$-even Higgs mass is $(X_t)_{\rm max} \simeq \pm\sqrt{6}\,M_S \approx \pm 2.4\,M_S$ in the RG results, the corresponding on-shell two-loop diagrammatic computation found a maximal value for m_h at $(X_t)_{\rm max} \approx 2M_S$.[8] Moreover, in the RG results are symmetric under $X_t \to -X_t$ and has a (local) minimum at $X_t = 0$. In contrast, the two-loop diagrammatic computation yields m_h values for positive and negative X_t that differ significantly from each other and the local minimum in m_h is shifted slightly away from $X_t = 0$ [17].

[8] A local maximum for m_h is also found for $X_t \simeq -2M_S$, although the corresponding value of m_h at $X_t \simeq +2M_S$ is significantly larger [8, 17].

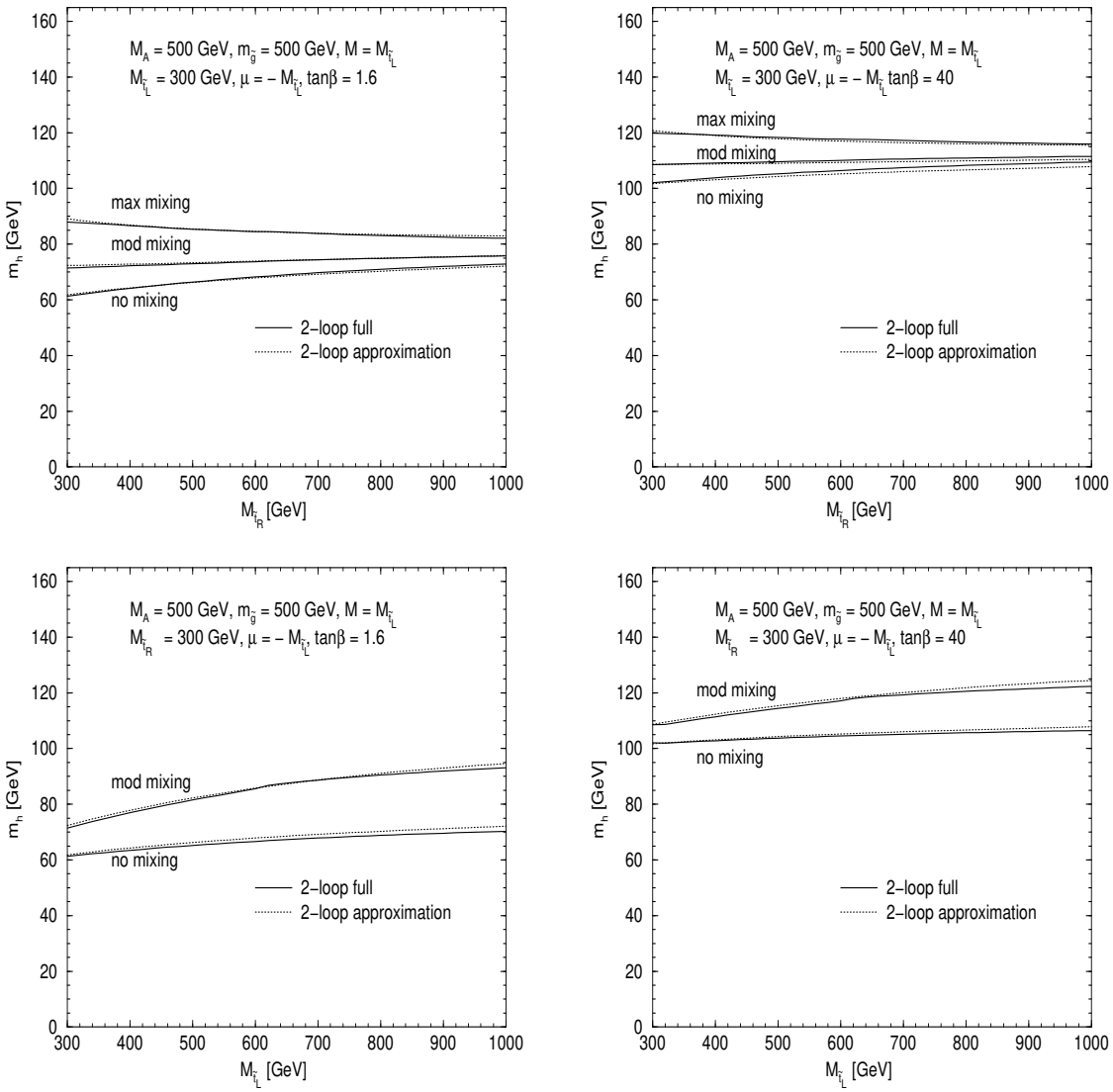

Figure 24: m_h as a function of $M_{\tilde{t}_R}$ or $M_{\tilde{t}_L}$, calculated from the full formula and from the approximation formula for varied $M_{\tilde{t}_R}$ ($M_{\tilde{t}_L}$), $M_{\tilde{t}_L}$ ($M_{\tilde{t}_R}$) = 300 GeV, $M_A = 500$ GeV, $m_{\tilde{g}} =$ 500 GeV and $\tan\beta = 1.6$ or 40.

In this section, it is shown that this apparent discrepancy is caused by the different renormalization schemes employed in the two approaches, leading to differences in the leading-logarithmic contributions. It will furthermore be shown that in the analytic approximation employed in this paper, the dominant numerical contribution of the new genuine non-logarithmic two-loop contributions of the FD result [7, 8] can be absorbed into an effective one-loop expression by choosing an appropriate scale for the running top-quark mass in different terms of the expression.

6.1 Approximation formulas for m_h

Within the RG approach the following approximation for m_h has been obtained [9–11, 18], taking into account terms up to $\mathcal{O}(\alpha\alpha_s)$:

$$m_h^2 = m_h^{2,\rm tree} + \frac{3}{2}\frac{G_F\sqrt{2}}{\pi^2}\overline{m}_t^4\left\{-\ln\left(\frac{\overline{m}_t^2}{\overline{M}_S^2}\right) + \frac{\overline{X}_t^2}{\overline{M}_S^2}\left(1 - \frac{1}{12}\frac{\overline{X}_t^2}{\overline{M}_S^2}\right)\right\}$$
$$- 3\frac{G_F\sqrt{2}}{\pi^2}\frac{\alpha_s}{\pi}\overline{m}_t^4\left\{\ln^2\left(\frac{\overline{m}_t^2}{\overline{M}_S^2}\right) + \left[\frac{2}{3} - 2\frac{\overline{X}_t^2}{\overline{M}_S^2}\left(1 - \frac{1}{12}\frac{\overline{X}_t^2}{\overline{M}_S^2}\right)\right]\ln\left(\frac{\overline{m}_t^2}{\overline{M}_S^2}\right)\right\}, \quad (118)$$

where we have introduced the notation $\overline{M}_S, \overline{X}_t$ to emphasize that the corresponding quantities are $\overline{\rm MS}$ parameters, which are evaluated at the scale $\mu = M_S$:

$$\overline{M}_S \equiv M_S^{\overline{\rm MS}}(M_S), \quad \overline{X}_t \equiv X_t^{\overline{\rm MS}}(M_S), \quad (119)$$

and $\overline{m}_t \equiv m_{t,\rm SM}^{\overline{\rm MS}}(m_t)$ as defined in eq. (82).

Concerning the FD result, we consider the dominant one-loop and two-loop terms and we focus on the case $M_A \gg M_Z$, for which the result for m_h^2 can be expressed in a particularly compact form, see Sects. 5.3.1 and 5.3.2,

$$m_h^2 = m_h^{2,\rm tree} + m_h^{2,\alpha} + m_h^{2,\alpha\alpha_s}, \quad (120)$$

and neglect the non-leading terms of $\mathcal{O}(M_Z^2/M_A^2)$. M_t in the following denotes the top quark pole mass. Assuming that $M_S \gg M_t$ and neglecting the non-leading terms of $\mathcal{O}(M_t/M_S)$ and $\mathcal{O}(M_Z^2/M_t^2)$, one obtains the following simple result for the one-loop and two-loop contributions

$$m_h^{2,\alpha} = \frac{3}{2}\frac{G_F\sqrt{2}}{\pi^2}M_t^4\left\{-\ln\left(\frac{M_t^2}{M_S^2}\right) + \frac{X_t^2}{M_S^2}\left(1 - \frac{1}{12}\frac{X_t^2}{M_S^2}\right)\right\}, \quad (121)$$

$$m_h^{2,\alpha\alpha_s} = -3\frac{G_F\sqrt{2}}{\pi^2}\frac{\alpha_s}{\pi}M_t^4\left\{\ln^2\left(\frac{M_t^2}{M_S^2}\right) - \left(2 + \frac{X_t^2}{M_S^2}\right)\ln\left(\frac{M_t^2}{M_S^2}\right) - \frac{X_t}{M_S}\left(2 - \frac{1}{4}\frac{X_t^3}{M_S^3}\right)\right\}. \quad (122)$$

The corresponding formulae, in which terms up to $\mathcal{O}(M_t^4/M_S^4)$ are kept, can be found in Ref. [18].

In eqs. (121)-(122) the parameters M_t, M_S, X_t are on-shell quantities. Using eq. (82), the on-shell result for m_h^2, eqs. (120)–(122), can easily be rewritten in terms of the running top-quark mass $\overline{m}_t$. While this reparameterization does not change the form of the one-loop result, it induces an extra contribution at $\mathcal{O}(\alpha\alpha_s)$. Keeping again only terms that are not suppressed by powers of $\overline{m}_t/M_S$, the resulting expressions read

$$m_h^{2,\alpha} = \frac{3}{2}\frac{G_F\sqrt{2}}{\pi^2}\overline{m}_t^4\left\{-\ln\left(\frac{\overline{m}_t^2}{M_S^2}\right) + \frac{X_t^2}{M_S^2}\left(1 - \frac{1}{12}\frac{X_t^2}{M_S^2}\right)\right\}, \quad (123)$$

$$m_h^{2,\alpha\alpha_s} = -3\frac{G_F\sqrt{2}}{\pi^2}\frac{\alpha_s}{\pi}\overline{m}_t^4\left\{\ln^2\left(\frac{\overline{m}_t^2}{M_S^2}\right) + \left(\frac{2}{3} - \frac{X_t^2}{M_S^2}\right)\ln\left(\frac{\overline{m}_t^2}{M_S^2}\right)\right.$$
$$\left. + \frac{4}{3} - 2\frac{X_t}{M_S} - \frac{8}{3}\frac{X_t^2}{M_S^2} + \frac{17}{36}\frac{X_t^4}{M_S^4}\right\}, \quad (124)$$

in accordance with the formulae given in Ref. [17] and in Sect. 5.3.2.

We now compare the diagrammatic result expressed in terms of the parameters $\overline{m}_t$, M_S, X_t ,eqs. (123)-(124), with the RG result of eq. (118), which is given in terms of the $\overline{\rm MS}$ parameters $\overline{m}_t$, $\overline{M}_S$, $\overline{X}_t$ eq. (119). While the X_t–independent logarithmic terms are the same in both the diagrammatic and RG results, the corresponding logarithmic terms at two loops that are proportional to powers of X_t and $\overline{X}_t$, respectively, are different. Furthermore, eq. (124) does not contain a logarithmic term proportional to X_t^4, while the corresponding term proportional to $\overline{X}_t^4$ appears in eq. (118). To check whether these results are consistent, one must relate the on-shell and $\overline{\rm MS}$ definitions of the parameters M_S and X_t.

Finally, we note that the non-logarithmic terms contained in eq. (124) correspond to genuine two-loop contributions that are not present in the RG result of eq. (118). They can be interpreted as a two-loop finite threshold correction to the quartic Higgs self-coupling in the RG approach. In particular, note that eq. (124) contains a term that is linear in X_t This is the main source of the asymmetry in the two-loop corrected Higgs mass under $X_t \to -X_t$ obtained by the diagrammatic method. The non-logarithmic terms in eq. (124) give rise to a numerically significant increase of the maximal value of m_h of about 5 GeV in this approximation.

6.2 On-shell and $\overline{\rm MS}$ definitions of M_S and X_t

Since the parameters $p = \{m^2_{\tilde{t}_1}, m^2_{\tilde{t}_2}, \theta_{\tilde{t}}, m_t\}$ of the t–$\tilde{t}$ sector are renormalized differently in different schemes, the parameters M_S and X_t also have a different meaning in these schemes. The relation between these parameters in the $\overline{\rm MS}$ and in the on-shell scheme have been derived in Ref. [18] and read in leading order in m_t/M_S:

$$\overline{M}_S^2 = M_S^{2,\rm OS} - \frac{8}{3}\frac{\alpha_s}{\pi} M_S^2 \,, \tag{125}$$

$$\overline{X}_t = X_t^{\rm OS} \frac{M_t}{\overline{m}_t(M_S)} + \frac{8}{3}\frac{\alpha_s}{\pi} M_S \,. \tag{126}$$

As previously noted, it is not necessary to specify the definition of the parameters that appear in the $\mathcal{O}(\alpha_s)$ terms. Thus, we use the generic symbol M_S^2 in the $\mathcal{O}(\alpha_s)$ terms of eqs. (125)–(126). The corresponding results including terms up to $\mathcal{O}\left(m_t^4/M_S^4\right)$ can be found in Ref. [18].

Finally, the evaluation of the ratio $M_t/\overline{m}_t(M_S)$ is needed. In leading order in m_t/M_S it is given by [18]:

$$\overline{m}_t(M_S) = \overline{m}_t \left[1 + \frac{\alpha_s}{\pi} \ln\left(\frac{m_t^2}{M_S^2}\right) + \frac{\alpha_s}{3\pi}\frac{X_t}{M_S}\right] , \tag{127}$$

where $\overline{m}_t \equiv m_{t,\rm SM}^{\overline{\rm MS}}(m_t)$ is given in terms of M_t by eq. (82). Note that the term in eq. (127) that is proportional to X_t is a threshold correction due to the supersymmetry-breaking stop-mixing effect. Inserting the result of eq. (127) into eq. (126) yields:

$$\overline{X}_t = X_t^{\rm OS} + \frac{\alpha_s}{3\pi} M_S \left[8 + \frac{4X_t}{M_S} - \frac{X_t^2}{M_S^2} - \frac{3X_t}{M_S} \ln\left(\frac{m_t^2}{M_S^2}\right)\right] . \tag{128}$$

It is interesting to note that $\overline{X}_t \neq 0$ when $X_t^{\rm OS} = 0$. Moreover, it is clear from eq. (128) that the relation between X_t defined in the on-shell and the $\overline{\rm MS}$ schemes includes a leading logarithmic effect, which has to be taken into account in a comparison of the leading logarithmic contributions in the RG and the two-loop diagrammatic results.

A remark on the regularization scheme is in order here. In effective field theory, the running top-quark mass at scales below M_S is the SM running coupling of eq. (82), which is calculated in dimensional regularization. This is matched onto the running top-quark mass as computed in the full supersymmetric theory. One could argue that the appropriate regularization scheme for the latter should be dimensional reduction (DRED) [20], which is usually applied in loop calculations in supersymmetry.[9] The result of such a change would be to modify slightly the two-loop non-logarithmic contribution to m_h that is proportional to powers of X_t. Of course, the physical Higgs mass is independent of scheme. One is free to re-express eqs. (121)-(122) (which depend on the on-shell parameters M_t, M_S, X_t) in terms of parameters defined in any other scheme. In this paper, we find $\overline{\rm MS}$–renormalization via DREG to be the most convenient scheme for the comparison of the diagrammatic and RG results for m_h.

6.3 Comparing the RG and diagrammatic results

In order to directly compare the two-loop diagrammatic and RG results, we must convert from on-shell to $\overline{\rm MS}$ parameters. Inserting eqs. (125)-(128) into eqs. (123)-(124), one finds

$$m_h^{2,\alpha} = \frac{3}{2}\frac{G_F\sqrt{2}}{\pi^2}\overline{m}_t^4\left\{-\ln\left(\frac{\overline{m}_t^2}{\overline{M}_S^2}\right)+\frac{\overline{X}_t^2}{\overline{M}_S^2}\left(1-\frac{1}{12}\frac{\overline{X}_t^2}{\overline{M}_S^2}\right)\right\}, \tag{129}$$

$$\begin{aligned} m_h^{2,\alpha\alpha_s} = {} & -3\frac{G_F\sqrt{2}}{\pi^2}\frac{\alpha_s}{\pi}\overline{m}_t^4\left\{\ln^2\left(\frac{\overline{m}_t^2}{\overline{M}_S^2}\right)+\left[\frac{2}{3}-2\frac{\overline{X}_t^2}{\overline{M}_S^2}\left(1-\frac{1}{12}\frac{\overline{X}_t^2}{\overline{M}_S^2}\right)\right]\ln\left(\frac{\overline{m}_t^2}{\overline{M}_S^2}\right)\right. \\ & \left.+\frac{\overline{X}_t}{\overline{M}_S}\left(\frac{2}{3}-\frac{7}{9}\frac{\overline{X}_t^2}{\overline{M}_S^2}+\frac{1}{36}\frac{\overline{X}_t^3}{\overline{M}_S^3}+\frac{1}{18}\frac{\overline{X}_t^4}{\overline{M}_S^4}\right)\right\}+\mathcal{O}\left(\frac{\overline{m}_t}{\overline{M}_S}\right). \end{aligned} \tag{130}$$

Comparing eq. (130) with eq. (118) shows that the logarithmic contributions of the diagrammatic result expressed in terms of the $\overline{\rm MS}$ parameters $\overline{m}_t$, $\overline{M}_S$, $\overline{X}_t$ agree with the logarithmic contributions obtained by the RG approach. The differences in the logarithmic terms observed in the comparison of eqs. (123)-(124) with eq. (118) have thus been traced to the different renormalization schemes applied in the respective calculations. The fact that the logarithmic contributions obtained within the two approaches agree after a proper rewriting of the parameters of the stop sector is an important consistency check of the calculations. In addition to the logarithmic contributions, eq. (130) also contains non-logarithmic contributions, which are numerically sizable.

In Fig. 25, we compare the diagrammatic result for m_h in the leading m_t^4 approximation to the results obtained by RG techniques, for two different values of $\tan\beta$. While the

[9] In order to obtain the corresponding DRED result, one simply has to replace the term $4\alpha_s/3\pi$ in the denominator of eq. (82) by $5\alpha_s/3\pi$.

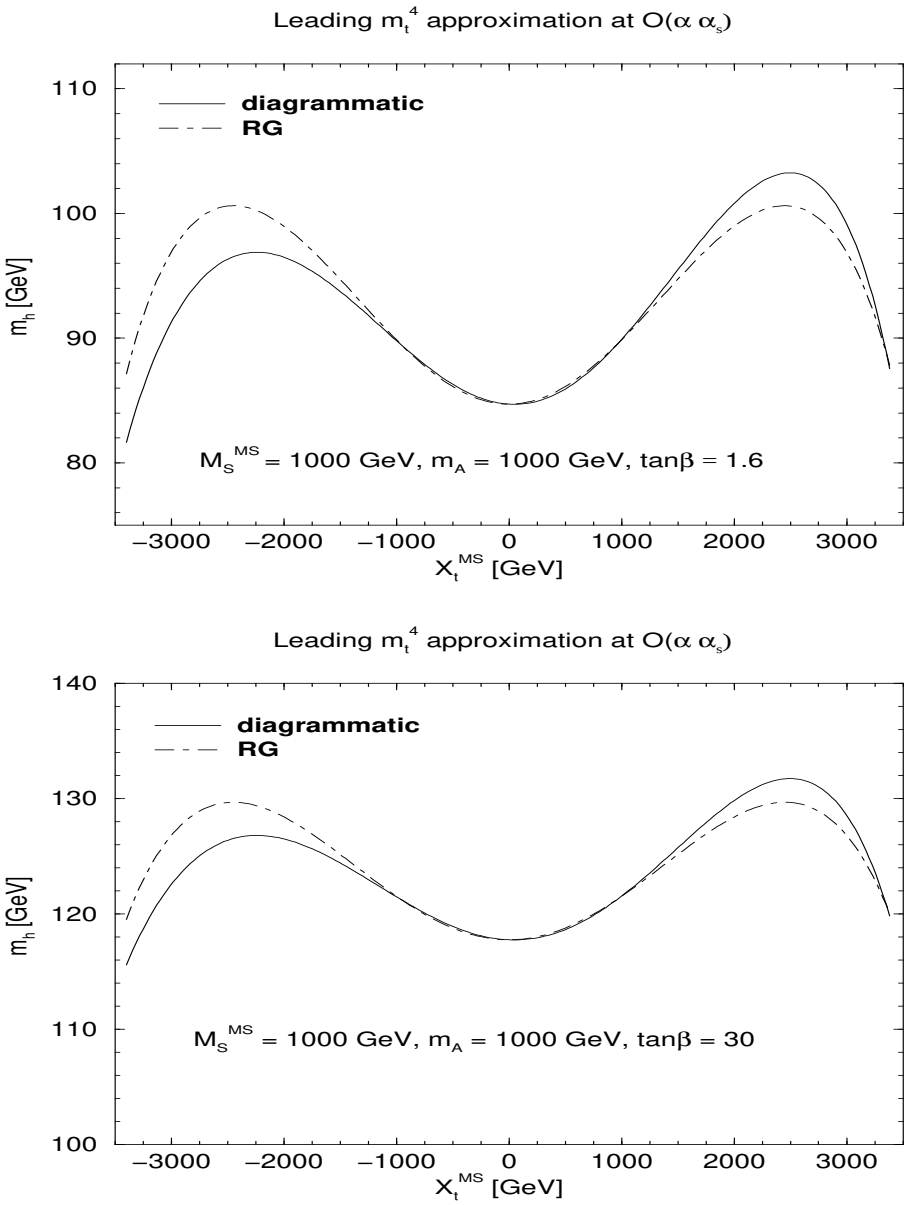

Figure 25: Comparison of the diagrammatic two-loop $\mathcal{O}(\alpha\alpha_s)$ result for m_h, to leading order in $\overline{m}_t/\overline{M}_S$ (eqs. (129)-(130)) with the RG result of eq. (118). Note that the latter omits the one-loop threshold corrections due to stop mixing in the evaluation of $\overline{m}_t(M_S)$. Since this quantity enters in the definition of $\overline{X}_t$, see eq. (126), the meaning of $X_t^{\rm MS}$ plotted along the x-axis is slightly different for the diagrammatic curve, where $X_t^{\rm MS} = \overline{X}_t$, and the RG curve, where $X_t^{\rm MS} = \overline{X}_t\,[1 + (\alpha_s/3\pi)(X_t/M_S)]$. See text for further details. The two graphs above are plotted for $\overline{M}_S = M_A = (m_{\tilde{g}}^2 + \overline{m}_t^2)^{1/2} = 1$ TeV for the cases of $\tan\beta = 1.6$ and $\tan\beta = 30$, respectively.

diagrammatic result expressed in terms of $\overline{m}_t$, $\overline{M}_S$, $\overline{X}_t$ agrees well with the RG result in the region of no mixing in the stop sector, sizable deviations occur for large mixing. In particular, the non-logarithmic contributions give rise to an asymmetry under the change of sign of the parameter $\overline{X}_t$, while the RG result is symmetric under $\overline{X}_t \to -\overline{X}_t$. In the approximation considered here, the maximal value for m_h in the diagrammatic result lies about 4 GeV higher than the maximal value of the RG result for $\tan\beta = 1.6$. The differences are slightly smaller for $\tan\beta = 30$. In addition, as previously noted, the maximal-mixing point $(\overline{X}_t)_{\rm max}$ (where the radiatively corrected value of m_h is maximal) is equal to its one-loop value, $(\overline{X}_t)_{\rm max} \simeq \pm\sqrt{6}M_S$, in the RG result of eq. (118), while it is shifted in the two-loop diagrammatic result. However, Fig. 25 illustrates that the shift in $(\overline{X}_t)_{\rm max}$ from its one-loop value, while significant in the two-loop on-shell diagrammatic result, is largely diminished when the latter is re-expressed in terms of $\overline{\rm MS}$ parameters.

The differences between the diagrammatic and RG results shown in Fig. 25 can be attributed to non-negligible non-logarithmic terms proportional to powers of X_t. Clearly, the RG technique can be improved to incorporate these terms. In Ref. [11], it was shown that the leading two-loop contributions to m_h^2 given by the RG result of eq. (118) could be absorbed into an effective one-loop expression. This was accomplished by considering separately the X_t–independent leading double logarithmic term (the "no-mixing" contribution) and the leading single logarithmic term that is proportional to powers of $\overline{X}_t$ (the "mixing" contribution) at $\mathcal{O}(\alpha\alpha_s)$. Both terms can be reproduced by an effective one-loop expression, where $\overline{m}_t$ in eq. (129), which appears in the no-mixing and mixing contributions, is replaced by the *running* top-quark mass evaluated at the scales μ_t and $\mu_{\tilde{t}}$, respectively:

$$\text{no mixing: } \mu_t \equiv (\overline{m}_t \overline{M}_S)^{1/2}\,, \qquad \text{mixing: } \mu_{\tilde{t}} \equiv \overline{M}_S\,. \tag{131}$$

That is, at $\mathcal{O}(\alpha\alpha_s)$, the leading double logarithmic term is precisely reproduced by the single-logarithmic term at $\mathcal{O}(\alpha)$, by replacing $\overline{m}_t$ with $\overline{m}_t(\mu_t)$, while the leading single logarithmic term at two loops proportional to powers of $\overline{X}_t$ is precisely reproduced by the corresponding non-logarithmic terms proportional to $\overline{X}_t$by replacing $\overline{m}_t$ with $\overline{m}_t(\overline{M}_S)$.

Applying the same procedure to eq. (130) and rewriting it in terms of the running top-quark mass at the corresponding scales as specified in eq. (131), we obtain

$$m_h^{2,\alpha} = \frac{3}{2}\frac{G_F\sqrt{2}}{\pi^2}\left\{-\overline{m}_t^4(\mu_t)\ln\left(\frac{\overline{m}_t^2(\mu_t)}{\overline{M}_S^2}\right) + \overline{m}_t^4(M_S)\frac{\overline{X}_t^2}{\overline{M}_S^2}\left(1 - \frac{\overline{X}_t^2}{12\overline{M}_S^2}\right)\right\}, \tag{132}$$

$$m_h^{2,\alpha\alpha_s} = -3\frac{G_F\sqrt{2}}{\pi^2}\frac{\alpha_s}{\pi}m_t^4\left\{\frac{1}{6}\ln\left(\frac{m_t^2}{M_S^2}\right) + \frac{X_t}{M_S}\left(\frac{2}{3} - \frac{1}{9}\frac{X_t^2}{M_S^2} + \frac{1}{36}\frac{X_t^3}{M_S^3}\right)\right\}. \tag{133}$$

Indeed, the X_t–independent leading double logarithmic term and the leading single logarithmic term that is proportional to powers of $\overline{X}_t$ have disappeared from the two-loop expression eq. (133), having been absorbed into an effective one-loop result (132), (denoted henceforth as the "mixed-scale" one-loop RG result). Of the terms that remain in eq. (133), there is a subleading one-loop logarithm at two loops which is a remnant of the no-mixing contribution. But, note that the magnitude of the coefficient (1/6) has been reduced from the corresponding coefficients that appear in eqs. (122)-(130) (-2 and 2/3, respectively). In addition, the

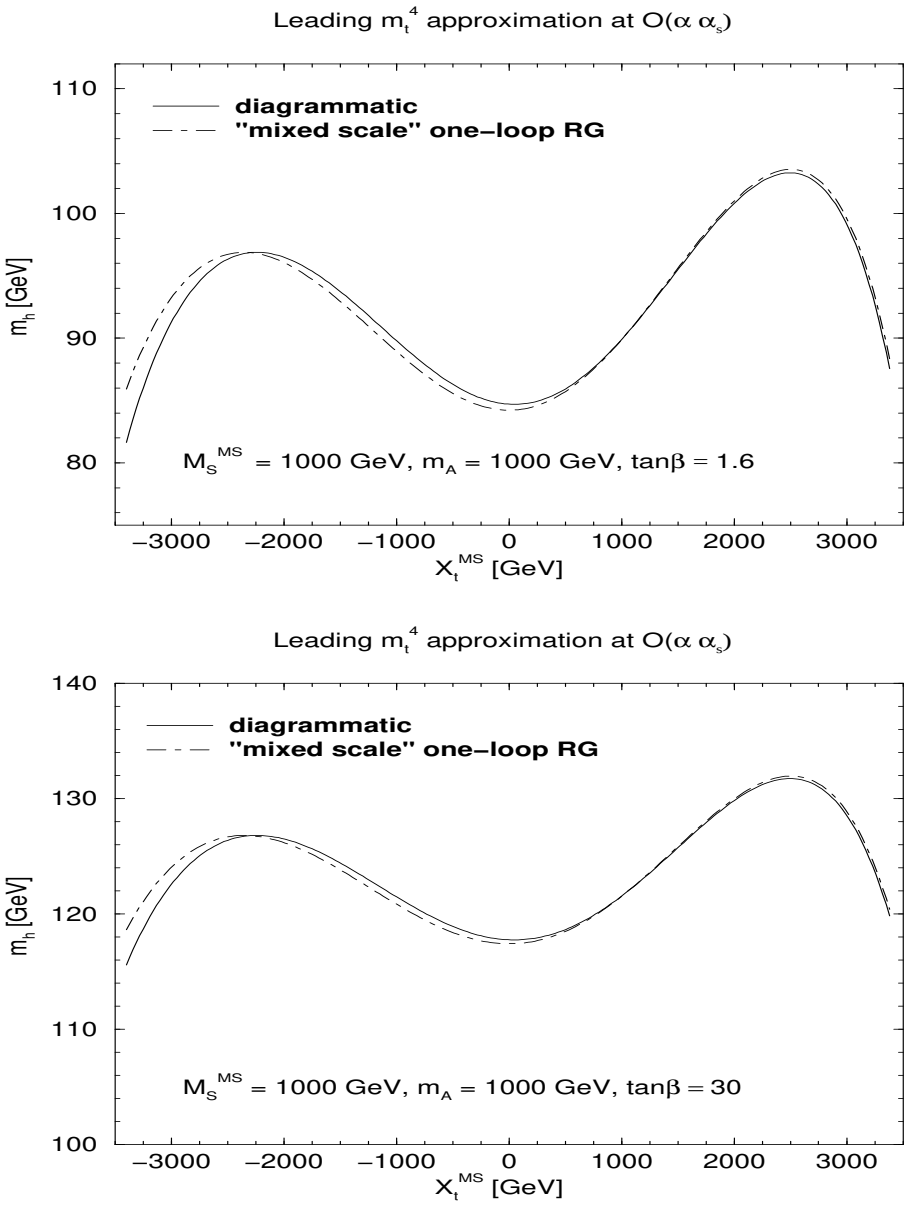

Figure 26: Comparison of the diagrammatic two-loop $\mathcal{O}(\alpha\alpha_s)$ result for m_h, to leading order in $\overline{m}_t/\overline{M}_S$ (eqs. (129)-(130)) with the "mixed-scale" one-loop RG result of eq. (132). Note that the latter now includes the threshold corrections due to stop mixing in the evaluation of $\overline{m}_t(M_S)$ in contrast to the RG results depicted in Fig. 25. "Mixed-scale" indicates that in the no-mixing and mixing contributions to the one-loop Higgs mass, the running top quark mass is evaluated at different scales according to eq. (131). See text for further details. The two graphs above are plotted for $\overline{M}_S = M_A = (m_{\tilde{g}}^2 + \overline{m}_t^2)^{1/2} = 1$ TeV for the cases of $\tan\beta = 1.6$ and $\tan\beta = 30$, respectively.

remaining leftover two-loop non-logarithmic terms are also numerically insignificant. We conclude that the "mixed-scale" one-loop RG result provides a very good approximation to m_h^2, in which the most significant two-loop terms have been absorbed into an effective one-loop expression.

To illustrate this result, we compare in Fig. 26 the diagrammatic two-loop result expressed in terms of $\overline{\rm MS}$ parameters (eqs. (129)-(130)) with the "mixed-scale" one-loop RG result of eq. (132) as a function of $\overline{X}_t$. The difference between the solid and dashed lines of Fig. 26 is precisely equal to the leftover two-loop term given by eq. (133), which is seen to be numerically small. Hence, within the simplifying framework under consideration (*i.e.*, only leading t–$\tilde{t}$ sector-contributions are taken into account assuming a simplified stop squared-mass matrix (92), with $\overline{M}_S$, $M_A \gg \overline{m}_t$ and $m_{\tilde{g}} = m_{\tilde{q}}$), we see that the "mixed-scale" one-loop result for m_h provides a very good approximation to a more complete two-loop result for all values of $\overline{X}_t$.[10]

7 Conclusions

Using the Feynman diagrammatic method we have calculated the dominant $\mathcal{O}(\alpha\alpha_s)$ corrections to the masses of the neutral $\mathcal{CP}$-even Higgs bosons in the MSSM. The two-loop result, supplemented by the subdominant electroweak two-loop corrections, has been implemented into the prediction based on the complete diagrammatic one-loop on-shell result. The results have been obtained using the on-shell scheme, which means a renormalization of all sectors of the MSSM at one-loop order and of the Higgs boson sector at two-loop order. In our two-loop calculation we have imposed no restrictions on the parameters of the Higgs and scalar top sector of the model. Thus the results are valid for arbitrary values of the relevant MSSM parameters. The complete result has been implemented into the `FORTRAN` program *FeynHiggs* [28] which is available via its WWW page `www.feynhiggs.de` .
In this way we provide the at present most precise prediction for m_h and m_H based on Feynman-diagrammatic calculations.

The two-loop corrections lead to a large reduction of the one-loop on-shell result. We have performed a detailed analysis of the dependence of m_h on the various MSSM parameters. Concerning the scalar top sector the analysis has been carried out in terms of the (unphysical) soft SUSY breaking parameters $M_{\tilde{t}_L}$, $M_{\tilde{t}_R}$ and X_t as well as in terms of the physical parameters $m_{\tilde{t}_2}$, $\Delta m_{\tilde{t}} \equiv m_{\tilde{t}_2} - m_{\tilde{t}_1}$ and $\theta_{\tilde{t}}$.

A scan over the parameters $\mu, M, m_{\tilde{g}}, M_A$ and X_t has been performed in order to determine the maximally possible value for m_h as a function of $\tan\beta$, the so called $m_h^{\rm max}$ scenario, which is meanwhile used by all LEP collaborations in order to obtain conservative $\tan\beta$ bounds.

[10] Strictly speaking, the analytic approximations discussed here break down when $\overline{m}_t \overline{X}_t \sim \overline{M}_S^2$. Thus, one does not expect an accurate result for the corresponding formulae when $\overline{X}_t$ is too large [9–11, 17]. In practice, one should not trust the accuracy of the analytic formulae once $\overline{X}_t > (\overline{X}_t)_{\rm max}$.

By means of a Taylor expansion of the diagrammatic two-loop result we have derived the leading logarithmic and non-logarithmic as well as subleading contributions to the lightest Higgs-boson mass m_h up to $\mathcal{O}(\alpha\alpha_s)$. This result has been incorporated into a compact analytical formula for m_h^2, which can easily be implemented for numerical evaluation. It contains the tree-level expression, leading and subleading one-loop contributions, the leading logarithmic and non-logarithmic two-loop contributions, and the subleading two-loop electroweak corrections. This formula is valid for general mixing in the scalar top sector and arbitrary choices of the parameters in the Higgs sector of the model. It has been included into the Fortran code *FeynHiggsFast*, thus allowing a very fast and reasonably accurate evaluation of m_h. The code is also available via the WWW page `www.feynhiggs.de` .
The approximation formula has been compared with the full diagrammatic result, in which the complete one-loop and the dominant two-loop corrections of $\mathcal{O}(\alpha\alpha_s)$ are taken into account without Taylor expansion. Good agreement, better than 2 GeV, is found for most parts of the MSSM parameter space. Larger deviations, exceeding a few GeV, can occur for large mixing in the $\tilde{t}$ sector, $|X_t/m_{\tilde{q}}| \gtrsim 2$. The effect of the corrections of $\mathcal{O}(\alpha\alpha_s)$ of shifting the maxima for m_h towards smaller values of $|X_t/m_{\tilde{q}}|$ can easily be read off from the compact formula by analytically determining the extrema of m_h.

We have compared the results for the lightest $\mathcal{CP}$-even Higgs-boson mass obtained from the two-loop $\mathcal{O}(\alpha\alpha_s)$ diagrammatic calculation in the on-shell scheme with the results of the RG approach. In order to compare these approaches, one must note two important facts. First, the two calculations are performed in different renormalization schemes. Hence, the resulting expressions actually depend on soft-supersymmetry-breaking parameters whose definitions differ at the one-loop level. Second, the diagrammatic calculation includes genuine non-logarithmic two-loop corrections to the lightest $\mathcal{CP}$-even Higgs-boson mass. However, after re-expressing the one-loop and the two-loop terms of the on-shell diagrammatic result in terms of $\overline{\rm MS}$ parameters, i.e. applying the same renormalization scheme for both approaches, we have shown that the discrepancy in the logarithmic dependence on M_S of both expressions disappears. This constitutes an important consistency check of the calculations. There remain, however, genuine non-logarithmic two-loop contributions in the diagrammatic result. They give rise to an asymmetry under $X_t \to -X_t$, while the RG computations only yield results that are symmetric under the change of sign of X_t. Moreover, the non-logarithmic two-loop contributions of the on-shell diagrammatic computation, in the approximations considered in this paper, can increase the predicted value of m_h by as much as 3 GeV. In Ref. [11], it was shown that the leading two-loop contributions to m_h^2 could be absorbed into an effective one-loop expression by using the running top quark mass $\overline{m}_t$ at two different scales: The running top-quark mass that appears in the X_t–independent one-loop expression for m_h^2 is evaluated at the scale $\mu_t = (M_S m_t)^{1/2}$. In the corresponding X_t–dependent terms, the running top quark mass is evaluated at the scale $\mu_{\tilde{t}} = M_S$. The result, which we call the "mixed-scale" one-loop RG expression neatly incorporates the leading two-loop effects. In this paper, we have extended this result by explicitly including stop mixing effects in evaluating the running parameter $\overline{m}_t(M_S)$. By doing so, we are able to incorporate some portion of the genuine leading non-logarithmic two-loop contributions. The remaining terms

at this order would then be identified with two-loop threshold corrections to the effective Higgs quartic coupling at the scale M_S. Remarkably, the latter turn out to be numerically small. This means that the mixed-scale one-loop RG expression for m_h provides a rather accurate estimate of the radiatively-corrected mass of the lightest $\mathcal{CP}$-even Higgs boson of the MSSM.

Acknowledgements

S.H. and G.W. thank M. Carena and C. Wagner for their collaboration on the $m_h^{\rm max}$ scenario. We thank M. Carena, H. Haber and C. Wagner for their collaboration on the comparison of the FD and the RG result.

References

[1] H. Haber and G. Kane, *Phys. Rep.* **117** (1985) 75.
H.P. Nilles, *Phys. Rep.* **110** (1984) 1.

[2] G. Kane, C. Kolda and J. Wells, *Phys. Rev. Lett.* **70** (1993) 2686, hep-ph/9210242;
J. Espinosa and M. Quirós, *Phys. Rev. Lett.* **81** (1998) 516, hep-ph/9804235.

[3] H. Haber and R. Hempfling, *Phys. Rev. Lett.* **66** (1991) 1815.

[4] Y. Okada, M. Yamaguchi and T. Yanagida, *Prog. Theor. Phys.* **85** (1991) 1;
J. Ellis, G. Ridolfi and F. Zwirner, *Phys. Lett.* **B 257** (1991) 83; *Phys. Lett.* **B 262** (1991) 477;
R. Barbieri and M. Frigeni, *Phys. Lett.* **B 258** (1991) 395;
J. Bagger, K. Matchev, D. Pierce and R. Zhang, *Nucl. Phys.* **B 491** (1997) 3.

[5] A. Dabelstein, *Z. Phys.* **C 67** (1995) 495; *Nucl. Phys.* **B 456** (1995) 25.

[6] P. Chankowski, S. Pokorski and J. Rosiek, *Nucl. Phys.* **B 423** (1994) 437.

[7] S. Heinemeyer, W. Hollik and G. Weiglein, *Phys. Rev.* **D 58** (1998) 091701, hep-ph/9803277; *Phys. Lett.* **B 440** (1998) 296, hep-ph/9807423.

[8] S. Heinemeyer, W. Hollik and G. Weiglein, *Eur. Phys. Jour.* **C 9** (1999) 343, hep-ph/9812472.

[9] J. Casas, J. Espinosa, M. Quirós and A. Riotto, *Nucl. Phys.* **B 436** (1995) 3, E: *ibid.* **B 439** (1995) 466, hep-ph/9407389.

[10] M. Carena, J. Espinosa, M. Quirós and C. Wagner, *Phys. Lett.* **B 355** (1995) 209, hep-ph/9504316;
M. Carena, M. Quirós and C. Wagner, *Nucl. Phys.* **B 461** (1996) 407, hep-ph/9508343.

[11] H. Haber, R. Hempfling and A. Hoang, *Z. Phys.* **C 75** (1997) 539, hep-ph/9609331.

[12] R. Hempfling and A. Hoang, *Phys. Lett.* **B 331** (1994) 99, hep-ph/9401219.

[13] R.-J. Zhang, *Phys. Lett.* **B 447** (1999) 89, hep-ph/9808299.

[14] J. Espinosa and R. Zhang, *Nucl. Phys.* **B 586** (2000) 3, hep-ph/0003246.

[15] S. Heinemeyer, W. Hollik, J. Rosiek and G. Weiglein, hep-ph/0102081.

[16] S. Heinemeyer, W. Hollik and G. Weiglein, *Eur. Phys. Jour.* **C 16** (2000) 139, hep-ph/0003022.

[17] S. Heinemeyer, W. Hollik and G. Weiglein, *Phys. Lett.* **B 455** (1999) 179, hep-ph/9903404.

[18] M. Carena, H. Haber, S. Heinemeyer, W. Hollik, C. Wagner, and G. Weiglein, *Nucl. Phys.* **B 580** (2000) 29, hep-ph/0001002.

[19] J. Gunion, H. Haber, G. Kane and S. Dawson, *The Higgs Hunter's Guide*, Addison-Wesley, 1990.

[20] W. Siegel, *Phys. Lett.* **B 84** (1979) 193;
D. Capper, D. Jones, P. van Nieuwenhuizen, *Nucl. Phys.* **B 167** (1980) 479.

[21] C. Bollini, J. Giambiagi, *Nuovo Cim.* **B 12** (1972) 20;
J. Ashmore, *Nuovo Cim. Lett.* **4** (1972) 289;
G. 't Hooft, M. Veltman, *Nucl. Phys.* **B 44** (1972) 189.

[22] A. Djouadi, P. Gambino, S. Heinemeyer, W. Hollik, C. Jünger and G. Weiglein, *Phys. Rev.* **D 57** (1998) 4179, hep-ph/9710438.

[23] J. Küblbeck, M. Böhm and A. Denner, *Comp. Phys. Comm.* **60**, 165 (1990);
H. Eck and J. Küblbeck, *Guide to FeynArts 1.0* (Univ. of Würzburg, 1992);
H. Eck, *Guide to FeynArts 2.0* (Univ. of Würzburg, 1995).

[24] T. Hahn, hep-ph/0012260; (see `www.feynarts.de`).

[25] G. Weiglein, R. Scharf and M. Böhm, *Nucl. Phys.* **B 416** (1994) 606, hep-ph/9310358;
G. Weiglein, R. Mertig, R. Scharf and M. Böhm, in *New Computing Techniques in Physics Research 2*, ed. D. Perret-Gallix (World Scientific, Singapore, 1992), p. 617.

[26] G. 't Hooft, M. Veltman, *Nucl. Phys.* **B 153** (1979) 365.

[27] A. Davydychev and J.B. Tausk, *Nucl. Phys.* **B 397** (1993) 123;
F. Berends and J.B. Tausk, *Nucl. Phys.* **B 421** (1994) 456.

[28] S. Heinemeyer, W. Hollik and G. Weiglein, *Comp. Phys. Comm.* **124** (2000) 76, hep-ph/9812320; hep-ph/0002213; see `www.feynhiggs.de` .

[29] S. Heinemeyer, W. Hollik and G. Weiglein, KA-TP-5-2001.

[30] A. Djouadi, P. Gambino, S. Heinemeyer, W. Hollik, C. Jünger and G. Weiglein, *Phys. Rev. Lett.* **78** (1997) 3626, hep-ph/9612363.

[31] P. Janot, in *Physics at LEP2*, eds. G. Altarelli, T. Sjöstrand and F. Zwirner, CERN 96-01, Vol. 2, p. 309.

[32] A. Quadt, *private communication.*

[33] M. Carena, S. Pokorski and C. Wagner, *Nucl. Phys.* **B406** (1993) 59, hep-ph/9303202;
W. de Boer et al., *Z. Phys.* **C 71** (1996) 415, hep-ph/9603350.

[34] Andringa et al., ALEPH 2000-074 CONF 2000-051, DELPHI 2000-148 CONF 447, L3 Note 2600, OPAL Technical Note TN661;
S. Heinemeyer, W. Hollik and G. Weiglein, *JHEP* **06** (2000) 009, hep-ph/9909540;
A. Dedes, S. Heinemeyer, P. Teixeira-Dias and G. Weiglein, *Jour. Phys.* **G 26** (2000) 582, hep-ph/9912249.

[35] Particle Data Group, *Eur. Phys. Jour.* **C15** (2000) 1.

[36] M. Carena and P. Zerwas, in *Physics at LEP2*, CERN 96-01, eds. G. Altarelli, T. Sjöstrand and F. Zwirner, hep-ph/9602250.

[37] M. Carena, S. Heinemeyer, C. Wagner and G. Weiglein, hep-ph/9912223.

[38] F. Abe et al., CDF Collaboration, hep-ex/9810029;
B. Abbott et al., D0 Collaboration, hep-ex/9808029;
R. Partridge, in *Proceedings of the 29th International Conference on High-Energy Physics*, Vancouver 1998, eds. A. Astbury, D. Axen and J. Robinson (World Scientific, Singapore, 1999), p. 107.

[39] A. Pilaftsis and C. Wagner, *Nucl. Phys.* **B 553** (1999) 3, hep-ph/9902371.